THE STUDY OF THE ENANTIOSELECTIVE [4+2] CYCLOADDITION REACTION OF ORTHO-HYDROXYSTYRENE AND AZLACTONE: COMPUTATIONAL SIMULATIONS

NAPASSORN JENSUPAKARN

A THESIS SUBMITTED IN PARTIAL FULFILLMENT
OF THE REQUIREMENT FOR THE DEGREE OF
MASTER OF SCIENCE IN NANOSCIENCE AND NANOTECHNOLOGY
COLLEGE OF NANOTECHNOLOGY
KING MONGKUT'S INSTITUTE OF TECHNOLOGY LADKRABANG
2019

KMITL-2019-NT-M-001-004

THE STUDY OF THE ENANTIOSELECTIVE [4+2] CYCLOADDITION REACTION OF ORTHO-HYDROXYSTYRENE AND AZLACTONE: COMPUTATIONAL SIMULATIONS

NAPASSORN JENSUPAKARN

A THESIS SUBMITTED IN PARTIAL FULFILLMENT
OF THE REQUIREMENT FOR THE DEGREE OF
MASTER OF SCIENCE IN NANOSCIENCE AND NANOTECHNOLOGY
COLLEGE OF NANOTECHNOLOGY
KING MONGKUT'S INSTITUTE OF TECHNOLOGY LADKRABANG
2019

KMITL-2019-NT-M-001-004

การศึกษาการเลือกเกิดอิแนนทิโอเมอร์ของปฏิกิริยา [4+2] ไซโคลแอดดิชัน ระหว่างออร์โธ-ไฮดรอกซีสไตรีนกับอาซแลคโตนโดยใช้ การจำลองแบบการคำนวณ

THE STUDY OF THE ENANTIOSELECTIVE [4+2] CYCLOADDITION REACTION OF ORTHO-HYDROXYSTYRENE AND AZLACTONE: COMPUTATIONAL SIMULATIONS

นภัสสร เจนศุภการ
NAPASSORN JENSUPAKARN

วิทยานิพนธ์นี้เป็นส่วนหนึ่งของการศึกษาตามหลักสูตรปริญญาวิทยาศาสตรมหาบัณฑิต
สาขาวิชานาโนวิทยาและนาโนเทคโนโลยี
วิทยาลัยนาโนเทคโนโลยีพระจอมเกล้าลาดกระบัง
สถาบันเทคโนโลยีพระจอมเกล้าเจ้าคุณทหารลาดกระบัง
พ.ศ. 2562
KMITL-2019-NT-M-001-004

Thesis Title	The Study of the Enantioselective [4+2] Cycloaddition Reaction of *ortho*-Hydroxystyrene and Azlactone: Computational Simulations
Student	Miss Napassorn Jensupakarn
Student ID	59607012
Degree	Master of Science
Program	Nanoscience and Nanotechnology
Year	2019
Thesis Advisor	Dr. Kanokthip Boonyarattanakalin
Thesis Co-advisor	Dr. Matthew Paul Gleeson

ABSTRACT

Theoretical studies have been undertaken to investigate the enantioselective [4+2] cycloaddition reaction between *o*-hydroxystyrene and azlactone catalyzed by (a) chiral BINOL-phosphoric acid (CPA) only and (b) by CPA combining with chiral bicyclic guanidine (TBO). An increase in enantioselectivity is experimentally observed under the latter conditions. Density functional theory (DFT) methods have been carrier out to study the cycloaddition reaction mechanism insight into the origin of the enantioselectivity for both the catalytic conditions. The results indicated that both the mono- and co-catalytic processes proceed via stepwise [4+2] cycloaddition reactions involving three key steps, which are (1) C-C and (2) C-O bond formations, and (3) ring opening of the azlactone, as a result of the formation of an oxygenous cycle with one chiral center. The structures and energetics of the intermediates and transition states formed on the potential energy surface of the competing enantioselective reactions are discussed to rationalize the origin of greater enantioselectivity under the co-catalytic conditions. The results indicated that the tightly binding of strong acidic CPA and strong basic TBO gives a greater blocking of one face, leading to control of facial selectivity via noncovalent interactions found between the substrates and the catalysts.

Keywords : [4+2] Cycloaddition reaction, density functional theory, chiral phosphoric acid, chiral bicyclic guanidine, enantioselectivity

หัวข้อวิทยานิพนธ์	การศึกษาการเลือกเกิดอิแนนทิโอเมอร์ของปฏิกิริยา [4+2] ไซโคลแอดดิชัน ระหว่างออร์โธ-ไฮดรอกซีสไตรีนกับอาซแลคโตนโดยใช้การจำลองแบบการคำนวณ
นักศึกษา	นางสาวนภัสสร เจนศุภการ
รหัสประจำตัว	59607012
ปริญญา	วิทยาศาสตรมหาบัณฑิต
สาขาวิชา	นาโนวิทยาและนาโนเทคโนโลยี
พ.ศ.	2562
อาจารย์ที่ปรึกษาวิทยานิพนธ์	ดร.กนกทิพย์ บุณยรัตกลิน
อาจารย์ปรึกษาวิทยานิพนธ์ร่วม	ดร.แมทธิว พอล กลีสัน

บทคัดย่อ

งานวิจัยนี้ได้ทำการศึกษาเชิงทฤษฎีของการเลือกเกิดอิแนนทิโอเมอร์ของปฏิกิริยา [4+2] ไซโคลแอดดิชันระหว่างออร์โธ-ไฮดรอกซีสไตรีนกับอาซแลคโตนโดยมี (1) เงื่อนไขที่ใช้ไครัลฟอสฟอริกแอซิดเป็นตัวเร่งปฏิกิริยาเพียงชนิดเดียวและ (2) เงื่อนไขที่ใช้ตัวเร่งปฏิกิริยาไครัลฟอสฟอริกแอซิดร่วมกับตัวเร่งปฏิกิริยาไครัลเกานิดีน จากผลการทดลองพบว่าการเลือกเกิดของสารผลิตภัณฑ์อิแนนทิโอเมอร์ในเงื่อนไขที่ใช้ตัวเร่งปฏิกิริยา 2 ชนิดมีค่าเพิ่มขึ้น เมื่อเทียบกับเงื่อนไขที่ใช้ตัวเร่งปฏิกิริยาเพียงชนิดเดียว ดังนั้นกลไกการเกิดปฏิกิริยาและการเลือกเกิดอิแนนทิโอเมอร์ของปฏิกิริยา [4+2] ไซโคลแอดดิชันนี้ จึงถูกนำมาศึกษาโดยใช้การจำลองแบบการคำนวณด้วยระเบียบวิธีทฤษฎีฟังก์ชันนอลความหนาแน่น จากผลการคำนวณพบว่ากลไกการเกิดปฏิกิริยา [4+2] ไซโคลแอดดิชันระหว่างสารออร์โธ-ไฮดรอกซีสไตรีนกับอาซแลคโตน ประกอบด้วย 3 ขั้นตอนหลัก คือ การเกิดพันธะระหว่างอะตอมคาร์บอน-คาร์บอน การเกิดพันธะระหว่างอะตอมคาร์บอน-ออกซิเจน และการเปิดวงของอาซแลคโตน ทำให้ได้สารผลิตภัณฑ์ที่มีจำนวนอะตอมไครัลในโมเลกุล 1 อะตอม จากการวิเคราะห์โครงสร้างและค่าพลังงานของสารมัธยันต์และสารในสถานะทรานซิชันบนพื้นผิวพลังงานศักย์สามารถอธิบายและให้เหตุผลการเลือกเกิดระหว่างคู่อิแนนทิโอเมอร์ของปฏิกิริยานี้ได้ว่า ตัวเร่งปฏิกิริยาไครัลฟอสฟอริกแอซิดและไครัลเกานิดีนจะมีแรงอันตรกิริยาระหว่างกันมากเนื่องจากความเป็นกรด-เบสทำให้การเข้าปฏิกิริยาระหว่างสารเกิดในบริเวณที่จำกัด และอันตรกิริยานอนโควาเลนซ์ระหว่างสารตั้งต้นและตัวเร่งส่งผลต่อการชอบเข้าทำปฏิกิริยาระหว่างสารเพียงด้านใดด้านหนึ่ง นั่นคือปฏิกิริยาที่ใช้ตัวเร่งปฏิกิริยา 2 ชนิดมีความจำเพาะที่สูงกว่าซึ่งสอดคล้องกับผลการทดลองจากงานวิจัยอ้างอิง

คำสำคัญ : ปฏิกิริยา [4+2] ไซโคลแอดดิชัน; ระเบียบวิธีทฤษฎีฟังก์ชันนอลความหนาแน่น; ตัวเร่งไครัลฟอสฟอริกแอซิด; ตัวเร่งไครัลเกานิดีน; การเลือกอิแนนทิโอเมอร์

ACKNOWLEDGMENT

I would like to acknowledge several people, who contributed to the research and this thesis, and have supported me in several ways almost three years.

First of all, I would like to express my sincere gratitude my thesis advisor, Dr. Kanokthip Boonyarattanakalin, and my thesis co-advisor, Dr. Matthew Paul Gleeson, for their continuous guidance and support during my Master's study and research work. They not only provided valuable suggestions throughout my research, but they also encourage me to complete this work and improve myself as much as possible. I have gained a lot of knowledge and experience, particularly skills of English language. I would like to thank for their kindness, patience, motivation, and immense knowledge contributing to a quality of this work.

I am thankful to Associate Professor Dr. Duangkamol Gleeson for her helpful suggestion and her kind support and for serving as my thesis committee's members.

A Heartfelt thanks to my supportive family for taking care of many familial tasks for all of my life and praying for me through hard times during my Master's student life. Thanks for always staying beside me all the times whether I am tired or happy.

I would also like to thanks members in Nano Materials Research Laboratory (NMRL) and Computational & Medicinal Chemistry Laboratory (CMCL) for their help, useful advice, and friendship as well as for giving good times. Furthermore, my special thanks to my close friends for listening and cheering me.

Finally, I would like to acknowledge College of Nanotechnology and at King Mongkut's Institute of Technology Ladkrabang (KMITL).

Napassorn Jensupakarn

CONTENTS (I)

Page

ABSTRACT(ENGLISH) I

ABSTRACT(THAI) II

ACKNOWLEDGMENT III

CONTENTS IV

LIST OF TABLES VI

LIST OF ILLUSTRATIONS VII

CHAPTER 1 INTRODUCTION 1

1.1 Introduction 1

1.2 Objectives of this work 2

1.3 Scope of this work 3

1.4 Expected results of this work 3

CHAPTER 2 BACKGROUND AND LITERATURE REVIEW 4

2.1 The Diels-Alder reaction 4

2.1.1 Types of DA reactions 5

2.1.2 Mechanistic pathways of Diels-Alder reactions 7

2.1.3 *o*-Hydroxystyrene as a conjugate diene 9

2.1.4 Azlactone as a dienophile 11

2.1.5 Enantioselective DA reaction 15

2.2 Example of oxygenous cyclic framework 24

2.3 Computational chemistry 25

2.3.1 Quantum Mechanics 25

2.3.2 The Born-Oppenheimer approximation 27

2.3.3 Electronic spatial and spin orbitals 28

2.3.4 Hartree products 29

2.3.5 The Slater determinant 30

2.3.6 The Hartree-Fock theory 32

2.3.7 Basis sets 33

2.3.8 Density Functional Theory 37

CONTENTS (II)

Page

2.3.9 Exchange-correlation functionals 39

2.4 Literature reviews 42

CHAPTER 3 COMPUTATIONAL METHODOLOGY 48

3.1 Molecular models 48

3.2 Computational details 49

3.3 Keto-Enol tautomerization 51

CHAPTER 4 RESULTS AND DISCUSSION 53

4.1 Mono-catalytic DA reaction 57

4.1.1 The effect of CPA substituents 65

4.2 Co-catalytic DA reaction 67

4.3 Discussion of enantioselective catalytic reaction 74

CHAPTER 5 CONCLUSION 75

REFERENCES 77

APPENDIX 86

APPENDIX A: Supporting Information 87

APPENDIX B: Publication 92

AUTHOR BIOGRAPHY 101

LISTS OF TABLES

Table **Page**

4.1 The computed QM energies of all stationary points obtained in this study. 56

4.2 The key interaction distances in the mono-catalytic reaction obtained at the QM (M062X/6-31G(d)//3-21G) level of theory..... 64

4.3 The QM relative enthalpies ΔH and free energies ΔG of the stationary points obtained in this study for mono-catalytic system using CPA-a and CPA-b.....67

4.4 The key interaction distances in the co-catalytic reaction obtained at the QM (M062X/6-31G(d)//3-21G) level of theory.....73

LISTS OF ILLUSTRATIONS (I)

Figure **Page**

2.1 Basic DA reaction of a diene and a dienophile forming a cyclohexene. 4
2.2 The simple molecular orbital diagram for DA reaction of butadiene and ethylene. 6
2.3 Representation of the energy-level diagrams for normal, neutral, and inverse electron-demand DA cycloadditions. 7
2.4 Schematic representation of energy profile for concerted (thick line) and stepwise (dashed line) mechanisms of DA reaction between butadiene with ethylene 8
2.5 *o*-Hydroxystyrene involved catalytic enantioselective reactions [24]. 10
2.6 Resonance structure of *o*-QMs 10
2.7 The E/Z geometric isomer of *o*-QMs 11
2.8 Keto-enol tautomerization 12
2.9 The design of asymmetric [4+2] cycloadditions of azlactones with o-QMs..... 14
2.10 Achiral and chiral Brønsted acid catalysts..... 17
2.11 *S* and *R* configurations of BINOL-derived axially chiral phosphoric acids..... 18
2.12 Bifunctional activation of CPA catalysis (a) a neutral electrophile and a nucleophile forming hydrogen bond with a catalyst (b) a cationic electrophile forming an ion pair with anionic conjugate bases of a catalyst (X=NR, O, C) [52]. 19
2.13 Goodman's and Quadrant representation of CPA catalyst. 20
2.14 Chiral [5,5]-bicyclic guanidine substituted by *t*-butyl groups and its geometry optimized at the M06-2X/6-31G* level. 22
2.15 Schematic representation of plausible mono- and bifunctional activation modes of bicyclic guanidinium catalyst (R = Ph, t-Bu). 23
2.16 Face-on and side-on ternary complexes..... 24
2.17 The structure of DHC and examples of their biologically active molecules. 25
2.18 Comparison of Slater and Gaussian Basis Functions for 1S orbital. 35
2.19 The energy profile of monocoordination and dicoordination pathways..... 43

LISTS OF ILLUSTRATIONS (II)

Figure **Page**

2.20 3D structures associated with antiperiplanar; r, and synclinal; s, transition states in (a) dicoordination (TSr and TSs) and (b) monocoordination (TSmr and TSms) models obtained at ONIOM (B3LYP/6-31G*:HF/3-21G) level. 44

2.21 3D structures and schematic representation models of TSαr_{syn}-A and TSβS_{syn}-A. The 3,3′-substituents of BINOL-phosphoric acid and substrates are represented to ball model and tube model, respectively. 45

2.22 The DFT optimized structures of the (E)- and (Z)-o-QM intermediates (IM'). [20] 46

3.1 The scope of this study. 48

3.2 Molecular models used for computational calculation with 6-31G* (in black) and 3-21G (in blue) basis sets 49

3.3 Schematic representation models of the (a) si and (b) re face additions for mono-catalytic system and that of the (c) *si* and (d) *re* face additions for co-catalytic system. 51

3.4 a) *o*-Hydroxystyrene and b) azlactone tautomers and their relative energies. 52

4.1 The QM ΔG energy profile of endo and exo pathways of DA reaction involving CPA and TBO catalysts. 54

4.2 Optimized structures of TS1 for endo and exo approaches in co-catalytic reactions. 54

4.3 QM ΔG reaction profile of both (*S*)- and (*R*)- products for the mono-catalytic reaction. Solid and dashed lines denote path a and b, respectively. 57

4.4 Schematic 2D illustration of the DA mechanism catalyzed by chiral phosphoric acid. 58

4.5 QM optimized structures associated with (*S*)-product in mono-catalysis obtained at the M06-2X/6-31G*//3-21G level. 60

4.6 QM optimized structures associated with (*S*)-product via path a in mono-catalysis obtained at the M06-2X/6-31G*//3-21G level. 61

LISTS OF ILLUSTRATIONS (III)

Figure **Page**

4.7 QM optimized structures associated with (*R*)-product in mono-catalysis obtained at the M06-2X/6-31G*//3-21G level..... 62
4.8 QM optimized structures associated with (*R*)-product via path a in mono-catalysis obtained at the M06-2X/6-31G*//3-21G level. 63
4.9 3D structures of INT1 and INT2 in mono-catalysis of (*S*)- and (*R*)- isomers. 64
4.10 Models of CPA derivatives used for computational calculations 65
4.11 The QM ΔG energy profile of CPA, CPA-a, and CPA-b for mono-catalysis. 66
4.12 QM optimized structures associated with (*S*)-product in mono-catalysis involving (a) CPA-a and (b) CPA-b obtained at the M06-2X/6-31G*//3-21G level.. 66
4.13 QM ΔG reaction profile of (*S*)- and (*R*)- products for the co-catalytic reaction.. 67
4.14 Schematic 2D illustration of the catalytic DA mechanism observed for chiral phosphoric acid merging with chiral bicyclic guanidine catalyst. 68
4.15 QM optimized structures associated with (*S*)-product in co-catalysis obtained at the M06-2X/6-31G*//3-21G level..... 70
4.16 QM optimized structures associated with (*R*)-product in co-catalysis obtained at the M06-2X/6-31G*//3-21G level..... 71
4.17 3D structures of TS1 and TS2 in co-catalysis of (*S*)- and (*R*)- isomers. 73
4.18 The relationship between the RDS energy difference and enantiomeric ratio for mono- and co- catalytic systems.....74

CHAPTER 1
INTRODUCTION

1.1 Introduction

Diels-Alder (DA) reaction is one of the most useful methods for synthesis of six-membered carbo- and heterocyclic compounds, both simple and complex molecules, in organic chemistry that are pronounced as fundamental structures in a wide range of natural products and pharmaceutically active molecules such as dihydrocoumarin (DHC) scaffolds. DA reaction is formally a [4+2] cycloaddition between a conjugated diene and a dienophile. In general, a diene reacts with a dienophile in stereoselective manner due to effect of internal and external factors on its reactivity including steric effects, catalysts, and reactants that induce various asymmetric transformations of products. In many cases, the great improvement in enantioselectivity to DA cycloadditions requires a type of chiral organocatalysts for controlling the formation of cyclic product in a favorable way, along with metal-free processes. With a molecule with a chiral center, the products can exist in two enantiomers, *S*- and *R*- isomers. As a part of continuing efforts to develop enantioselective DA reactions, an acid-base bifunctional organic catalyst can lead to efficient chiral induction through the simultaneous activation of both nucleophile and electrophile reaction partners by hydrogen-bonding interactions. Most of enantioselective DA reactions have been achieved using one catalyst to improve yields as well as enantiomeric ratios, however, the recent research showed the success in enhancing the enantioselectivity in asymmetric DA reaction of *o*-hydroxystyrene and azlactone by the use of cooperative catalysis that consists of two different catalysts, chiral phosphoric acid and chiral bicyclic guanidine, in order to o develop new catalytic system. Unfortunately, the yield of products was found to be decreased in comparison with the mono-catalytic condition. Although, the selectivity in DA cycloadditions have been investigated by both experimental and theoretical studies, the experimental studies cannot explain the actual catalytic DA reactions. Consequently, computational

methods are used to gain mechanistic insights into the enantioselective DA reaction based on this previous research work.

A Quantum Mechanics (QM) calculation is a computational tool for investigating chemical reactions and molecular properties. In this work, we focused on *o*-hydroxystyrene and azlactone as versatile reactants, which allow different organic transformations, existing the ring bearing an oxygen atom. For chiral catalysts, we concentrated on phosphoric acid and guanidine as chiral Brønsted acid and base, respectively that had been used in the experimental research as mentioned above. To explore the mechanism insight of Diels-Alder reaction of o-hydroxylstyrene with azlactone catalyzed by chiral phosphoric acid and chiral guanidine, Quantum computational methods have been used as practical tools to study the systems at the molecular level explaining the experimental results by using the M06-2X functional with 6-31G* and 3-21G basis sets in QM calculations.

1.2 Objectives of this work

1.2.1 To investigate the possible enantioselective Diels-Alder reaction catalyzed by only CPA and both CPA and TBO catalysts

1.2.2 To study the unusual phenomena in the enantioselective cycloaddition of *o*-hydroxystyrene and azlactone due to the use of bifunctional chiral organocatalysts

1.2.3 To explain and support the experimental observations using computational calculations, concerning both the mechanism and the origin of enantioselectivity in the Diels-Alder reaction

1.3 Scope of this work

This study is divided into two catalytic systems in which each system has two enantioselective channels including the formation of (*S*)-product and (*R*)-product.

System	Absolute configuration
1. Mono-catalysis using CPA only	1.1 (*S*)-product
	1.2 (*R*)-product
2. Co-catalysis using both CPA and TBO	1.1 (*S*)-product
	1.2 (*R*)-product

1.4 Expected results of this work

1.4.1 Reveal the Diels-Alder reaction mechanisms based on the different catalytic systems : mono- and co-catalysis using DFT calculations

1.4.2 Understand and rationalize the origin of enantioselectivity in the Diels-Alder reactions

1.4.3 Show the difference between mono- and co-catalytic Diels-Alder reactions

1.4.4 Support the synergy of computation and experiment

CHAPTER 2

BACKGROUND AND LITERATURE REVIEW

2.1 The Diels-Alder reaction

Diels-Alder (DA) reaction is formally a [4+2] cycloaddition reaction to produce an unsaturated six-membered ring from a conjugated diene and a dienophile. This reaction was firstly reported by Otto Diels and Kurt Alder in 1928 [1] and become one of the most important and useful for synthesis of cyclic frameworks in organic chemistry [2]. In DA reactions, the movement of 4π-electrons of a diene and 2π-electrons of an alkene, commonly termed a dienophile, rearrange themselves leads to bond cleavage and formation of two new σ-bonds and one π-bond within the ring structure (Figure 2.1). Later, the range of dienes and dienophiles has been extended when dienes and/or dienophiles containing at least one heteroatoms (O, N, S) to form carbon-heteroatom or heteroatom-heteroatom bonds, they can directly access to structurally diverse six-membered heterocycles. These carbo- and heterocyclic systems are frequently found in core structures in a number of natural products and biologically active molecules [3]. The DA reaction has remained as an efficient way for constructing simple and complex molecules through traditional transformations. Undoubtedly, these DA cycloadditions have attracted much attention in the area of pharmaceutical and agrochemical applications [4]. Interestingly, they also have a potential to apply in nanotechnology, for example, the preparation of hydrogel nanoparticles for drug delivery systems [5].

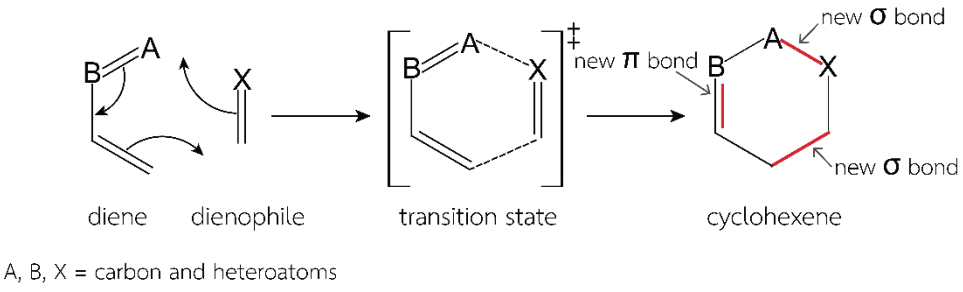

Figure 2.1 Basic DA reaction of a diene and a dienophile forming a cyclohexene.

2.1.1 Types of DA reactions

Reactants used for DA reactions consist of a diene, which is a compound with 1,3-conjugated system, and a dienophile, which is a substituted alkene. Any atoms on the diene and/or dienophile fragments replaced by one or more heteroatoms can create a number of cyclohexene with different positions of heteroatom. These reactions are called hetero Diels-Alder (HDA) reactions. Due to DA reactions controlled by orbital interaction, the concept of frontier molecular orbitals (FMO) theory has been utilized to rationalize [4+2] cycloadditions [6].

According to FMO theory, the reactivity and the stereochemistry are controlled by the interaction between the highest occupied molecular orbital (HOMO) and the lowest unoccupied molecular orbital (LUMO). In the reaction of two reactants, electrons from the HOMO of one reactant transfer to the LUMO of the other in the way of the smallest HOMO-LUMO energy gap. As shown in Figure 2.2, four p atomic orbitals on the diene are overlapped to create different levels of potential energy of four molecular orbitals that depend on the number of nodes. When two orbitals between adjacent atoms are overlapped on the same sign of the wave functions ψ to form a bonding molecular orbital (π-orbital), the probability of the electron density between the two carbon nuclei of bonding atoms are increased, resulting in the more stable and lower energy orbitals. However, the overlap of two orbitals with the opposite sign provides an anti-bonding molecular orbital (π^*-orbital), which is separated from each other by a region of zero electron density called a nodal plane. Then, the orbital jumps to the higher energy level. Overall, the diene has four possible energy levels of the wave functions from the lowest energy to the highest energy, including ψ_1, ψ_2, ψ_3, and ψ_4, respectively. The complete overlap of molecular orbitals allows the electrons to distribute all around to the four atoms, leading to the minimization of electronic repulsion. The two of the total four electrons from the two π bonds of the diene are filled in the lowest energy of molecular orbitals ψ_1 first following filling the upper ψ_2 with the two remaining electrons of the diene. Hence, ψ_2 is the HOMO level and ψ_3 is the LUMO level. As happened in the dienophile with just two electrons from one π bond, the HOMO and the LUMO are ψ_1 and ψ_2, respectively.

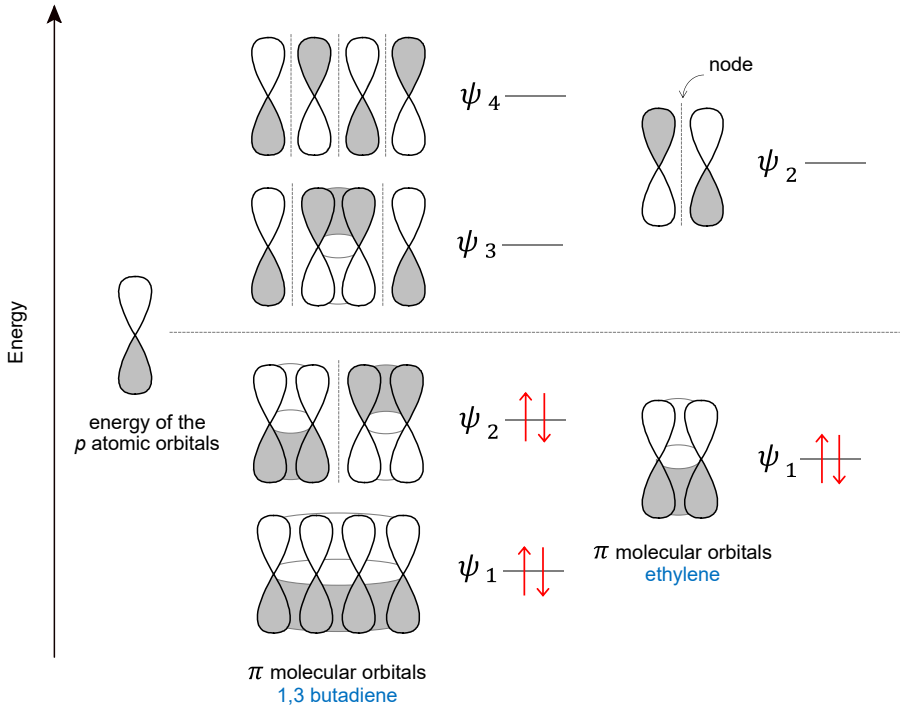

Figure 2.2 The simple molecular orbital diagram for DA reaction of butadiene and ethylene.

Basically, the simplest DA reaction of 1,3-butadiene with ethylene requires high temperature and high pressure conditions; however, the cyclohexene product is obtained in very low yields [7]. This may result from the poor reactivity by means of small difference in electrophilicity power of a diene-dienophile pair [8]. Internal and external factors are consequently used for an enhancement of orbital interactions [9].

In the case of substitutions on substrates for changing their electronic features, DA reactions can be classified into three types according to HOMO-LUMO interaction with respect to the direction of electron flow (Figure 2.3). These three types of DA reactions are (1) normal electron demand where electron donating group (EDG) on diene and electron withdrawing group (EWG) on dienophile promote the reaction; (2) neutral electron demand where there are no EDG and EWG to facilitate the reaction; and (3) inverse electron demand additions where EDG on dienophile and EWG on diene activate the reaction. Within the normal DA reactions, EDG on the diene increases the HOMO energy of the diene, while EWG on the dienophile lowers the LUMO of the

dienophile. As a result, the $HOMO_{diene}$-$LUMO_{dienophile}$ gap is reduced. Consequently, the activation energy of the cycloaddition is decreased; hence the electron transfer is energetically favorable from the diene HOMO to the dienophile LUMO. On the contrary, in case of the inverse DA reaction, the energy separation between the $HOMO_{diene}$ and $LUMO_{dienophile}$ is increased by the presence of EDG on the dienophile and EWG on the diene, which lead to the electron-rich dienophile and the electron-poor diene, respectively. Hence, the electrons flow from the dienophile HOMO to the diene LUMO. For the neutral DA reaction, both reactants can be an electron donor and an electron acceptor because the energy gap between $HOMO_{diene}$-$LUMO_{dienophile}$ and $LUMO_{diene}$- $HOMO_{dienophile}$ is not much different. Therefore, the electron-donating and electron-withdrawing substituents can accelerate the chemical reaction.

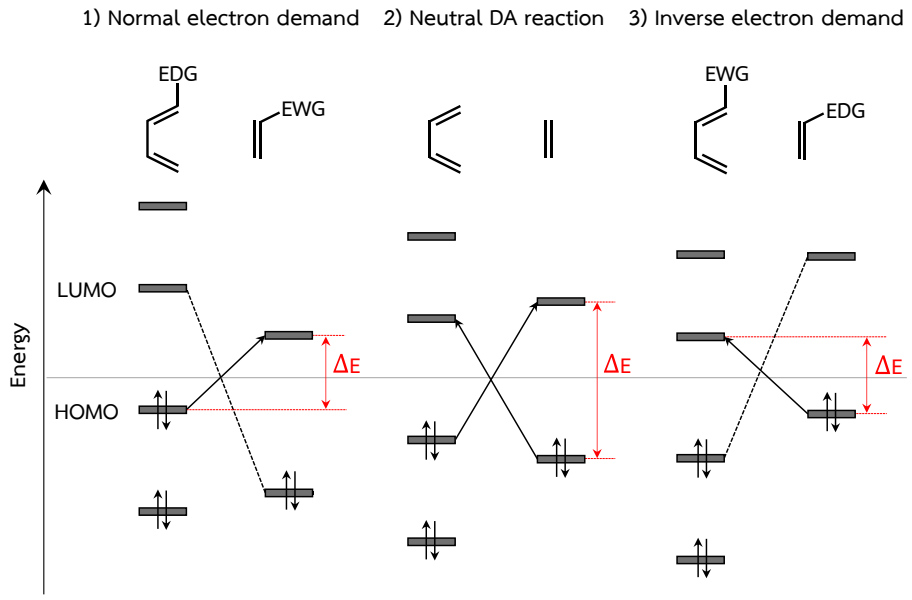

Figure 2.3 Representation of the energy-level diagrams for normal, neutral, and inverse electron-demand DA cycloadditions.

2.1.2 Mechanistic pathways of Diels-Alder reactions

The cyclic product obtained from cycloadditions is called as a *cycloadduct*. As the two new bonds are formed between the reactants for all DA reactions, there are two possible mechanisms for these [4+2] processes: concerted and stepwise pathways.

In a concerted pathway, the two new bonds are formed in a single step. Thus, the formation of the adduct proceeds via only one transition state (TS) without any intermediate. In the concerted TS, if the two forming bonds elongate to the same extent at the same time, this reaction is called synchronous. In contrast, if one bond is a greater extent than the other bond, this reaction is called asynchronous. The latter is a result of unsymmetrical diene and/or dienophile by adding various substituted groups. The means of the difference between the distances of the bonds being formed are measured in order to show the extent of asynchronicity. Alternatively, a stepwise pathway involves two TSs separated by one of two intermediates (INTs), which are diradical and zwitterion species, followed by a subsequent ring closure.

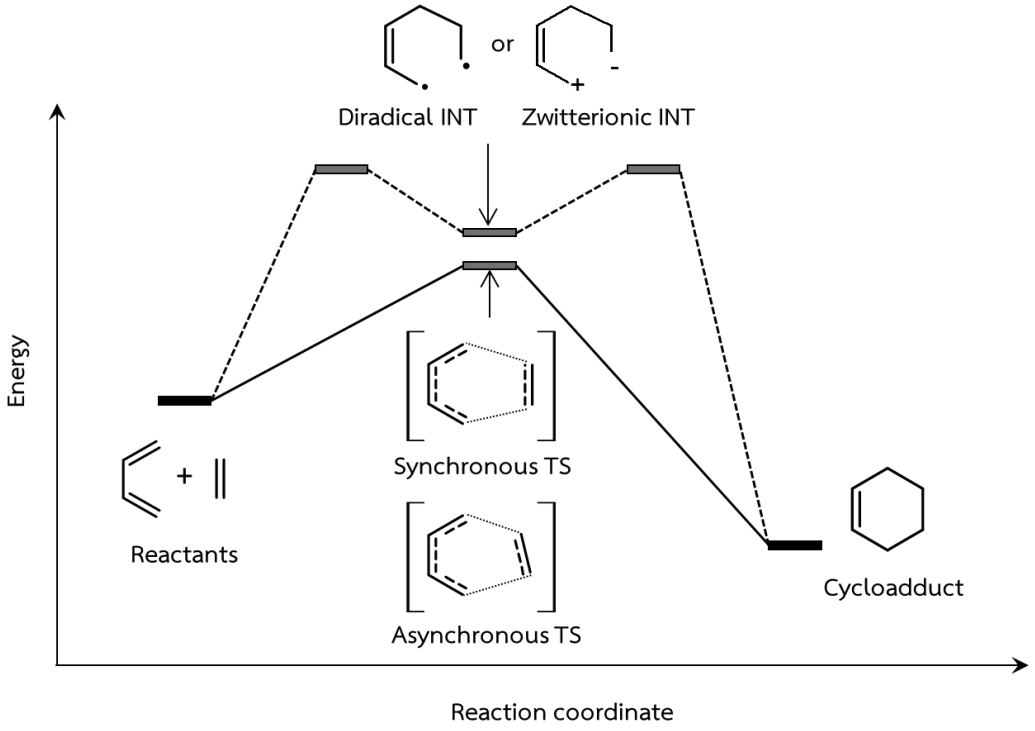

Figure 2.4 Schematic representation of energy profile for concerted (thick line) and stepwise (dashed line) mechanisms of DA reaction between butadiene with ethylene

The mechanism of DA reactions has long been the subject of controversy [10-13]. Thus, experimental and theoretical studies have been devoted to investigating this

part. For example, the DA reaction between butadiene and ethylene can occur through either a synchronous concerted or a stepwise pathway. Although, the one-step mechanism is favored by ~2-7 kcal/mol over the latter, it still require a high energy of activation [11]. As mentioned above, the opposite electronic features of electron-donating and electron-withdrawing substituents on the diene and dienophile can increase the reaction rate by decreasing the HOMO-LUMO energy gap [14]. In this research, *ortho*-hydroxystyrene and azlactone, which are served as the oxa-diene and the dienophile, respectively, have been focused on the study of the DA reaction. These two reaction partners will be introduced in the following sections.

2.1.3 *o*-Hydroxystyrene as a conjugate diene

A styrene substituted with a hydroxyl group at *ortho* position refers to *o*-hydroxystyrenes that have been exhibited their great potential as versatile reactants including nucleophiles [15-19] and electrophiles [20, 21] as illustrated in Figure 2.5. In the former, *o*-hydroxystyrene is activated by an acid catalyst through the formation of hydrogen bond with a hydroxyl group, thereby facilitating nucleophilic addition to electrophiles. For the latter in contrast, *o*-hydroxystyrene is protonated by an acid catalyst to form either a tertiary carbocation or its neutral resonance structure, an *o*-QM form, which acts as a potent electrophile to readily attack with nucleophiles in addition reactions. For all of these reactions, an *o*-hydroxyl group in the styrene plays a crucial role as an activating group in both reactivity and enantioselectivity via forming a hydrogen bond with a chiral catalyst [20-23]. *o*-Hydroxystyrenes have been recently recognized as a promising oxa-diene to undergo [4+2] cycloaddition reaction by converting them into *ortho*-quinone methide (*o*-QM) intermediates [24].

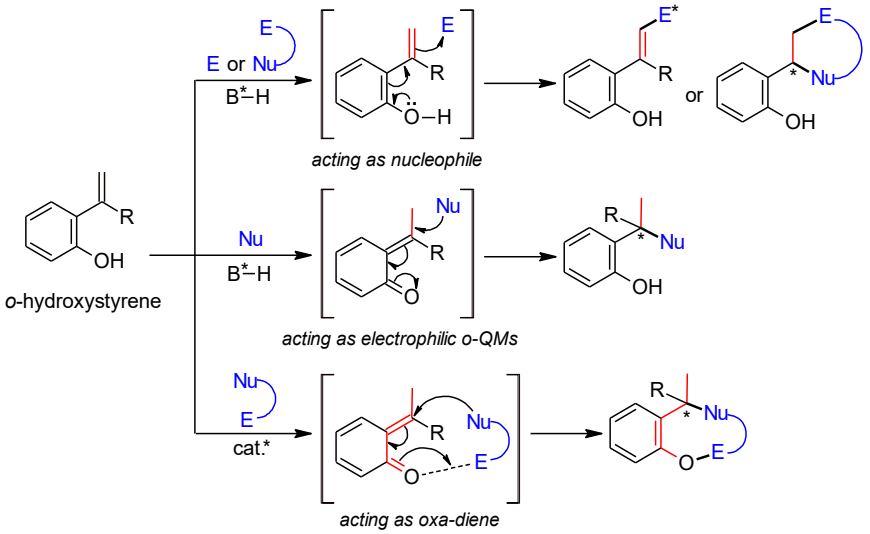

Figure 2.5 *o*-Hydroxystyrene involved catalytic enantioselective reactions [24].

o-QMs are highly reactive intermediates with short lifetimes due to much more polarized, thus their driving force to rapidly rearomatize either by Michael addition with nucleophiles or, more usefully, by [4+2] cycloaddition reaction with dienophiles for stabilization [25, 26]. This is a result of the transient nature of *o*-QMs. Regarding electron density distribution of the two resonance forms, *o*-QM is a non-aromatic core structure with no charge while the ionic form has a zwitterionic character with an increasing polarity, which is stabilized by its aromatic resonance structure. This dipolar form contains both negative and positive charges on the oxygen and exocyclic carbon atoms, respectively, thus simultaneously reacting with both nucleophile and electrophile (Figure 2.6). The electron donating effect of the oxygen atom makes *o*-QMs less electrophilic. Many researches have been reported *o*-QM served as an electron-deficient diene mostly react with dienophiles in inverse-electron-demand DA reactions [27, 28].

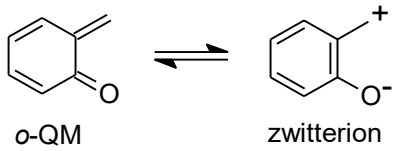

Figure 2.6 Resonance structure of *o*-QMs

The geometric isomer of o-QMs can be either *E*- or *Z*-configuration depending on the substituent effects. If the R^1 substituent is smaller than the oxygen atom of the carbonyl group, *E*-configuration is preferred because of steric repulsion. In contrast, if the R^1 substituent is replaced by bulkier group than the carbonyl oxygen, *Z*-configuration is preferred (Figure 2.7).

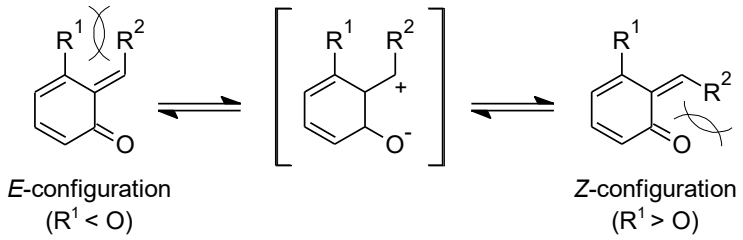

Figure 2.7 The *E/Z* geometric isomer of o-QMs

Consequently, *o*-QMs is potentially utilized in cycloadditions for production of various fused oxygen-containing rings [29]. A range of methods have been developed to generate *o*-QMs, including acid or base catalysis [26, 30]. In particular, chiral Brønsted acid catalysis has been extensively explored as a major method for in situ generation of *o*-QMs from *o*-hydroxystyrenes via protonation [20]. However, the conversion of *o*-hydroxystyrenes into *o*-QMs under organocatalytic asymmetric reactions, especially cycloadditions, still remains underdeveloped and has become a challenging nowadays [24, 31]. Based on the previous experiment [24], the use of *o*-hydroxystyrenes as oxa-diene precursors under the catalysis of a chiral BINOL-derived phosphoric acid is the focus of this work.

2.1.4 Azlactone as a dienophile

The selection of a suitable dienophile to attack the oxadiene requires a molecule bearing both nucleophilic and electrophilic sites for facilitating cycloaddition reactions. Azlactones or oxazole-5-(4H)-ones, which are five-membered oxygen- and nitrogen-containing heterocycles, have been regarded to be a suitable candidate due to their multiple reactive sites allowing for several different transformations in which its C2 and C5 positions are electrophilic centres, whereas its C4 position is nucleophilic site. The

utility of azlactones as a reaction partner in [4+2] cycloadditions has been explored that can exhibit either diene [32, 33] or dienophile [34, 35]. Recently, keto-enol tautomerization of the azlactone was studied using DFT calculations [36]. The keto form of the azlactone is converted into its enol tautomer through an enolate intermediate by a base-mediated reaction and this transformation can also occur backward in the same way. However, the keto azlactone is more stable than the enol such as by $\Delta G_{keto \rightarrow enol}$ of 14.4 kcal/mol in the case of 2,4-diphenyl substituted azlactone (in supporting information of [36]).

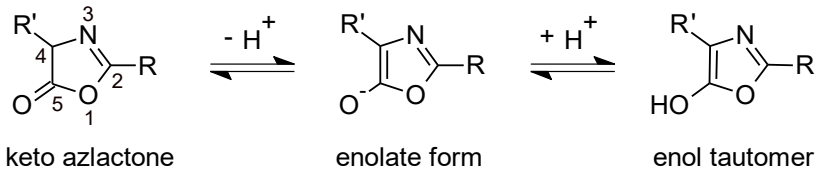

Figure 2.8 Keto-enol tautomerization

The DA reactions usually take advantage of the C4 nucleophilic and C5 electrophilic atoms of the azlactone serving as a dienophile to undergo the cycloaddition process, allowing the formation of unsatursated six-membered rings such as γ, δ-unsaturated δ-lactones and -lactams. The two new forming bonds can occur either in one-step or two-step mechanisms. In 2011, Terada and Nii confirmed the stepwise [4+2] cycloaddition involving azlactone by using HPLC that proceeded via the initial Michael addition at the C4 position of the azlactone, followed by subsequent cyclization reaction at its C5 position to give a cycloadduct [37]. Whereas, in 2015, Hu and co-workers indicated that the concerted pathway of the inverse-electron-demand DA (IEDDA) reaction of azlactones with o-QMs is preferred by the use of th Operando IR experiments [38]. Whether the cycloaddition is concerted or stepwise, the enolate oxygen atom occuring during the catalytic reaction facilitates intramolecular ring opening at the C2 position of the azlactone moiety as a result of the cyclic product bearing a quaternary amino acid moiety. This utilizes the production of quaternary α-amino acid derivatives, which are valuable substrates in bioorganic and medicinal chemistry [39]. On the other side, olefinic azlactones were employed as

pronucleophiles acting as dienes that shown in the few reports [32, 33]. Overall, the azlactone can be activated by the use of either chiral Brønsted acid or chiral Brønsted base catalysts, in particular chiral phosphoric acid and chiral guanidine, respectively, which are bifunctional organocatalysts and thereby providing an excellent yield and enantioselectivity.

Since the azlactones, possessing both nucleophilic and electrophilic properties owing to their interconversion of keto and enol forms, would be the best option being enolates to efficiently react with o-QMs, some DA cycloadditions of azlactones with *o*-QMs have been reported in recent years [38, 40-42] in which the chiral catalysts play an important role to assist in the enolization of the azlactones into an active dienophile via the enolization to undergo the [4+2] cycloadditions with in situ-generated o-QMs in chiral environment. The obtained products are chiral dihydrocoumarins containing a quaternary amino acid moeity, which are a unique structural motif holding pharmaceutcal activities. Very recently, Chen's group established merging chiral phosphoric acid and chiral bicyclic guanidine catalyzed [4+2] cycloaddition reaction of the azlactones with o-QMs [24]. Regardless of their further application of the products, these DA reactions still need to develop highly efficient catalytic asymmetric strategies [41].

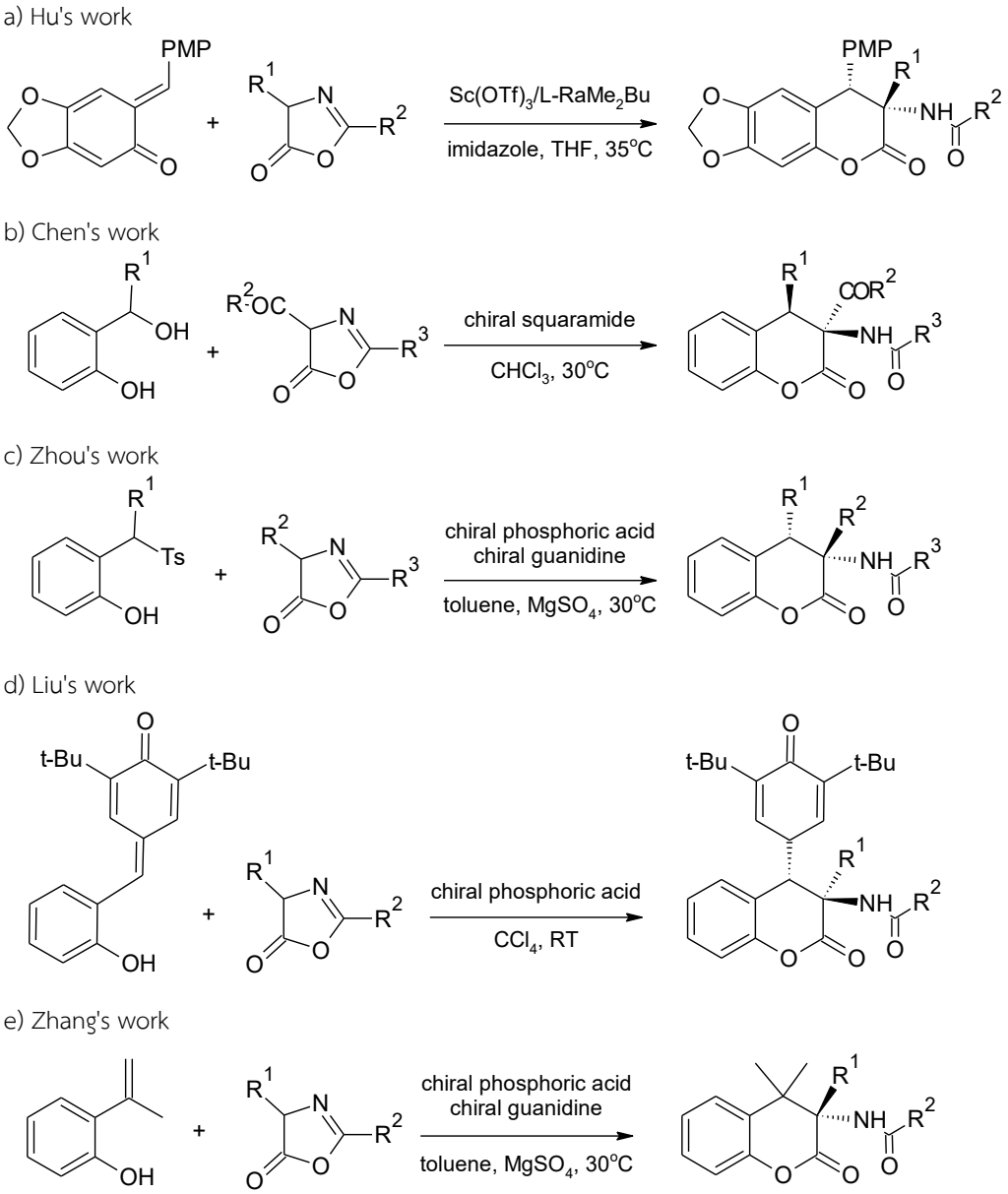

Figure 2.9 The design of asymmetric [4+2] cycloadditions of azlactones with *o*-QMs.

Catalysts play an essensial role in reactant activation, in particular chiral catalysts, which exhibit as key elements contributing to an enantioselective version of reactions including the parent DA cycloadditions. Even though the possible reaction pathways can be identified by experiments [37, 38], they lack a deep explanation of the mechanisms and also enantioselective control that are able to be carried out by the utility of computational chemistry [43].

2.1.5 Enantioselective DA reaction

The enantioselective version of DA reactions has been greatly interested in the synthesis of carbo- and heterocycles with a number of stereogenic centers by the use of chiral catalysts [44]. Catalysts enhance the rate of reaction by decreasing energy pathway via the presence of lower-energy TSs. The goal of enantioeslective catalysis is the generation of one enantiomer over the other by means of asymmetric induction. Many natural products have important biological activity and great potential in fields of medicine. However, these useful compounds difficult to synthesize due to their structural complexity and specific stereochemistry. An apparently small difference in absolute stereochemistry can cause a major effect on the activity, for example, the different behavior of (*S*)- and (*R*)- enantiomers of warfarin in anticoagulant therapy [45]. Therefore, enantiomerically pure compounds have advantage over racemic mixtures, especially in the application of pharmaceuticals, agrochemicals and drugs. For these reasons, it obviously requires enantioselective synthesis for production of a single enantiomer. In the area of enantioselective synthesis, a chiral catalyst plays an important inducing chirality for an achiral precursor into a chiral product via asymmetric transformations, giving one enantiomeric form in larger quantity than the other. A pair of exhibits in biological activities due to its mirror images of each other and hence its difference in three dimensional structures arrangement of atoms.

Among types of catalysts, catalysis using small organic molecules as chiral catalysts, known as organocatalysis, has been emerged for asymmetric reactions coming with a wide range of advantages such as metal-free catalysis and atom-economic process making much attention in asymmetric synthesis [46, 47]. The role of chiral organocatalysts not only accelerate chemical reactions as same as general catalysts, but also potentially participate in stereocontrol for asymmetric transformations along with environmentally friendly procedures, affording only one enantiomeric form. The use of small purely organic molecules as catalysts has become rapidly growing area of asymmetric catalysis and has been focusing on researches because of several advantages of organocatalysts such as nontoxic, low-cost, easy to handle, and stable to oxygen and water which cloud be stored for a long period of time. In addition, their environment-friendly, the absence of transition metals of

organocatalysis and their application for large-scale synthesis seem to be especially attractive for enantioselective processes without metal contamination. Oraganocatalysts have a crucial role for the synthesis of enantiomerically enriched products. Organocatalysts can be classified into four major classes depending on the chemical nature of the catalysts: Lewis base (LB) catalysts, Lewis acid (LA) catalysts, Brønsted acid (BA) catalysts, and Brønsted base (BB) catalysts. In LA and LB catalysis, the catalysis prefer the activation of the catalysts and the substrates to form covalent bond by accepting and donating pair of electrons, respectively. On the other side, BA and BB is conceptually related to (partial) protonation and deprotonation, respectively on catalytic modes. In this work, we focused on chiral Brønsted-acid and chiral Brønsted base catalysts.

2.1.5.1 Chiral phosphoric acid as chiral Brønsted acid catalyst

The fundamental role of LA catalysts is to lower the energy of LUMO and to promote nucleophilic addition to the activation of C-X bonds (X=C, O, N). The combination of a metal-centered Lewis acid with a chiral ligand results in the formation of a chiral LA catalyst and enantioselective versions of the chiral LA catalyzed reaction have been developed. While LA catalysts have been widely used for carbon-carbon bond forming reactions, Brønsted acids using small organic molecules have been mainly employed as catalysts for the formation and cleavage of carbon-oxygen bonds. In comparison to Lewis acids, Brønsted acids are easy to handle, stable in the presence of oxygen and water, and being stored for a long period of time. Although common Brønsted acids are developed to be stronger acids, these achiral acids still perform classic transformations [48]. Chiral Brønsted acids have been emerged as efficient catalysts and become a new class of organocatalysts for a number of enantioselective C-X bond formations along with environmentally friendly procedures.

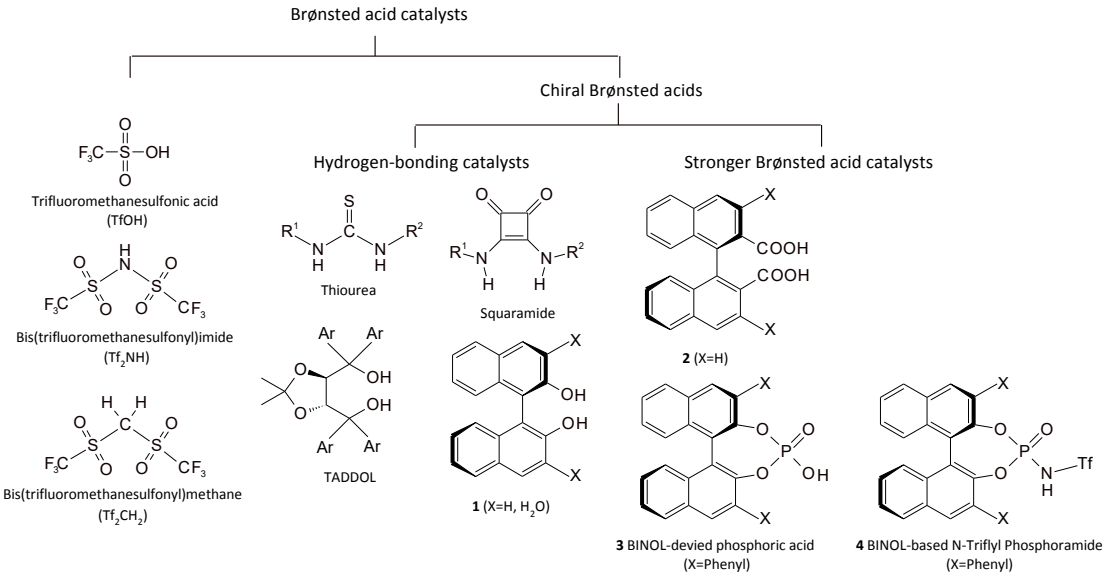

Figure 2.10 Achiral and chiral Brønsted acid catalysts

Chiral Brønsted acids are in general classified into 1) neutral and 2) stronger small organic molecules (Figure 2.10). Neutral Brønsted acids such as thiourea, TADDOL, and squaramide derivatives catalyze a range of organic transformations as hydrogen-bond donors via the formation of hydrogen-bond complex in transition state, whereas stronger Brønsted acids such as 1,1'-bi-2-naphtohol (BINOL) derivatives and phosphoric acids are protonated to form ion-pair transition states.

Since Akiyama [49] and Terada [50] independently accomplished to demonstrate the utility of a chiral phosphoric acid derived from BINOL as a chiral Brønsted acid catalyst in 2004, enantioselective BA catalysis have attracted much attention in the area of asymmetric synthesis. Afterwards, many variations of chiral phosphoric acids (CPAs) have been developed and exhibited excellent catalytic activity of chiral Brønsted acids for a range of CPA-catalyzed reactions through asymmetric transformations. A large number experimental and computational researches have been devoted to study insights into the activity and selectivity of chiral phosphoric acid catalysts. BINOL is an axially chiral molecule having C_2-symmetry that is utilized as a chiral source to create the ring structure. The structural feature of chiral phosphoric acids is based on (*S*)- or (*R*)-BINOL backbone with varying aryl substituents at the 3,3'-positions as a chiral environment in which the influence of steric and

electronic properties of the substituents is highly advantageous for enantioselective transformations.

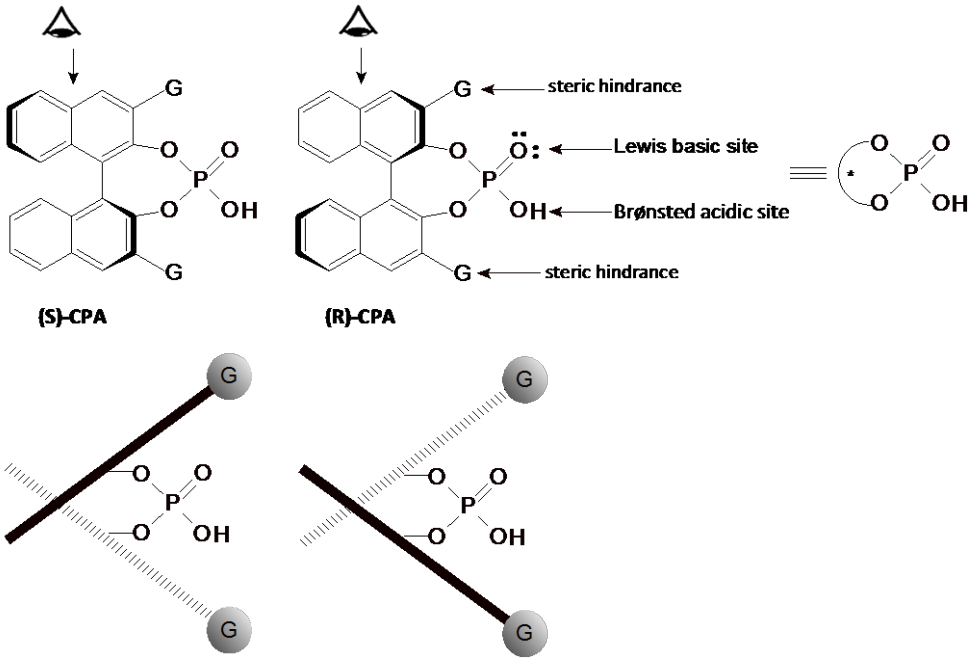

Figure 2.11 *S* and *R* configurations of BINOL-derived axially chiral phosphoric acids.

As researchers reported [51], chiral phosphoric acid derivatives have a bifunctional character consisting of a Brønsted acidic site and a Lewis basic site, allowing distinct activation modes including mono-, dual-, and bifunctional activation, in consequence of plenty of possible catalytic transformations. In cases of reactions involving CPAs, the catalysts functions through diverse interactions with substrates during the key stereoselective step wherein bifunctional activation covers a largest proportion of CPA-catalyzed procedures.

Within the bifunctional catalysis, the acidic and basic sites of the phosphoric acids simultaneously activate both substrates. The acidic proton (P-OH) of the catalyst activates an electrophile while the phosphoryl oxygen (P=O) forms hydrogen bond with a nucleophile. Computational studies on the reaction mechanism and transition structure for CPA-catalyzed reactions suggested that both hydrogen-bonding and ion-

pairing interactions created by the bifunctional catalyst play a crucial role in controlling stereochemical outcomes for achieving high enantioselectivities [52].

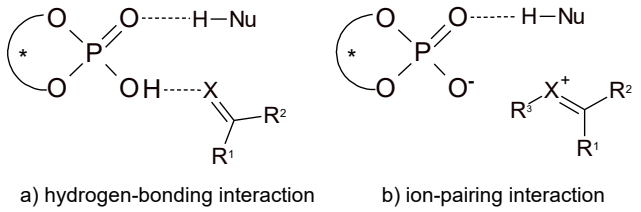

Figure 2.12 Bifunctional activation of CPA catalysis (a) a neutral electrophile and a nucleophile forming hydrogen bond with a catalyst (b) a cationic electrophile forming an ion pair with anionic conjugate bases of a catalyst (X=NR, O, C) [52].

In CPA-catalyzed reactions involving *o*-hydroxystyrenes, Liu and colleges [19] reported the asymmetric allylation reaction of 3-indolylmethanols and the styrene using CPA, leading to production of chiral oxindole with stereogenic center and new C-C bond in high enantioselectivity. They observed that the O-H group in *o*-hydroxystyrene as well as the NH group in the indole are important for generating hydrogen bonds with both basic and acidic sites of CPA, allowing the reactivity and enantioselectivity in the reaction. At the same time, Zhang group [17] presented the first asymmetric formal alkenylation reaction of isoindolo-β-carboline derived hydroxylactam with *o*-hydroxystyrene catalyzed by CPA. The two substrates are activated by the catalyst via ion-pair and hydrogen-bonding interactions. The reaction mechanism was proposed on the basis of the experimental results in which the lactam is protonated in the presence of CPA and thereby generate the corresponding ion and CPA cation. Then, this ionic intermediate and the styrene are activated by the catalyst via the dual action of ion pair and hydrogen bond to undergo enantioselective conjugate addition followed by hydrogen elimination, leading to formation of chiral isoindolo-β-carboline in high enantioselectivity.

The previous mention is well known for CPAs. A large number of asymmetric reaction involving CPA catalysts have been extensively studied in both experimental

and theoretical frameworks in order to explain the activity and stereoselectivity of these catalysts. Although there are experimental evidence base on X-ray diffraction analysis, an increasing number of computational studies has provided a deeper insight into asymmetric reaction catalyzed by CPAs in recent years [53-55] and the key stereocontrolling factors have been carried out.

(1) *Steric environment* around CPAs has been considered as the dominant controlling factor for stereoinduction in asymmetric synthesis in which the presence of the bulky 3 and 3' substituents creates a chiral binding pocket of the catalyst that restricts the orientation of reacting substrates. Models for predicting stereochemical outcomes of reactions has been proposed. The Quadrant projection is the earliest model suggested by Terada group [56] and Himo group [57] wherein the catalyst is viewed along the C_2-symmetric axis as a consequence of the substituents of the CPA occupying two of four quadrants and the substrates positioning in the empty quadrants (Figure 2.13). After that Goodman *et al.* [58] observed the catalyst across the C_2 axis, known as the Goodman projection, resulting in the phosphoryl group lying above and below the plane of the paper and having the substituents on different sides.

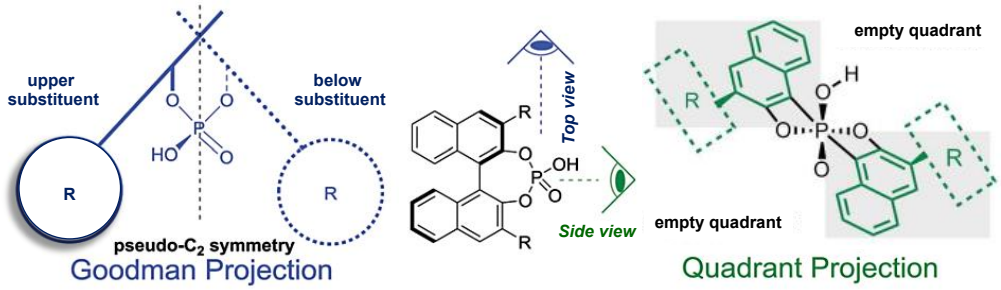

Figure 2.13 Goodman's and Quadrant representation of CPA catalyst.

(2) *Non-covalent interactions* have been shown to play a vital role for the attribution of stereoselectivity. The presence of aryl groups as well as chiral electrostatic environment of CPA can lead to stabilizing non-covalent interactions between substrates and the catalyst in the stereocontrolling TS.

These interactions include CH···O, CH···π, C=O···H, π-stacking, lone-pair···π, and also electrostatic interactions. An imbalance of multiple favorable interactions arises the difference in free energy between competing enantiomeric forms that yields a major and a minor product.

(3) *Acidity of CPA catalyst* pK_a has also proved the effect on reaction activity and stereoselectivity of asymmetric catalytic reactions. One way to understand these effects is to measure the pK_a values of CPAs and their derivatives as well as correlate a catalyst's acidity with the reactivity. Despite the difficulty of determining the acidity values by experimental methods, the pK_a's of parent phosphoric acids can be achieved by DFT-based predictions and the relationship between the structure and acidity are offered as a plausible clue to predict the trends in acidity for all related acids.

In CPA catalysis, activation occurs by lowering the substrate LUMO energy through either protonation state or hydrogen bonding of the catalyst. With computational studies, various activation modes of CPAs have been concluded [55]in which traditional LUMO lowering strategy occurs via dual and bifunctional activation that normally involves two points of contact.

2.1.5.2 Chiral bicyclic guanidine as chiral Brønsted base

In organic synthesis, Brønsted bases are alternative catalytic species for C-X bond formations by accepting a proton. Due to the absence of inducing stereoselectivity from these general base catalysts in contrary to a rapidly growing area of asymmetric synthesis, chiral Brønsted bases have been developed for promoting enantioselectivity in a number of reactions through asymmetric transformations [59]. The core structure of chiral base catalysts is typically based on nitrogen-containing functionalities such as tertiary amines, amidines, and guanidines. Among these, a guanidine consisting of three nitrogen atoms is classified as an organic superbase. A resonance stabilized guanidinium cation naturally forms when nitrogen's lone pair abstracts a proton from substrate or pro-nucleophile (NuH), which allows for double hydrogen bonding. Guanidine derivatives have been extensively explored as promoters for stereoselective reactions, for example, conjugate addition and Michael reactions. Especially, chiral bicyclic

guanidines have been shown to be efficient catalysts in a series of enantioselective transformations.

The utility of chiral bicyclic guanidines and has received much attention in delivering high levels of enantioselectivity [60, 61]. Among distinctive structural features of bicyclic guanidines, chiral [5,5]-bicyclic guanidine catalyst (1,4,6-Triaza-Bicyclo[3.3.0]-Oct-4-ene ; TBO), which is constructed as a fusion of two five-membered rings, will be examined in this study. Furthermore, the substitution of two *tert*-butyl (*t*-Bu) groups is added into the core TBO skeleton that leads to asymmetric structure with distinct top and bottom faces.

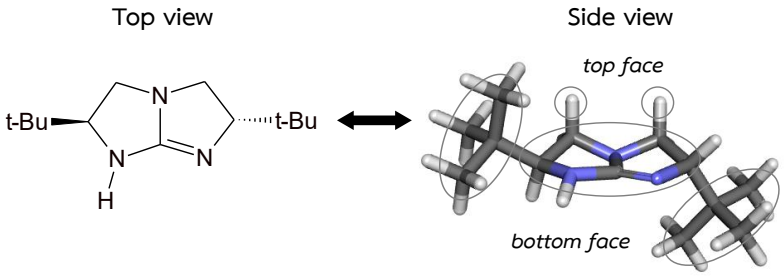

Figure 2.14 Chiral [5,5]-bicyclic guanidine substituted by *t*-butyl groups and its geometry optimized at the M06-2X/6-31G* level.

In a study of TBO catalytic mechanism, a proton transfer from the substrate to the neutral guanidine give the hydrogen-bonded complex between the guanidinium cation and the nucleophilic anion. This ion-pair complex is more stable than the neutral complex [62, 63]. The guanidinium ion can either activate the substrate via hydrogen-bonding interactions in a monofunctional or a bifunctional mode (Figure 2.14). In monofunctional activation mode, the protonated TBO interacts with a single substrate through dual hydrogen bonding. On the other hand, the bifunctionality of the guanidinium catalyst can activate both a nucleophile and an electrophile simultaneously. As revealed by computational studies [63, 64], there are two bifunctional activation modes of the bicyclic guanidinium catalyst, namely Brønsted acid and Brønsted-Lewis acid. In the bifunctional activation mode as Brønsted acid, the two guanidinium N-H protons form double hydrogen bonds with both substrates.

Whereas, in the mode of the Lewis and Brønsted acid activations, both N-H protons form dual hydrogen bonds with an electrophile while the central electrophilic carbon served as a Lewis acid on the guanidinium group is likely to interact with a nucleophile (Lewis base). However, if steric repulsion takes place in the interaction of a bulky nucleophile with the Lewis acidic central carbon via substituents on the catalyst, the other electrophile-nucleophilie arrangement in which the electrophile will interact with the central carbon instead of the nucleophile is possible.

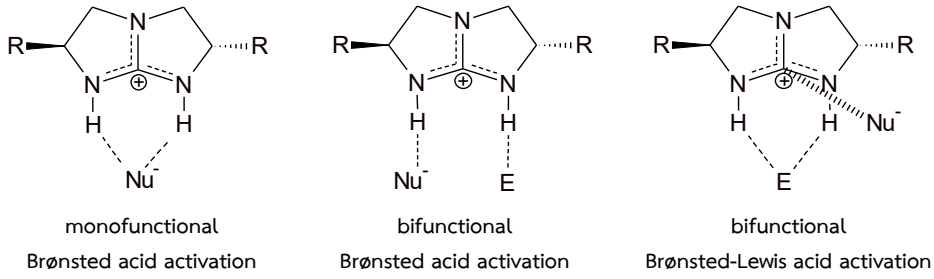

Figure 2.15 Schematic representation of plausible mono- and bifunctional activation modes of bicyclic guanidinium catalyst (R = Ph, t-Bu).

Furthermore, two types of catalyst-substrate complexes in the TS according to their geometries, namely face-on and side-on have been proposed. The face-on TS corresponds to the bifunctional Brønsted acid activation, whereas the side-on TS correlates with the Brønsted-Lewis acid activation. Based on calculated activation free energies, the side-on ternary complex TS is strongly preferred over the corresponding face-on TS due to stronger hydrogen bonding stabilization [62]. This indicates that the strength of hydrogen bond interactions plays an important role for stabilizing the TS structure as well as types of non-covalent interactions is a key factor for controlling the reactivity and the stereoselectivity including two competing enantiomeric TSs (*S*- and *R*-inducing TSs) [63].

It was reported that Brønsted acid activation based side-on TSs is more energetically favorable than the monofunctional binding mode due to stabilization of the stronger interactions of two N-H protons with the oxygen atom of dienolate and

especially with the lone pair of nitrogen atom on the diazocarboxylate (NH···N = 1.79 Å in TS).

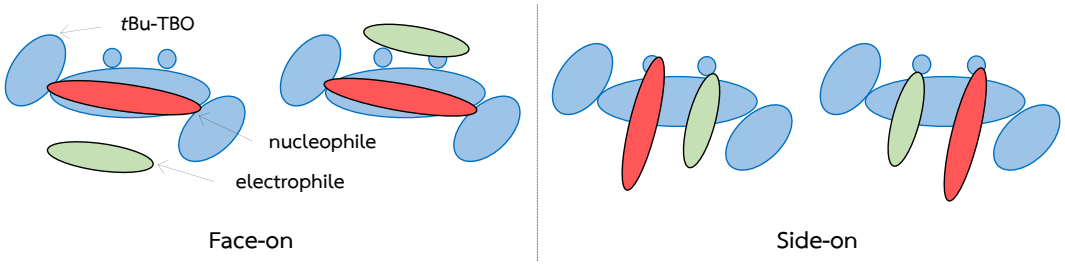

Figure 2.16 Face-on and side-on ternary complexes.

As reported by Wong and Ng [63], the ternary complexes are stable with respect to the ion-pair complex and play an important role in stabilizing the pre-TS complex and governing enantioselectivity. They found that the bifunctional Brønsted acid activation in which the two guanidinium N-H protons form hydrogen bonds with cyclopentenone and malonate ion simultaneously, is energetically more favorable due to forming the strongest hydrogen-bonding interactions.

The bicyclic guanidines have a bifunctional character bearing both a Brønsted acidic and a Brønsted basic sites in which the nitrogen base of the catalyst abstract a proton from pro-nucleophile (Nu-H) while the acidic N-H proton function as a hydrogen bond donor.

2.2 Example of oxygenous cyclic framework

Dihydrocoumarin scaffold (DHC) belongs to a privileged structural motif in numerous natural products [65-67] and pharmaceutically active molecules exhibiting a broad range of biological activities by distinct structural features of DHC derivatives as shown in Figure 2.17, for example, antimicrobial activity [68, 69], antioxidant activity [70, 71], antitumor activity [71], anti-inflammatory activity [72, 73], and histone deacetylase inhibitor [74, 75]. In addition, DHC is added as flavoring agent in foods [76] and as a fragrance ingredient in cosmetics [77, 78]. Owing to these diverse advantages, the development of efficient methodologies have received much attention for the

enantioselective synthesis of the purely DHC framework. Moreover, these oxygen-containing heterocycles can used as a platform for accessing diversity as well as complexity of molecules in a number of reactions.

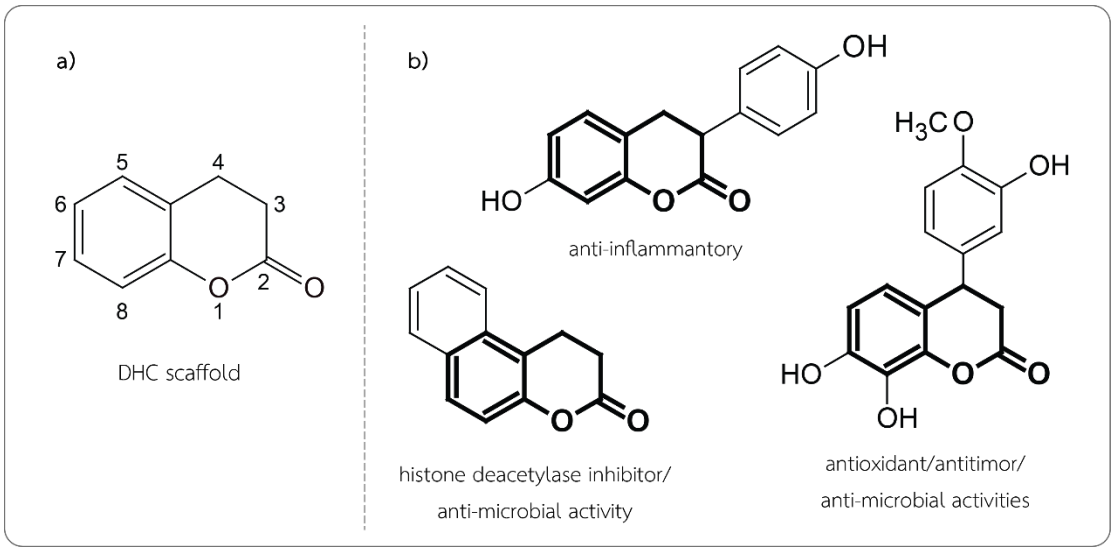

Figure 2.17 The structure of DHC and examples of their biologically active molecules.

2.3 Computational chemistry

Computational chemistry techniques is very useful for chemists such as reducing the scope of experiments, explaining observed phenomena, and predicting the results of future experiments as well as providing insight into properties of a molecule such as molecular bonding that cannot be obtained by experimental methods, to completely understand a chemical process.

2.3.1 Quantum Mechanics

Any molecular structure and dynamics can be modeled by Molecular Mechanics (MM) method based on classical mechanics. However, this method does not treat the electrons in a system due to the limitations of molecular size that are important for accurate energies and chemical reactions involving making and breaking bonds, which are directly dependent on the electron density. As a consequence, quantum mechanics (QM), which gives a mathematic description of the behavior of electrons,

has been chosen and the basic mathematical formulation of QM simulations starts with the time-independent and non-relativistic Schrödinger equation given by

$$\hat{H}\Psi(\mathrm{R},\mathrm{r}) = E\Psi(\mathrm{R},\mathrm{r})$$

This form is an eigenvalue equation in which Ψ and E are called the eigenfunction and eigenvalue, respectively. $\Psi(\mathrm{R},\mathrm{r})$ is a function of the electron r and nuclear R positions, called a wave function. $\hat{H}$ is the Hamiltonian operator for an interested system consisting of n electrons and N nuclei and E is the corresponding energy of the system. The operator $\hat{H}$ representing the total energy can be written as

$$\hat{H} = -\sum_{i=1}^{n}\frac{1}{2}\nabla_i^2 - \sum_{A=1}^{N}\frac{1}{2M_A}\nabla_A^2 - \sum_{i=1}^{n}\sum_{A=1}^{N}\frac{Z_A}{r_{iA}} + \sum_{i=1}^{n}\sum_{j<i}^{n}\frac{1}{r_{ij}} + \sum_{A=1}^{N}\sum_{B<A}^{N}\frac{Z_A Z_B}{R_{AB}} \quad (2.1)$$

Here, the subscripts A and B refer to the individual nuclei and M is the mass of each nucleus, while the subscripts i and j refer to the individual electrons. Z is the nuclear charge. R_{AB}, r_{iA}, and r_{ij} are the distances between nuclei A and B, electron i and nucleus A, and electrons i and j, respectively.

Where ∇^2 is the Laplacian operator of a particle;

$$\nabla^2 = \frac{\partial^2}{\partial x^2} + \frac{\partial^2}{\partial y^2} + \frac{\partial^2}{\partial z^2} \quad (2.2)$$

Equation 2.2 can be represented as

$$\hat{H} = \hat{T}_e(r) + \hat{T}_N(R) + \hat{V}_{eN}(r,R) + \hat{V}_{ee}(r) + \hat{V}_{NN}(R) \quad (2.3)$$

Here, the first two terms of the Hamiltonian operator is the kinetic energy of electrons ($\hat{T}_e$) and nuclei ($\hat{T}_N$), respectively, and the remaining three terms are the potential energies that account for the electrostatic attraction between electrons and nuclei ($\hat{V}_{eN}$), the repulsion between electrons ($\hat{V}_{ee}$), and between nuclei ($\hat{V}_{NN}$),

respectively. After the wave function has been defined by solving the Schrödinger equation, any systematic property can be determined by taking the expectation value of the operator for an interested property, for example, energy E given by

$$\langle E \rangle = \int \Psi^* \hat{H} \Psi \tag{2.4}$$

Nevertheless, the Schrödinger equation cannot be solved exactly in common due to the mathematical difficulties of systems with more than one electron. Thus, a number of approximations are required.

2.3.2 The Born-Oppenheimer approximation

The Born-Oppenheimer approximation (BOA) is the most fundamental approximation and is firstly used to simplify the calculations under the assumption that the motion of electrons and nuclei are independent because nuclei are much heavier than electrons and consequently electrons move much faster than nuclei. Therefore, in the BOA, electrons are considered as moving in the field of fixed nuclei, it results that the kinetic energy of nuclei can be abandoned and the repulsive potential due to the nuclear-nuclear interactions can be considered as a constant. At this point, the Hamiltonian operator in equation 2.3 can be rewritten as in the following

$$\hat{H} = \hat{T}_e(r) + \hat{V}_{eN}(r, R) + \hat{V}_{ee}(r) + \hat{V}_{NN}(R) \tag{2.5}$$

Due to this approximation, the wave function depends only on the nuclear positions but not on the nuclear movement and thus the full wave function can be considered as the combination of the contributions of electrons and nuclei.

$$\Psi(R, r) = \Psi_e(R, r)\Psi_N(R,) \tag{2.6}$$

Here, Ψ_e is the electronic wave function and Ψ_N is the nuclear wave function. R and r denote the coordinates of nuclei and electrons, respectively. Hence, for each nuclear position, the Schrödinger equation can be solved in order to obtain the energy

that is contributed by electrons. The electronic Schrödinger equation by applying the BOA is

$$\hat{H}_e \Psi_e(R,r) = E_e \Psi_e(R,r) \tag{2.7}$$

Where $\hat{H}_e$ is the so-called electronic Hamiltonian operator describing the motion of n electrons in the field of N nuclei

$$\hat{H}_e = \hat{T}_e(r) + \hat{V}_{eN}(r,R) + \hat{V}_{ee}(r) \tag{2.8}$$

After that the resulting electronic energy must include the constant nucleus-nucleus repulsion term in order to obtain the final total energy for a stationary nuclei system.

$$E_{total} = E_e(R) + \hat{V}_{NN}(R) \tag{2.9}$$

2.3.3 Electronic spatial and spin orbitals

According to the BOA, both wave function and the electronic Hamiltonian operator in equation 2.7 are considered only the electronic contribution part, but they depends only on the spatial coordinates of electrons. Therefore, it is necessary to specify the electronic spin in order to completely describe an electron. The spin of an electron has two possible states: spin up and spin down, and their corresponding spin functions of spin variable ω are denoted by $\alpha(\omega)$ and $\beta(\omega)$, respectively, that are orthonormal according to the following equations

$$\int \alpha^*(\omega)\alpha(\omega)d\omega = \int \beta^*(\omega)\beta(\omega)d\omega = 1 \tag{2.10}$$

$$\int \alpha^*(\omega)\beta(\omega)d\omega = \int \beta^*(\omega)\alpha(\omega)d\omega = 0 \tag{2.11}$$

Both equations 2.10 and 2.11 can be rewritten by using the bra-ket notation as in the following

$$\langle\alpha|\alpha\rangle = \langle\beta|\beta\rangle = 1 \tag{2.12}$$

$$\langle\alpha|\beta\rangle = \langle\beta|\alpha\rangle = 0 \tag{2.13}$$

Consequently, the complete explanation of an electron contains three spatial coordinates x, y, z collected in the index r and one spin coordinate ω. These four coordinates can be represented as $\mathrm{x} = \{r, \omega\}$ and the wave function expressing both spatial and spin coordinates for one electron is called a spin orbital $\phi(\mathrm{x})$. Therefore, multiplying one spatial orbital $\psi(r)$ by both spin up $\alpha(\omega)$ and spin down $\beta(\omega)$ can give two possible spin orbitals.

$$\phi(\mathrm{x}) = \begin{cases} \psi(r)\alpha(\omega) \\ or \\ \psi(r)\beta(\omega) \end{cases} \tag{2.14}$$

The electronic wave function of a system containing n electrons can be written in a function of $\mathrm{x}_1, \mathrm{x}_2, \mathrm{x}_3, \ldots, \mathrm{x}_n$ as $\phi(\mathrm{x}_1, \mathrm{x}_2, \mathrm{x}_3, \ldots, \mathrm{x}_n)$. The additional requirement on a wave function to satisfy Pauli exclusion principle is that an n-electron wave function has to be antisymmetric with respect to the interchange of the coordinates x of any two electrons.

$$\phi(\mathrm{x}_1, \mathrm{x}_2, \mathrm{x}_3, \ldots, \mathrm{x}_n) = -\phi(\mathrm{x}_2, \mathrm{x}_1, \mathrm{x}_3, \ldots, \mathrm{x}_n) \tag{2.15}$$

2.3.4 Hartree products

To describe an electronic wave function for a system of n electrons, one simple approximation that considers all electrons in the system are independent is applied. In the case of non-interacting electrons in which each electron i occupies in each specific spin orbital, the Hamiltonian operator of a system can be expressed as a sum of each electronic Hamiltonian operator excluding an electron-electron repulsion term as presented in equation 2.16.

$$\widehat{H} = \sum_{i=1}^{n} h\,(i) \tag{2.16}$$

Where $h(i)$ is one-electron Hamiltonian operator containing both kinetic and potential energies of electron i. The eigenfunctions corresponding to the operator $h(i)$ are the spin orbitals, and hence the eigenvalue equation is

$$h(i)\phi_j(\mathrm{x}_i) = \epsilon_i\phi_j(\mathrm{x}_i) \tag{2.17}$$

When assuming each electron i moving in an individual orbital, the n-electron wave function Ψ^{HP}, namely a Hartree product, can be inscribed as a product of one-electron wave functions or of spin orbitals of each electron $\phi_j(\mathrm{x}_i)$.

$$\Psi^{HP}(\mathrm{x}_1, \mathrm{x}_2, \mathrm{x}_3, \ldots, x_n) = \phi_i(\mathrm{x}_1)\phi_j(\mathrm{x}_2)\phi_k(\mathrm{x}_3)\ldots\phi_l(\mathrm{x}_n) \tag{2.18}$$

The total energy can be determined from a sum of all spin orbital energies ϵ_i.

$$E = \epsilon_i + \epsilon_j + \epsilon_k + \cdots + \epsilon_n \tag{2.19}$$

Nevertheless, this independent electron approximation called Hartree approximation, does not explain an electron correlation due to the Hartree product violating the antisymmetric principle. The appropriate method in order to obtain correctly antisymmetric wave function is using Slater determinant.

2.3.5 The Slater determinant

To achieve a more accurate solution to the electronic Schrödinger equation, the antisymmetric wave function of n-electron system can be made by constructing the Slater determinant as presented in equation 2.16.

$$\Psi(\mathrm{x}_1,\mathrm{x}_2,\mathrm{x}_3,\ldots,\mathrm{x}_n)=\frac{1}{\sqrt{n!}}\begin{vmatrix}\phi_1(\mathrm{x}_1) & \phi_2(\mathrm{x}_1) & \cdots & \phi_n(\mathrm{x}_1)\\ \phi_1(\mathrm{x}_2) & \phi_2(\mathrm{x}_2) & \cdots & \phi_n(\mathrm{x}_2)\\ \vdots & \vdots & \ddots & \vdots\\ \phi_1(\mathrm{x}_n) & \phi_2(\mathrm{x}_n) & \cdots & \phi_n(\mathrm{x}_n)\end{vmatrix}\begin{matrix}\downarrow \text{ electrons}\\ \\ \\ \\ \xrightarrow[\text{orbitals}]{}\end{matrix} \tag{2.16}$$

Where $\frac{1}{\sqrt{n!}}$ is the normalization factor and $\phi_i(\mathrm{x}_i)$ are orthonormal spin orbitals. The rows and columns of an n-electron Slater determinant are labeled by electrons and spin orbitals, respectively. Each row refers to the distribution of each electron in n spin orbitals, while each column shows the contribution of n electrons in each spin orbital. Equation 2.16 can be written by using short-hand notation. If swap two rows of the determinant relating to an exchange of a pair of one-electron coordinates, the sign of the determinant changes.

$$\frac{1}{\sqrt{n!}}\begin{vmatrix}\phi_1(\mathrm{x}_{\mathbf{1}}) & \phi_2(\mathrm{x}_{\mathbf{1}}) & \cdots & \phi_n(\mathrm{x}_{\mathbf{1}})\\ \phi_1(\mathrm{x}_{\mathbf{2}}) & \phi_2(\mathrm{x}_{\mathbf{2}}) & \cdots & \phi_n(\mathrm{x}_{\mathbf{2}})\\ \vdots & \vdots & \ddots & \vdots\\ \phi_1(\mathrm{x}_n) & \phi_2(\mathrm{x}_n) & \cdots & \phi_n(\mathrm{x}_n)\end{vmatrix}=-\frac{1}{\sqrt{n!}}\begin{vmatrix}\phi_1(\mathrm{x}_{\mathbf{2}}) & \phi_2(\mathrm{x}_{\mathbf{2}}) & \cdots & \phi_n(\mathrm{x}_{\mathbf{2}})\\ \phi_1(\mathrm{x}_{\mathbf{1}}) & \phi_2(\mathrm{x}_{\mathbf{1}}) & \cdots & \phi_n(\mathrm{x}_{\mathbf{1}})\\ \vdots & \vdots & \ddots & \vdots\\ \phi_1(\mathrm{x}_n) & \phi_2(\mathrm{x}_n) & \cdots & \phi_n(\mathrm{x}_n)\end{vmatrix} \tag{2.17}$$

This mathematical property makes wave function corresponding to the antisymmetric principle. If any two columns are identical meaning two electrons in a system occupying in the same spin orbital, the determinant is zero.

$$\frac{1}{\sqrt{n!}}\begin{vmatrix}\phi_{\mathbf{1}}(\mathrm{x}_1) & \phi_{\mathbf{1}}(\mathrm{x}_1) & \cdots & \phi_n(\mathrm{x}_1)\\ \phi_{\mathbf{1}}(\mathrm{x}_2) & \phi_{\mathbf{1}}(\mathrm{x}_2) & \cdots & \phi_n(\mathrm{x}_2)\\ \vdots & \vdots & \ddots & \vdots\\ \phi_{\mathbf{1}}(\mathrm{x}_n) & \phi_{\mathbf{1}}(\mathrm{x}_n) & \cdots & \phi_n(\mathrm{x}_n)\end{vmatrix}=0 \tag{2.18}$$

This property satisfy the Pauli exclusion principle, which states that no two electrons have the same four quantum numbers. The normalized antisymmetric wave function of an n-electron system in equation 2.16 can be shortened in the ket notation as in the following

$$\Psi(\mathrm{x}_1,\mathrm{x}_2,\mathrm{x}_3,\ldots,\mathrm{x}_n)=|\phi_1\phi_2\phi_3\ldots\phi_n\rangle \tag{2.19}$$

As equation 2.17, if electrons i and j interchange their coordinates, it can be written as

$$|\phi_1, \dots, \phi_i, \dots, \phi_j, \dots, \phi_n\rangle = -|\phi_1, \dots, \phi_j, \dots, \phi_i, \dots, \phi_n\rangle \quad (2.20)$$

2.3.6 The Hartree-Fock theory

An improvement on the Hartree approximation known as the Hartree-Fock theory is the starting point for treatments of the electron correlation by using the Slater determinant, which incorporates exchange correlation. An antisymmetric wave function is represented using the Slater determinant of one-electron wave function. Additionally, this approximation connect to the variational principle, which states that the energy corresponding to a trial wave function Ψ_{trial} is an upper bound to the exact ground-state energy E_0.

$$E = \frac{\langle \Psi_{trial} | \hat{H} | \Psi_{trial} \rangle}{\langle \Psi_{trial} | \Psi_{trial} \rangle} \geq E_0 \quad (2.21)$$

Where $\langle \Psi_{trial} | \Psi_{trial} \rangle$ is normalized as equal to 1. In the Hartree-fock theory, each electron is considered as moving independently in an average field of the other electrons. Thus, the potential energy due to the electron-electron interaction is given as

$$V^{eff} = \sum_{j}^{n} \int \phi_j^*(r_2)\phi_j(r_2)\frac{1}{r_{12}}dr_2 - \int \phi_j^*(r_2)\phi_j(r_1)\frac{1}{r_{12}}\phi_i(r_2)dr_2 \quad (2.22)$$

Here, V^{eff} is called the effective potential. The first term represents the Coulomb repulsion in an average distance between two electrons at position r_1 and r_2 in the same spin orbital ϕ_j and the second term accounts for the exchange potential arising from the antisymmetry of the wave function. According to the variational principle, it has to find the best Slater determinant in order to obtain the

lowest possible energy by varying a set of spin orbitals. The Hartree-Fock equation is derived to determine the optimal spin orbital as presented in the following equation

$$\hat{f}_i \phi_i = \epsilon_i \phi_i \tag{2.23}$$

Where $\hat{f}$ is an effective Hamiltonian operator for one electron, called the Fock operator, and can be expressed as

$$\hat{f}_i = -\frac{1}{2}\nabla_i^2 - \sum_A^N \frac{Z_A}{r_{iA}} + V_i^{eff}(i) \tag{2.24}$$

In self-consistent field method, an initial set of spin orbitals for one electron is guessed. Then, this one-electron function is used to determine the average potential in equation 2.22. After that, the Hartree-Fock equation 2.23 can be solved in order to produce a new set of spin orbitals. These new spin orbitals are used to obtained an improved average potential. This cyclic process is repeated until the input and output spin orbitals are close enough or self-consistency. The resulting orbitals from this procedure are called Hartree-Fock spin orbitals. The obtained eigenvalues ϵ_i are called orbital energies.

In conclusion, the molecular orbitals and their related total energy can be determined by the representation of the molecular orbitals as the linear combinations of atomic orbitals (LCAO-MO). Then the coefficients in the linear combinations are evaluated by self-consistent field calculation (LCAO-MO-SCF) until convergence. Each atomic orbital is defined by using basis sets.

2.3.7 Basis sets

Basis sets is a set of atomic orbitals used to construct LCAO-MO to determine the molecular orbital in which atomic orbitals are represented as basis functions. There are two types of basis set commonly used in electronic structure calculations that are Slater-type orbitals (STO) and Gaussian-type orbitals (GTO).

2.3.7.1 Slater and Gaussian type orbitals

The formulation of spin orbitals can be reduced by replacing with spatial function that provide identical results by using both spatial orbital and spin function. Basis sets for Quantum chemical calculation, STOs are primarily used for atomic and diatomic systems with high accuracy requirements. Consider the radial function, the radial part of STO is an exponentially decaying function depending on increasing distance between an electron and the nuclear center, defined as

$$\mathcal{X}^{STO}(r) = Ne^{-\varsigma r} \tag{2.25}$$

Where r is the electron-nuclear distance, ς is the orbital exponent, and N is a normalization constant. In order to correctly determine the electronic wave function and the corresponding energy, the number of STOs on each nucleus and the orbital exponent of each STO has been chosen. The large number of STOs and the greater selecting of the orbital exponent will provide the more accurate final wave function and the obtained energy. However, the three- and four-center integrals or multicenter integrals are complicated to evaluate with computationally time-consuming. Then, an alternative GTO basis set is suggested for the problem of integral evaluation in which the Gaussian radial form is given by

$$\mathcal{X}^{GTO}(r) = Ne^{-\varsigma r^2} \tag{2.26}$$

The multicenter integrals are easy to accurately evaluate with Gaussian basis functions rather than STOs. However, at the nucleus, an exponential function of GTOs lacks the cusp behavior describing electrons near the nucleus (the core electrons) and its behavior at large distance is also differ from STOs. A GTO with zero slope does not represent the proper behavior of the exact molecular wave function near the nucleus, otherwise a STO has a cusp for describing the electron density at the nucleus.

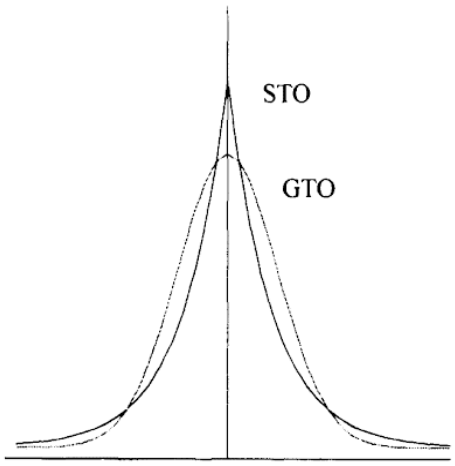

Figure 2.18 Comparison of Slater and Gaussian Basis Functions for 1S orbital.

Therefore, a larger basis set is needed to approach the quality of a Slater function, which are more correctly describe the qualitative features of the molecular orbitals, a STO can be approximated by a linear combination of GTOs. This combined functional form is called contracted GTO (CGTO).

$$\mathcal{X}^{STO}(r) \approx \mathcal{X}^{CGTO} = \sum_{i=1}^{k} a_i \mathcal{X}_i^{PGTO} \qquad (2.27)$$

Where a_i is the contraction coefficient. The individual Gaussian functions contributing to these contractions used to construct CGTO are referred to as primitive Gaussian type orbitals (PGTOs). In order to improve the accuracy of calculations, a number of PGTOs with different exponents are necessary to give a reasonable STO, allowing an improved representation of electron density close to the nucleus that are designated as the STO-nG.

2.3.7.2 Minimal Basis Sets

As mention previously, the used number of function is an important factor for calculations. The common minimal basis set is STO-kG that means the k number of primitive GTOs used to represent a single STO. The exponent and expansion coefficient are obtained by a fitting procedure to a STO or optimizing an atomic energy. The most

widely used smallest basis set is STO-3G. Consider STO-3G basis set for a carbon atom consisting of 1s, 2s, $2p_x$, $2p_y$, and $2p_z$ orbitals, each orbital is approximated as linear combination of three PGTOs and thus the carbon atom are built from 15 primitive functions.

2.3.7.3 Split Valence and Polarization Basis Sets

A single basis function for a minimal basis set, one basis function is used for each atomic orbital, known as a Single Zeta (SZ) basis set. Since each constituent atoms in a molecule is lower symmetric than isolated atoms, making the change of atomic orbital shapes, it is important to use orbitals with need more flexible shape for better explanation of molecular systems. At the SZ level, all of approximated orbitals are obtained in rough results that are insufficient for explanation. Therefore, increasing the number of functions allow the basis set for more accurate representation of atomic orbitals. Each atomic orbital is doubled its set of basis function, this basis set is called Double Zeta (DZ). For example, a DZ for a carbon atom consists of a total of 10 orbitals, including two 1s orbitals (1s and 1s'), two 2s orbitals (2s and 2s'), and six 2p orbitals ($2p_x$, $2p_y$, $2p_z$, $2p'_x$, $2p'_y$, and $2p'_z$). However, using the DZ basis for every orbital takes expensive computational cost.

The fact that the core electrons of an atom are less affected by chemical environment than the valence electrons. In particular, bond formation occur between valence orbitals. Thus, the core orbital is adequately described by a single basis function, while the DZ basis doubles only the number of valence orbitals. The valence orbital is split into two parts : an inner (compact orbital) and an outer (diffuse orbital) that are represented by two basis functions. This method is called a split valence basis set and its N-MPG notation is used. Here, N is represented the number of PGTOs for describing the inner (core) orbitals. After the hyphen, the two values indicate that the valence orbital consists of the two functions in which M and P are the numbers of PGTOs used to express the valence and the split valence set of Slater orbitals, respectively.

If consider a carbon atom in the 3-21G basis set, the 1s (core orbital) is represented by one contraction of three PGTOs. The two values after the hyphen indicate that both 2s and 2p orbitals (valences) are each described by two STOs.

Regarding the number 2 and 1, each valence orbitals (2s, $2p_x$, $2p_y$, and $2p_z$) is represented by a summation of two PGTOs and each split valence orbital (2s', $2p'_x$, $2p'_y$, and $2p'_z$) is represented by a single uncontracted PGTO, respectively. As a result, a split valence DZ for a carbon atom consists of a total of 9 basis functions.

To increase quality of the basis set is that consider transformation of orbital shapes. In a molecular formation involving bond forming, atoms are closer together and then their electron distribution create a polarization effect that distort the atomic orbitals from their normal shapes. At this point, a basis function for better describing distortion or polarization of an electron density is added to the basis set, called polarization function. The addition of this basis function with a higher angular momentum quantum number is used to modify the atomic orbital shape.

The next step to improve quality of the basis set is adding a basis function for describing distortion or polarization of an electron density caused by entering atoms to a molecule, called polarization function. This basis provide flexibility to orbital shape by using basis function with a higher angular momentum quantum number. For example, the distorted spherical 1s orbital of hydrogen atom takes into account 2p orbital. By mixing two opposite signs of p orbital lobes and one sign of s orbital lobe, the s orbital will shift to one side of the equal sign while the opposite sign decrease the other side of the s orbital. In the same way, 2p orbital can be polarized in one direction by adding 3d orbital. The asterisk (*) notation is used for the polarization basis set that means the 3d orbital used for adding to the 2p atomic orbital of a second row element in the periodic table. For example, the 6-31G* is the 6-31G basis set with d orbitals functions for the second row atom and also written as 6-31G(d). Consequently, a chemical bond involving 2p orbital can be explained by an asymmetric shape of electron density along the bonds. When atoms enter a molecule, an electron density the atomic orbitals are distorted or polarized in their electron density. At this point, is added to the basis set, called that changes the atomic orbital shape.

2.3.8 Density Functional Theory

To solve the correlation error in the total energy due to treatment of the electron-electron interactions in an average way in the Hartree-Fock approximation, Density

Functional Theory (DFT) is introduced. The basic idea of DFT is to determine electron density rather than the complicated n-electron wave function. Compared to the wave function, the electron density depends only on three spatial variables (x, y, z ; r). The electron correlation energy is the difference between the exact ground-state energy and the Hartree-Fock energy. The two Hohenberg-Kohn theorems are the fundamentals of DFT in which the first theorem states that all the systematic properties are uniquely determined using a functional of electron density and the second theorem states the minimum of the total energy functional that delivers the ground-state energy of a system is obtained using the exact ground-state density by applying the variational principle. The expectation value for the total electronic energy can be expressed in terms of the electron density $\rho(r)$ as in the following

$$E_0 \geq E_e[\rho(r)] = T_e[\rho(r)] + V_{ee}[\rho(r)] + V_{eN}[\rho(r)] \qquad (2.28)$$

However, the explicit density functional forms of both the kinetic and exchange-correlation terms remain unknown. Then, the Kohn-Sham scheme is introduced based on the idea of a reference system of non-interacting electrons. The energy functional of a system can be defined as

$$E_e[\rho(r)] = T_s[\rho(r)] + J[\rho(r)] + V_{eN}[\rho(r)] + E_{XC}[\rho(r)] \qquad (2.29)$$

Where $T_S[\rho]$ is the kinetic energy functional of the non-interacting reference system in which S denotes that the kinetic energy is obtained from the Slater determinant, $J[\rho]$ is the functional for the Coulomb part due to the electron-electron repulsion, $V_{eN}[\rho]$ is the electron–nuclear attraction functional, and $E_{XC}[\rho]$ is the exchange-correlation functional accounting for the kinetic and Coulomb correlation energies that are the difference in that energy contributions between the fictitious system of non-interacting electrons and the real interacting system as well as the exchange energy due to the antisymmetry requirement is also included in this functional as shown in equation 2.30.

$$E_{XC}[\rho] = (T[\rho] - T_s[\rho]) + (V_{ee}[\rho] - J[\rho]) \qquad (2.30)$$

Here, the first two terms collect the difference between kinetic energies of the real interacting and fictitious non-interacting electrons and the last two terms collect the difference between the full electron-electron interaction energy and the classic Coulomb energy equal to Hartree energy. In fact to relate the wave function to the electron density, the electron density is the probability to find an electron with spin in a volume element d^3r at the position r defined in terms of the wave function as the sum of the square of occupied spin orbitals.

$$\rho(r) = \sum_{i=1}^{n} \left|\phi_i^{KS}(r)\right|^2 \tag{2.31}$$

In order to find the ground-state density of a system, the Kohn-Sham equation is derived as in the following

$$\hat{H}_{KS}\phi_i = \epsilon_i\phi_i \tag{2.32}$$

Where $\hat{H}_{KS}$ is the Kohn-Sham operator for one electron expressed as

$$\hat{H}_{KS} = -\frac{1}{2}\nabla_i^2 + \int \frac{\rho(r_j)}{|r_i - r_j|} dr_2 + \frac{\delta E_{XC}[\rho]}{\delta\rho(r)} - \sum_A^N \frac{Z_A}{|r_i - R_A|} \tag{2.33}$$

In equation 2.33, the only unknown term is the exchange-correlation term. Consequently, a number of approximations have been proposed.

2.3.9 Exchange-correlation functionals

To treat the exchange-correlation term, Jacob's ladder have been introduced as the rung of the exchange-correlation functional can be divided into the exchange E_X and correlation E_C terms.

$$E_{XC}[\rho] = E_X + E_C \tag{2.34}$$

Local Density Approximation (LDA) is the simplest approximation based on a uniform electron gas model and thus the electron density can be considered as a constant.

$$E_{XC}^{LDA}[\rho(r)] = \int \rho(r)\epsilon_{xc}(\rho(r))dr \qquad (2.35)$$

Where ϵ_{xc} is the exchange and correlation energy for one electron within the volume element of a uniform electron density at the position r. In fact, the electron density distribution of any real system is inhomogeneous. Thus, this approximation is good enough for predicting physical properties such as molecular structures, but does not satisfy the accuracy of total energy calculations.

Generalized Gradient Approximation (GGA) is an improvement over the LDA by including the gradient of the electron density as a correction term. In this approximation, the exchange and correlation energies not only depend on the electron density, but also on its gradient $\nabla\rho(r)$, which is the first derivative of the density with respect to the same position and accounts for its inhomogeneity.

$$E_{XC}^{GGA}[\rho(r)] = \int \rho(r)\epsilon_{XC}^{GGA}\big(\rho(r), \nabla\rho(r)\big)dr \qquad (2.36)$$

Meta-Generalized Gradient Approximation (MGGA) is the development of the GGA by adding the higher order density gradient, which is the second derivative of the density, and the kinetic energy density as presented in equation 2.37.

$$E_{XC}^{MGGA}[\rho(r)] = \int \rho(r)\epsilon_{XC}^{MGGA}(\rho(r), \nabla\rho(r), \nabla^2\rho(r), \tau)dr \qquad (2.37)$$

Where $\nabla^2\rho(r)$ is the Laplacian of the electron density and τ is the kinetic energy density written in terms of the occupied Kohn-Sham orbitals as

$$\tau = \frac{1}{2}\sum_{i=1}^{n}\left|\nabla\phi_i^{KS}(r)\right|^2 \qquad (2.38)$$

Hybrid approximation is the evolution of the exchange-correlation functional to go beyond the previous approximations by a combination of the GGA exchange-correlation functional with a percentage of the exact Hartree-Fock exchange using a Slater determinant. The following equation connects the non-interacting reference and the fully interacting system by applying the adiabatic connection formula (ACF) involving the adjustable parameter λ (from 0 to 1), which switches on the electron-electron interaction.

$$E_{XC} = \int_0^1 \epsilon_{XC}^{\lambda} d\lambda \tag{2.39}$$

At $\lambda = 0$, electrons are non-interacting resulting in no correlation energy. Therefore, the exchange-correlation energy is composed of the exchange only that is approximated by Hartree-Fock method. If Hartree-Fock orbitals can be represented as Kohn-Sham orbitals, the exact exchange calculated from Kohn-Sham orbitals with Hartree-Fock method. On the other hand, at $\lambda = 1$, electrons are fully interacting containing both the exchange and correlation. Consequently, the exchange-correlation functional mixes a fraction of the Hartree-Fock exchange and the DFT exchange-correlation as in the following

$$E_{XC}^{hybrid} = \lambda_0 E_X^{HF} + (1 - \lambda_0) E_X^{DFT} + E_C^{DFT};\ 0 \geq \lambda \geq 1 \tag{2.40}$$

For example, the simplest approximation of the value of hybrid exchange-correlation functional at two end-points can be written as a linear combination

$$E_{XC}^{hybrid} = \frac{1}{2} E_{XC}^{\lambda=0} + \frac{1}{2} E_{XC}^{\lambda=1} \tag{2.41}$$

Equation 2.41 can be rewritten as

$$E_{XC}^{hybrid} = \frac{1}{2} E_X^{HF} + \frac{1}{2} (E_X^{DFT} + E_C^{DFT}) \tag{2.42}$$

There are various kinds of hybrid functionals. In this study, ***M06-2x***, which is a hybrid meta-GGA functional developed by Zhao and Truhlar at the University of Minnesota in 2006, were used in which the letter ***M*** and the number ***06*** denote Minnesota and the year 2006, respectively. The M06 family consists of M06-L, M06, M06-2X, and M06-HF accounting for 0%, 27%, 54%, and 100% of Hartree-Fock exchange, respectively. The ***2x*** indicates the functional with double the amount of Hartree-Fock exchange. The M06-2x functional gives the best performance for main-group thermochemistry, kinetics, electronic excitation energies, and noncovalent interactions including hydrogen bonding, excepting for systems involving transition metals. According to study on DFT methods, the large errors in reaction energy is originated from the conversion of π bonds into σ bonds. The M06-2x has been exhibited as the most reliable estimate for exploring DA reactions and types of cycloadditions due to giving small errors in bond transformations.

2.4 Literature reviews

In 2013, both mechanism and the origin of enantioselectivity in asymmetric transfer hydrogenation of ketamine with thaizoline catalyzed by chiral BINOL-phosphoric acid were investigated by Shibata and Yamanaka [65] using DFT calculations. Regarding the bifunctionality of the phosphoric acid, two pathways are possible: (1) monocoordination and (2) dicoordination models in which both pathways can occur in either antiperiplanar or synclinal orientation of the phenyl group of thaizoline with respect to the C=N bond of ketamine. In the former pathway, only one site of the catalyst makes a single point of contact to both ketamine and thaizoline. For the latter in contrast, both the Brønsted acid site (proton) and Lewis basic site (phosphoryl oxygen) of the catalyst give two points of contact to each reactant. For the resulting optimized structures shown in Figure 2.20, the two P-O bonds of the monocoordination TS structure can be regarded as a P-O single bond and a P=O double bond with bond lengths of ~1.53 and ~1.49 Å, respectively, whereas the two P-O bonds of the dicoordination TS structure have a bond length of ~1.51 Å. The computational results indicated that the pathway associated with the two-point coordination model is energetically preferred due to the fact that the negative charge

delocalizesover the O-P-O fragment resulting in the resonance stabilization as well as the formation of the H-bonding interactions. Consequently, only the dicoordination model was used for studying a more complex reaction, the enantioselective hydrogenation of ketamine and benzothaizoline catalyzed by BINOL-phosphoric acid.

Among eight possible their TS structures, TSαr_{syn}-A and TSβS_{syn}-A corresponding the enantiofacial selection are the two most energetically favored TSs, but the former was found to be 4.9 kcal/mol lower in energy than the latter (Figure 2.21). This is due mainly to the steric interactions of the 3,3′-substituents as the major factors controlling the enantioselectivity, in agreement with the experimental results.

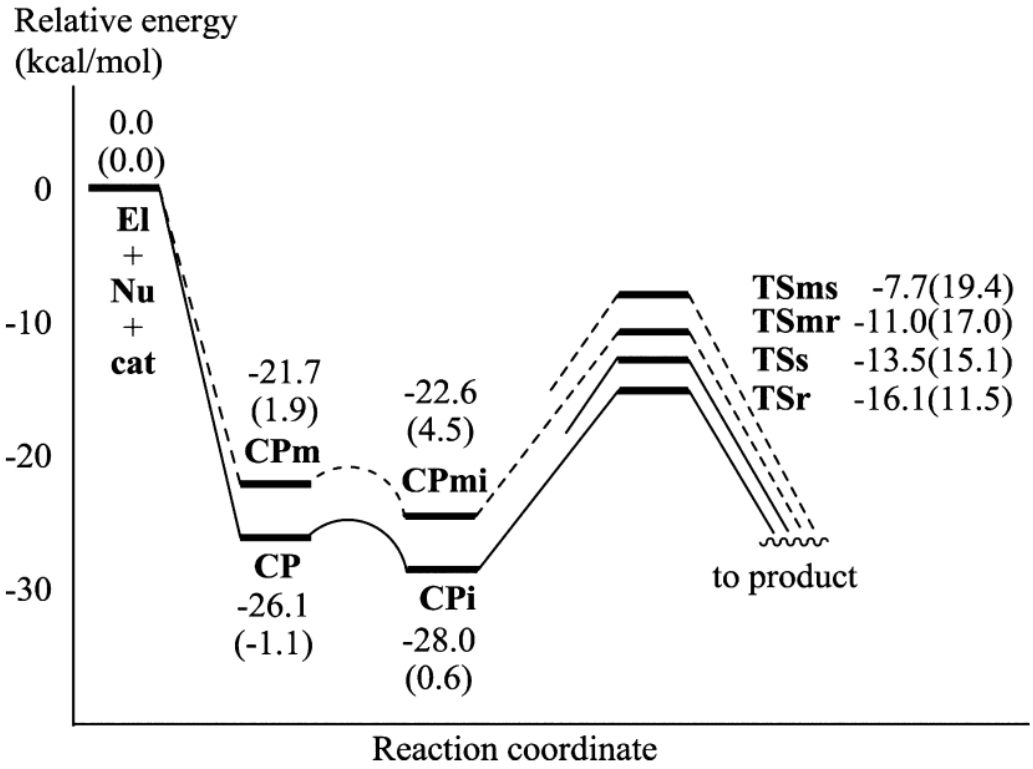

Figure 2.19 The energy profile of monocoordination and dicoordination pathways. The potential energy of the sum of ketimine (EI), thiazoline (Nu), and biphenyl phosphoric acid (cat) is set to 0 as a reference energy. Relative energies are given in parentheses (in kcal/mol).

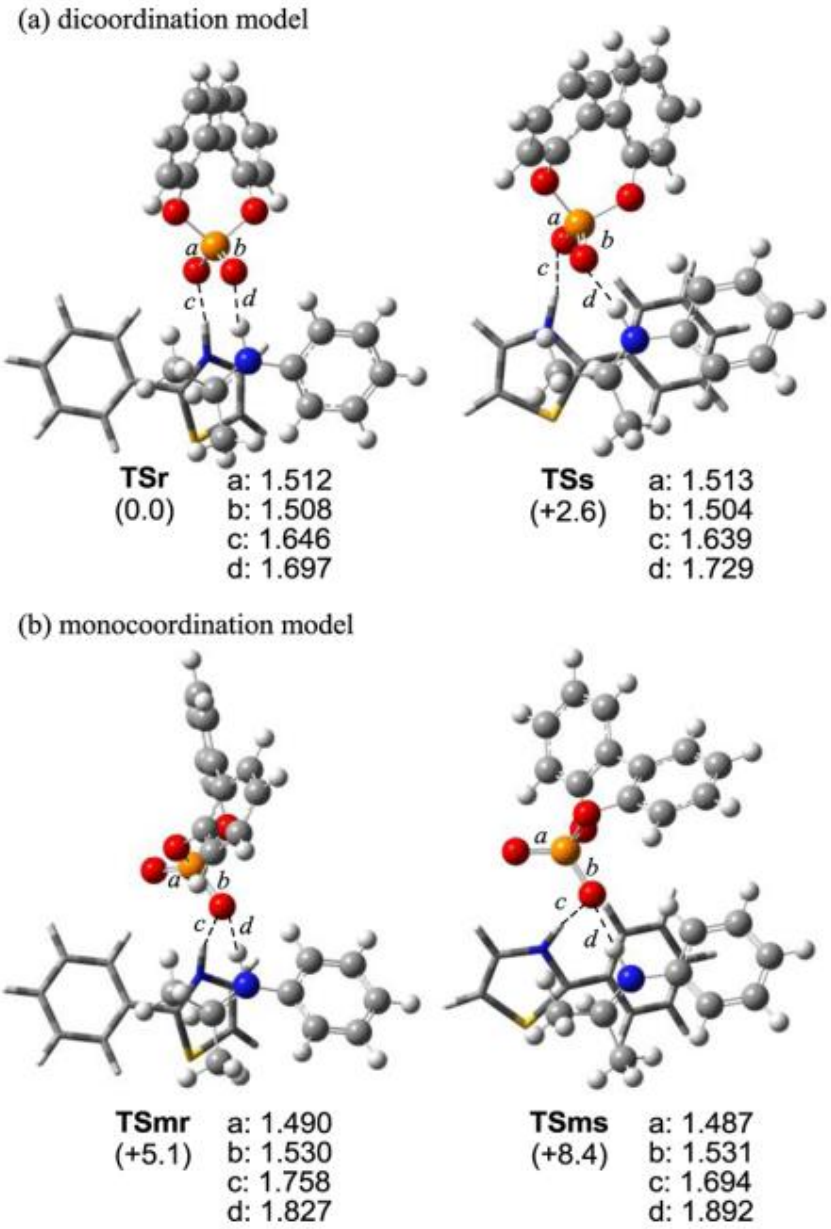

Figure 2.20 3D structures associated with antiperiplanar; r, and synclinal; s, transition states in (a) dicoordination (TSr and TSs) and (b) monocoordination (TSmr and TSms) models obtained at ONIOM (B3LYP/6-31G*:HF/3-21G) level (C, gray; O, red; N, blue; P, orange; S, yellow; biphenyl phosphoric acid and ketimine, ball and stick model; thiazoline, tube model). Bond lengths are in Å. The number in parentheses are relative energies (in kcal/mol).

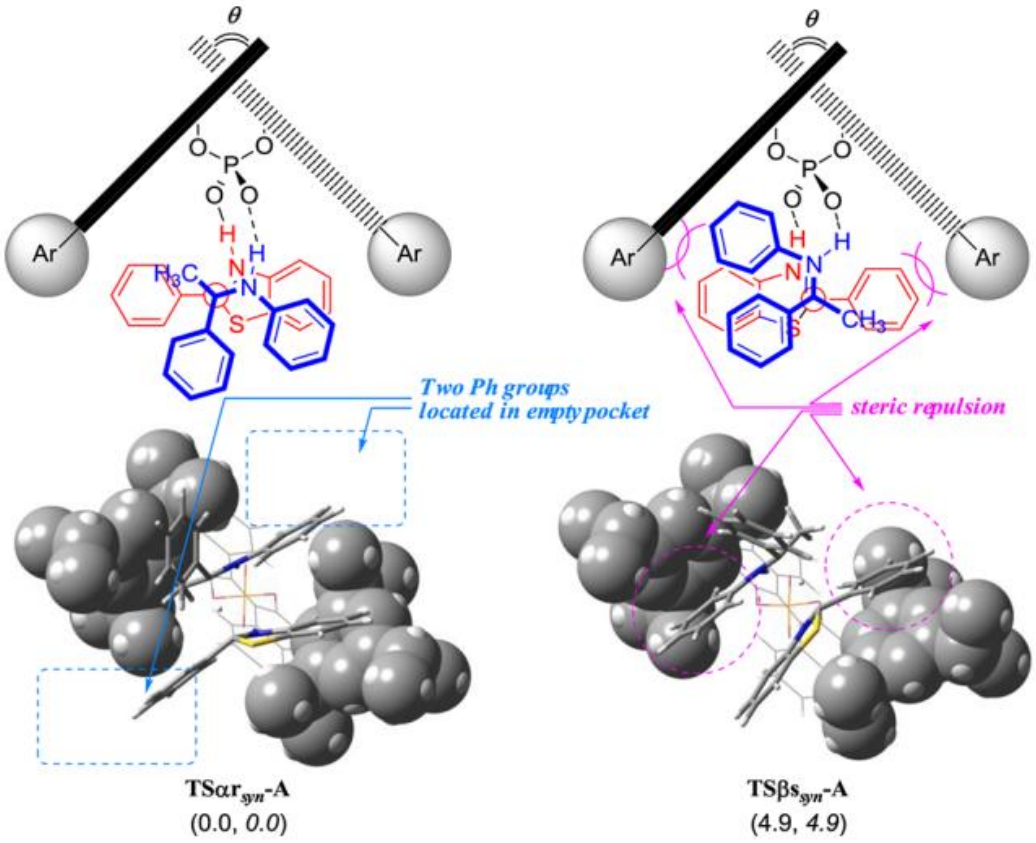

Figure 2.21 3D structures and schematic representation models of TSαr$_{syn}$-A and TS β S$_{syn}$-A. The 3,3′-substituents of BINOL-phosphoric acid and substrates are represented to ball model and tube model, respectively. Relative energy differences (in kcal/mol) are shown in parentheses. Relative solution-phase energies (PCM, toluene) are shown in italics.

In 2014, the Sun group [20] successfully used *o*-hydroxystyrenes as *o*-QM precursors under the catalysis of chiral phosphoric acid for organocatalytic asymmetric transfer hydrogenation (ATH). The structures and the reaction mechanism were carried out using DFT calculations at the B3LYP/6-31G(d) level. The ATH mechanism involves the initial generation of *o*-QM intermediate followed by the nucleophilic addition with Hantzsch esters or indoles. The protonation of *o*-hydroxystyrene gives the key intermediate, which has two resonance forms including ionic and *o*-QM forms. The calculated results indicated that the *o*-QM intermediate, where the C–C bond lengths in the six-membered ring are distinct as shown in Figure 2.22, is more represented than

its resonance structure, the zwitterionic form, where the bond lengths in the ring should be equal. Furthermore, although the *E* isomer of *o*-QM was found to be 2.1 kcal/mol more stable than the *Z* isomer, the activation barrier for the formation of (*Z*)-*o*-QM is smaller than that for (*E*)-*o*-QM, thus the (*Z*)-*o*-QM is clearly preferred to be generated for the subsequent addition reaction.

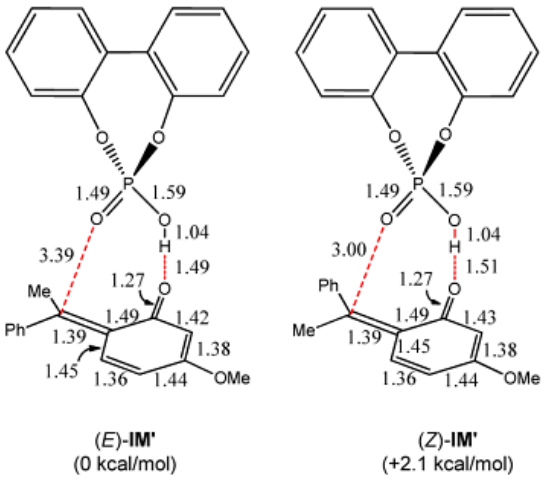

Figure 2.22 The DFT optimized structures of the (*E*)- and (*Z*)-*o*-QM intermediates (IM'). The numbers in parentheses are relative Gibbs free energies (in kcal/mol) [20]

In 2016, Yu-Chen Zhang and colleagues [24] established the new cooperative catalysis involving chiral BINOL-derived phosphoric acid and chiral guanidine for the [4+2] cycloaddition between *o*-hydroxystyrene and azlactone, resulting in the formation of dihydrocoumarin scaffolds in high yields and excellent enantioselectivities. The observed reaction was proposed to proceed via a cycloaddition followed by a subsequent ring opening. They found that merging CPA and TBO catalysts greatly improves the selectivity over using one type of catalysts. Moreover, when CPA or TBO was combined with achiral catalyst, the enantiomeric ratio was decreased. These results disguised that the chirality of both TBO and CPA catalysts plays a crucial role in asymmetric induction to attain high enantioselectivity. In the proposed activation mode of the reaction, the catalysts activated the substrates to

from the oxa-diene and enolized azlactone INT by hydrogen-bonding interactions where the phosphoryl oxygen of CPA formed a hydrogen bond with the NH group of TBO that contributed to the synergistic and matched interaction between them to create the chiral environment around the substrates.

CHAPTER 3
COMPUTATIONAL METHODS

In order to study the mechanisms insight into the origin of the enantioselectivity in the DA reaction of *o*-hydroxystyrene and azlactone catalyzed by *t*Bu-TBO and/or CPA catalysts, the two distinct catalytic systems were evaluated, as the mono-catalytic and co-catalytic systems, by the use of density functional theory. Moreover, each system was subdivided into two possible orientations of the approaching reactants, giving two enantiomeric products; (*S*)- and (*R*)-products. Hence, a scope of this study on enantioselective [4+2] cycloaddition reactions is summarized by Figure 3.1.

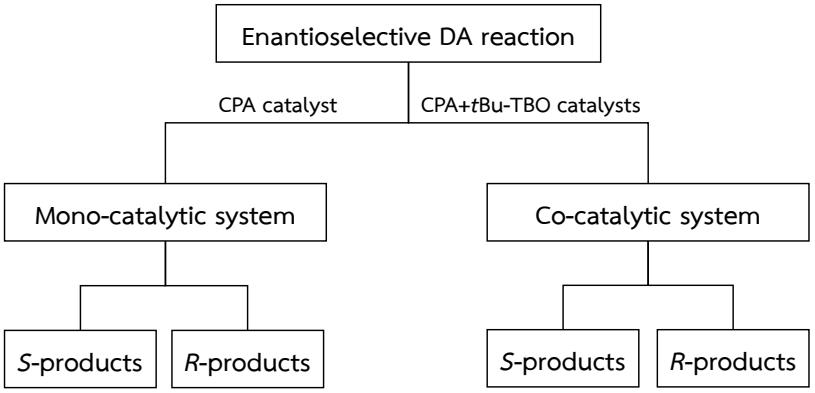

Figure 3.1 The scope of this study

3.1 Molecular models

In the catalytic DA reaction, GaussView 5.0.8 program [66] was used to model *o*-hydroxystyrene as the diene and azlactone as the dienophile, as well as both chiral catalysts in which (*R*)-BINOL-derived chiral phosphoric acid (CPA) substituted with phenyl groups at the 3 and 3' positions and chiral [5,5] bicyclic guanidine (1,4,6-Triaza-Bicyclo[3.3.0]-Oct-4-ene; TBO) bearing two *tert*-butyl groups function as Brønsted acid and Brønsted base catalysts, respectively. Despite the need to keep down computational cost, the two benzene rings, which is expected to be less influence in

the reaction, were removed from CPA structures (Figure 3.2) in a similar way to this research [65, 67].

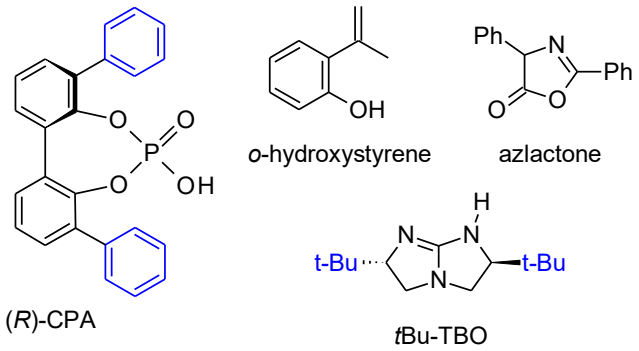

Figure 3.2 Molecular models used for computational calculation with 6-31G* (in black) and 3-21G (in blue) basis sets

The initial structure in this study consists of *o*-hydroxystyrene, azlactone, CPA, and *t*Bu-TBO. According to the Tain group report [68], two molecules of CPA were added into mono-catalytic system in which one CPA was put on the top position of both reactants and another one positioned below both reactants. On the other side, co-catalytic system consists of both reactants with one CPA and one *t*Bu-TBO, which is expected to capture CPA through hydrogen-bonding interactions [69]. These models were used to explore the catalytic DA processes including the reaction mechanism and selective control for DFT calculation under gas phase condition. The DFT at the M06-2X/6-31G*//M06-2X/3-21G level was used to carry out the output structures for being the suitable starting structural geometry for all four investigated systems.

3.2 Computational details

The QM calculations were performed in the Gaussian 09 program [70]. Density functional theory (DFT) calculations using M06-2X functional [71, 72] were used as recommended by Linder and Brinck [73, 74]. The 6-31G* basis set advised by Gayatri [75] was used for all atoms involved in bond breaking and formation of H-bonding. The 3-21G basis set was used for phenyl substituent of CPA and *t*Bu of as these play a

primarily a steric role. All structures were fully optimized to stable stationary points at the M06-2X/6-31G*//M06-2X/3-21G level of theory in gas phase. As shown in Figure 3.2, the calculations on the catalyst system were performed using two different basis sets in which the large basis set (6-31G*) was used to calculate the atoms in black color that participate a strong influence in the reaction while the less sensitive atoms in blue color were treated with the smaller basis set (3-21G) to reduce time consuming. Vibrational analysis was undertaken to confirm the identity of all stationary points obtained as either a minimum having only positive frequency and a transition state existing a single negative frequency, and to allow for the determination of the Gibbs's free energy corrections to the reaction profile. The vibration associated with the imaginary frequency was ensured to correspond to the expected bond forming and breaking processes. A further correction in form of single-point energies at the M06-2X/6-31+G** level were also performed.

To support and ensure that the potential of 6-31G* mixed with 3-21G basis set can be used instead of high-level basis sets, single-point calculations using the M06-2X density functional with 6-311+G(d,p) and with 6-311++G(d,p) basis sets were additionally calculated for the rate-determining steps only. Discovery Studio 4.5 Visualization (DSV) program was used for 3D structural analysis of stationary points. All 2D structures were drawn in ChemSketch program.

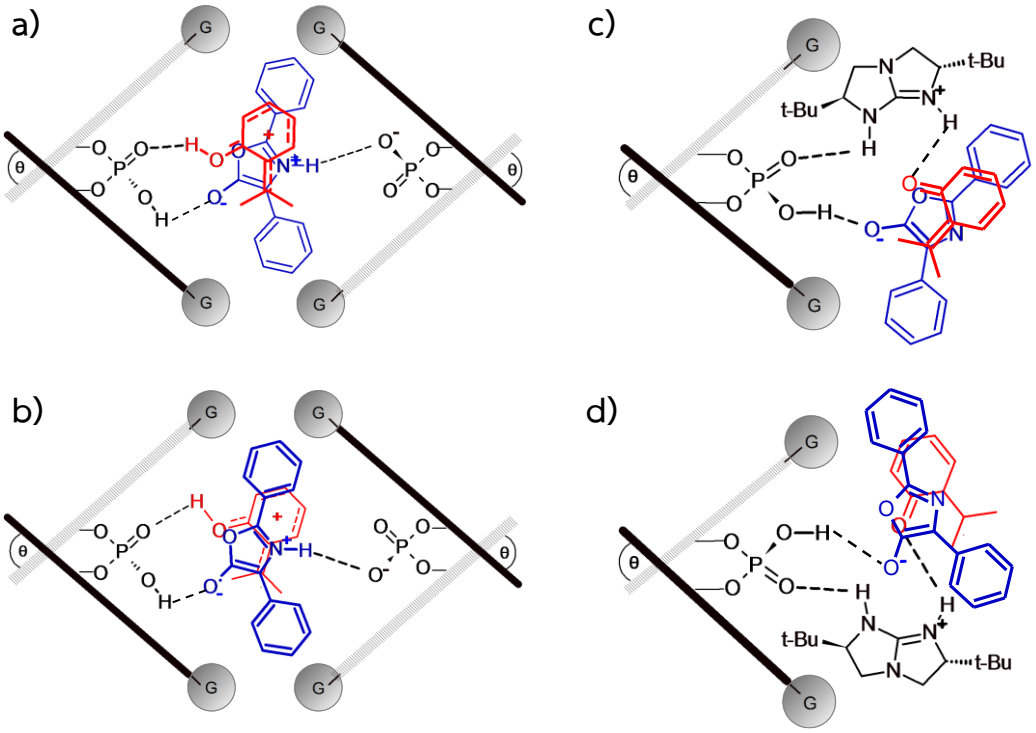

Figure 3.3 Schematic representation models of the (a) si and (b) re face additions for mono-catalytic system and that of the (c) si and (d) re face additions for co-catalytic system.

3.3 Keto-Enol tautomerization

According to these researches [29, 36] that *ortho*-quinone methide (*o*-QM) and azlactone can exist in both keto and enol forms. The structures of *o*-hydroxystyrene and azlactone are thus simulated in their higher energy tautomeric forms. Illustrations of these tautomers are shown in Figure 3.4.

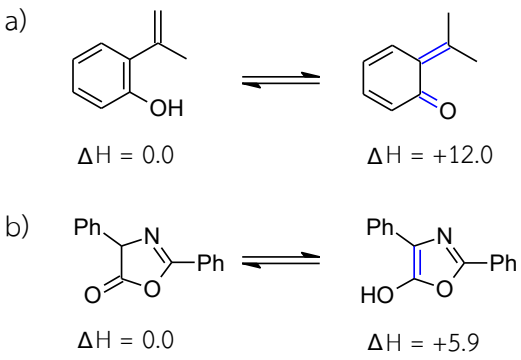

Figure 3.4 a) *o*-Hydroxystyrene and b) azlactone tautomers and their relative energies (in kcal/mol).

Both reactions should proceed via high energy tautomers of each reactant. The *o*-hydroxystyrene diene as *o*-QM is 12.0 kcal/mol higher in energy than the corresponding enol based on isolated gas phase calculations at the M06-2X/6-31+G(d,p) level. In comparison, the keto azlactone requires 5.9 kcal/mol to adopt the enol form needed to undergo reaction. Interestingly, modelling the reactants in these tautomers together with CPA and/or TBO led to additional proton rearrangement.

CHAPTER 4
RESULTS AND DISCUSSION

First of all, the approach mode of the reactants, *o*-hydroxystyrene and azlactone, was characterized in terms of *endo* and *exo* selectivities for co-catalytic system of interest only. The energy profile of *endo* and *exo* additions and the optimized structures corresponding to the TS are shown in Figure 4.1 and 4.2, respectively. In the both cases, the results indicated that these [4+2] cycloaddition reactions can proceed by a concerted mechanism through asynchronous TSs in which the difference between C···C and C···O distances in TS1 for *endo* is found to be 0.46 Å compared to 0.54 Å for *exo*. This is due to the stronger C···C bond formation in *endo*-TS1 (2.43 Å). The activation energies required for simultaneously forming the C-C and C-O bonds in one step is found to be 23.7 and 29.1 kcal/mol for *endo* and *exo* approaches, respectively. The *endo*-TS1 is ∼5 kcal/mol lower in free energy than the *exo*-TS1 due to the existence of overlap of secondary orbitals between the reactants, called secondary orbital interaction (SOI) [76-78]. While both of these TSs have the same number of H-bonding interactions, the *endo*-TS1 is also stabilized by SOI. Furthermore, the *endo* cycloadduct is more stable than the *exo* cycloadduct by 7.5 kcal/mol and therefore, the *endo* form is actually thermodynamically most favorable. Consequently, the *endo* approach has taken place in all studied DA reactions.

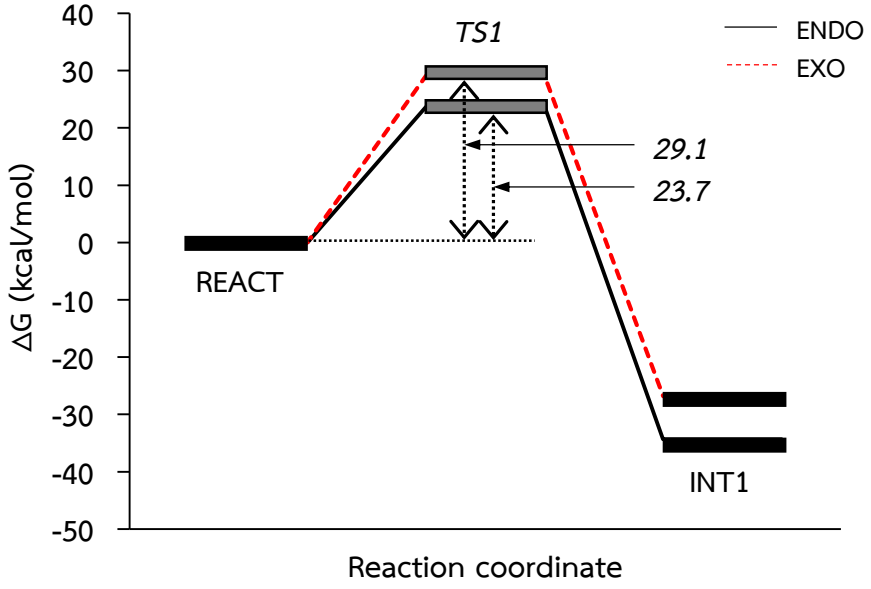

Figure 4.1 The QM ΔG energy profile of endo and exo pathways of DA reaction involving CPA and TBO catalysts.

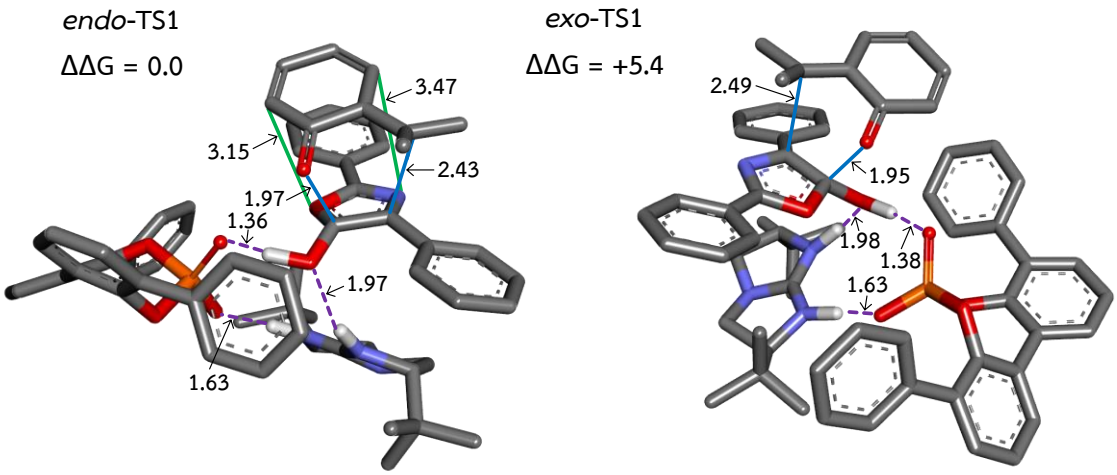

Figure 4.2 Optimized structures of TS1 for endo and exo approaches in co-catalytic reactions. Primary and secondary orbital interactions, and H-bonding interaction are displayed in blue and green solid, and purple dashed lines, respectively. The values are given in kcal/mol.

The structures and energetics of the mono- and co-catalytic models were evaluated in terms of both *si*- and *re*- based mechanisms. Both possible concerted and stepwise mechanisms of DA reactions were investigated; however, the free energy barrier height of the latter is then found to be ~8 kcal/mol lower than that of the former in the case of the co-catalytic system, but only the latter is observed in the mono-catalytic system. To the best of our knowledge, the stepwise reaction mechanism is only focused on studying for both the mono- and co-catalytic conditions. From the DFT calculations, the energies of the stationary points obtained for the *si*- and re- DA mechanisms with respect to the *endo* arrangement are given in Table 4.1.

Table 4.1 The computed QM energies of all stationary points obtained in this study. ΔH and ΔG correspond to the energy of optimized complexes using the M06-2X/6-31G(d)//3-21G level. ΔH SP and ΔG SP correspond to the single point energy of the optimized stationary point performed by using the M06-2X/6-31+G(d,p) level. The superscript 'a' and 'b' correspond to the single point energy of the optimized stationary point using the M062X functional with the 6-311+G(d,p) and 6-311++G(d,p) basis sets, respectively. The numbers in parentheses are the energies in the case of using the azlactone (Az.) as a base catalyst. All energies are given in kcal/mol.

State	(*S*)-product					(*R*)-product				
	ΔH	ΔG	ΔH SP	ΔH SP[a]	ΔH SP[b]	ΔH	ΔG	ΔH SP	ΔH SP[a]	ΔH SP[b]
Mono-catalysis										
REACT	0.0	0.0	0.0			0.0	0.0	0.0		
TS1	0.3	0.5	0.9			0.8	1.5	1.3		
INT1	-15.5	-15.8	-15.4	0.0	0.0	-14.9	-12.9	-15.2		
TS2	-1.3	-3.8	-3.5	13.9	13.9	-3.8	-4.9	-5.9		
INT2	-15.5	-14.6	-16.0			-21.8	-17.2	-19.7	0.0	0.0
TS3 (Az.)	0.8 (10.2)	0.6 (8.1)	-1.6 (10.5)			-9.1 (15.6)	-6.1 (15.8)	-8.9 (14.4)	10.5	10.6
PROD*	-2.1	-0.9	-3.2			-14.9	-14.5	-15.3		
PROD	-21.0	-17.7	-16.8			-28.7	-25.3	-27.0		
Co-catalysis										
REACT	0.0	0.0	0.0			0.0	0.0	0.0	0.0	0.0
TS1	11.6	11.7	10.8			15.5	15.7	14.8	15.6	15.6
INT1	-7.4	-4.3	-8.4	0.0	0.0	-8.2	-5.7	-8.1		
TS2	4.3	7.5	4.1	13.1	13.1	-2.2	-0.8	-3.9		
INT2	-26.8	-23.2	-26.9			-25.3	-22.0	-25.6		
TS3	-10.5	-7.1	-10.1			-8.4	-6.5	-9.2		
INT3	-26.5	-20.1	-22.6			-17.1	-17.9	-18.2		
PROD	-22.3	-18.2	-18.8			-29.0	-23.5	-25.2		

[a] Single-point calculations using the M062X/6-311+G(d,p) level.

[b] Single-point calculations using the M062X/6-311++G(d,p) level.

Since two DA mechanisms are possible: concerted and stepwise [4+2] cycloaddition processes, the results of mono-catalytic DA reaction are first described in the following section

4.1 Mono-catalytic DA reaction

Based on QM calculations, the mono-catalytic mechanism involves three main steps. The two first steps is stepwise [4+2] cycloaddition consisting of the first C-C bond formation and the second C-O bond formation. The final step is ring-opening reaction. The free energy reaction profile for the mono-catalytic system is shown in Figure 4.17.

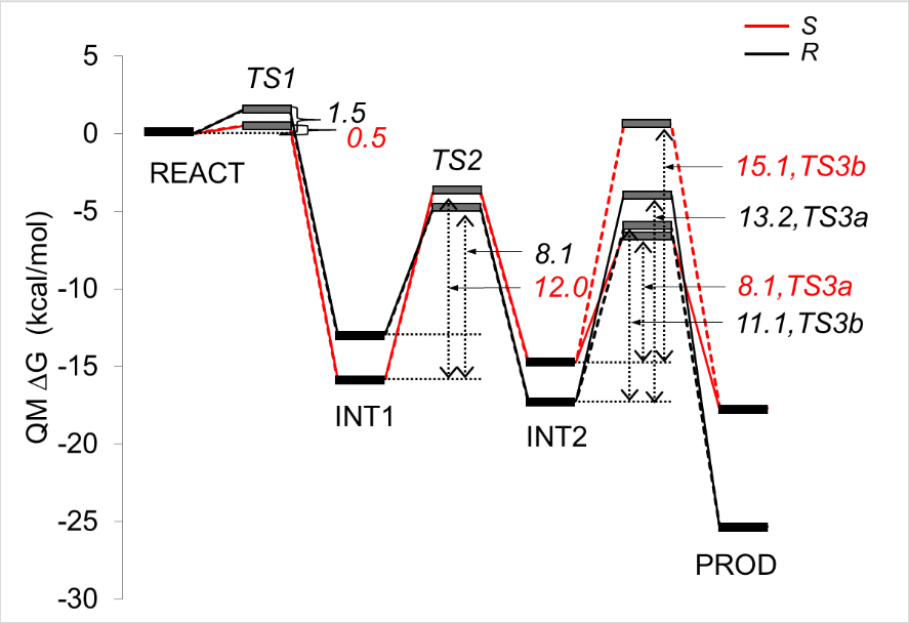

Figure 4.3 QM ΔG reaction profile of both (*S*)- and (*R*)- products for the mono-catalytic reaction. Solid and dashed lines denote path a and b, respectively.

The mono-catalytic model consists of the *o*-hydroxystyrene, azlactone, and two CPA molecules, which are placed on the top and bottom of the substrates. The optimized *si*- and *re*- based models have similar interactions, but their structures in three-dimensional arrangement are different due to the steric effects of the CPA phenyl substituents. The DA reaction mechanism catalyzed by CPA only is suggested according to Figure 4.18. The stationary points corresponding to the (*S*)- and (*R*)-

products are illustrated in Figure 4.18 and 4.10, respectively. In the mono-catalytic process, the protonated nitrogen atom of the azlactone, which is the most basic site among all the substrates, is initially formedby the phosphoric acid or **CPA1**, creating a partial negative charge on the oxygen atom of an azlactone enolate. The styrene tertiary carbocation intermediate is formed via the protonation of *o*-hydroxystyrene tautomer. Therefore, this resulting ion-pair easily undergoes the nucleophilic addition, allowing to C-C bond formation.

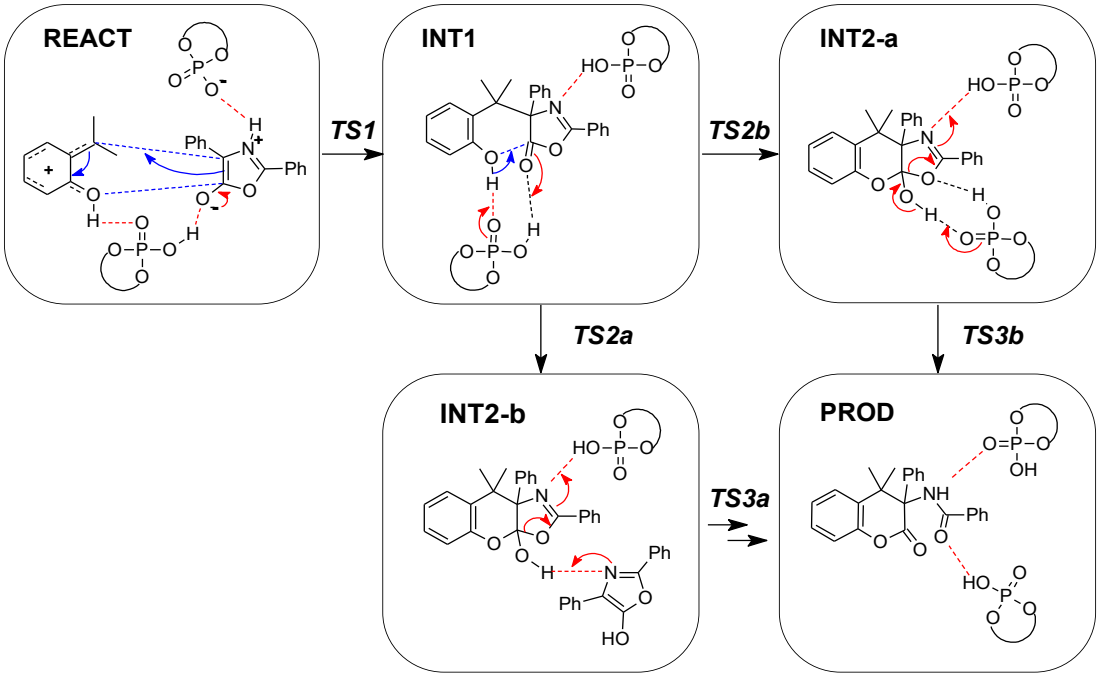

Figure 4.4 Schematic 2D illustration of the DA mechanism catalyzed by chiral phosphoric acid.

Step 1 involves the initial formation of a new σ-bond of the nucleophilic C4 atom of the azlactone with the tertiary carbon atom of the styrene, giving a dearomatized intermediate in **INT1** via an asynchronous TS (**TS1**). The difference between the C---C and C---O bond distances in **TS1-S** is found to be 0.45 Å compared to 0.51 Å in **TS1-R**. The barrier to reaction for **TS1-S** is only 0.5 kcal/mol, which is 1.0 kcal/mol lower in energy than **TS1-R**. It is observed that this step has the smallest barriers overall

reaction pathways for both (*S*)- and (*R*)- isomers due to the ion-pairing reaction. A little difference between **TS1-S** and **TS1-R** results from displaying comparable interactions.

CPA2 activates the dearomatized complex n step 2, to promote ring closure via a proton-shuttling process, thereby generating the DA adduct by C-O formation (**TS2**). The **TS2-S** and **TS2-R** barriers are found to be 12.0 and 8.1 kcal/mol, respectively, with the C---O bond distances of 1.77 and 1.76 Å, respectively. In **INT2** cycloadducts, the C-O bond length are approximately 1.4 Å. We notice that a big difference in barrier heights between TS2s is a direct result of the stability of INT1 rather than TS2 themselves.

Finally, step 3 involves ring-opening reaction and proton rearrangement. The protonation of the azlactone nitrogen by CPA1 leads to ring opening of the azlactone moiety via C-O bond cleavage. The proton transfer from the alcohol to a base is required. This can occur in both CPA (path b) and an additional azlactone molecule (path a) with more basic, thus giving rise to the two alternative pathways (Figure 4.18). Proton transfer to **CPA2** generates the enolate complex in the case of **TS3-b** with the ring-opening activation energy of 15.1 kcal/mol in comparison to 8.1 kcal/mol in the case of **TS3-a**, which is a second azlactone acting as the base. At this point, the increased basicity of the azlactone results in a much lower barrier of 7.1 kcal/mol for (*S*)-product, however, not help for (*R*)-product. Structural analysis shows that this is directly due to π-π stacking interactions among three phenyl rings of the complex, CPA, the second azlactone, stabilizing TS3-a for the (*S*)-product only in contrast to the (*R*)-product (Figure 4.20 vs 4.22). In the final step, proton rearrangement is subsequently required to form the corresponding amide group on the final bicyclic cyclic product in **PROD**.

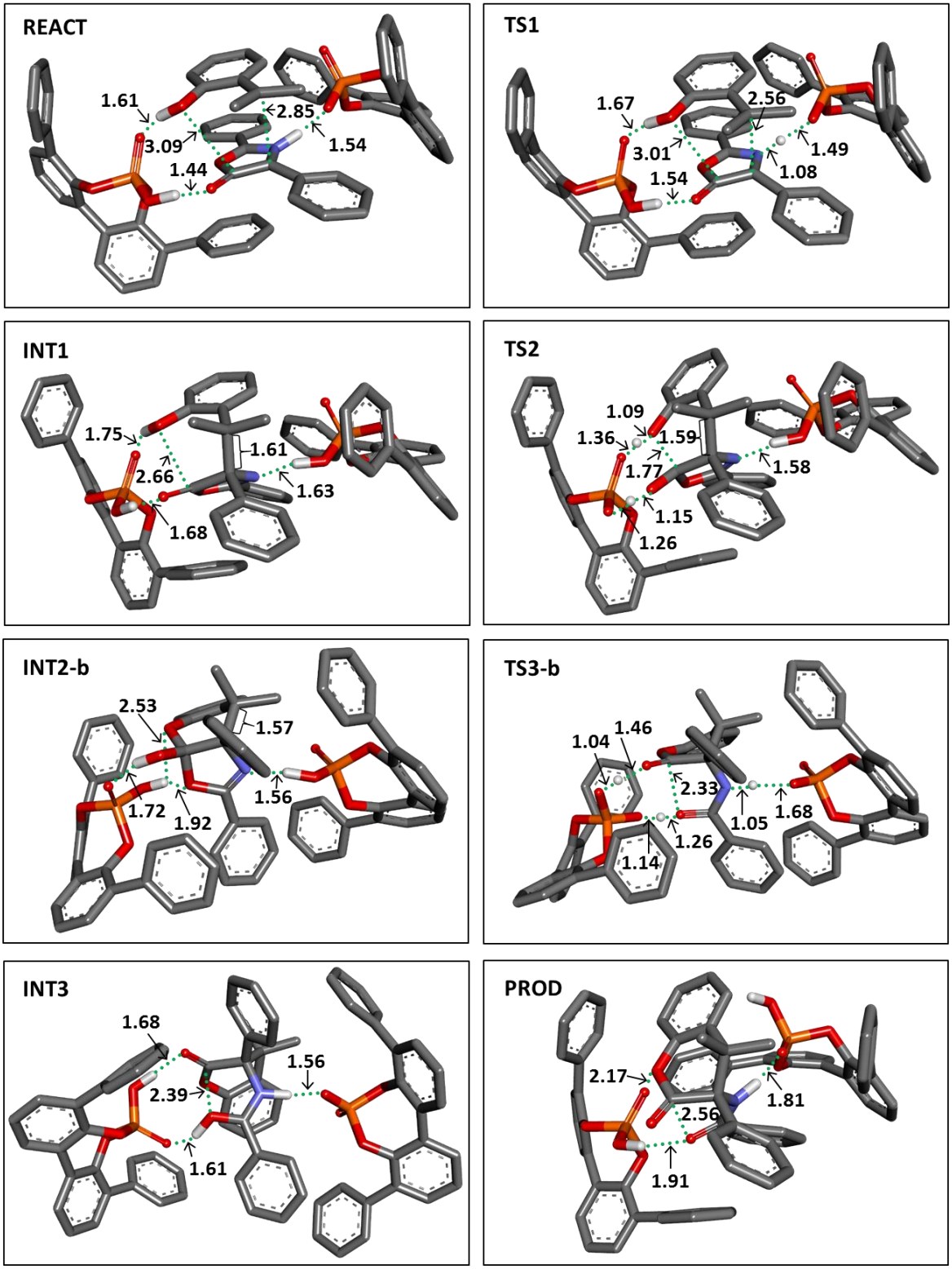

Figure 4.5 QM optimized structures associated with (*S*)-product in mono-catalysis obtained at the M06-2X/6-31G*//3-21G level. Polar hydrogens are shown only for clarity. Distances are reported in Angstroms Å.

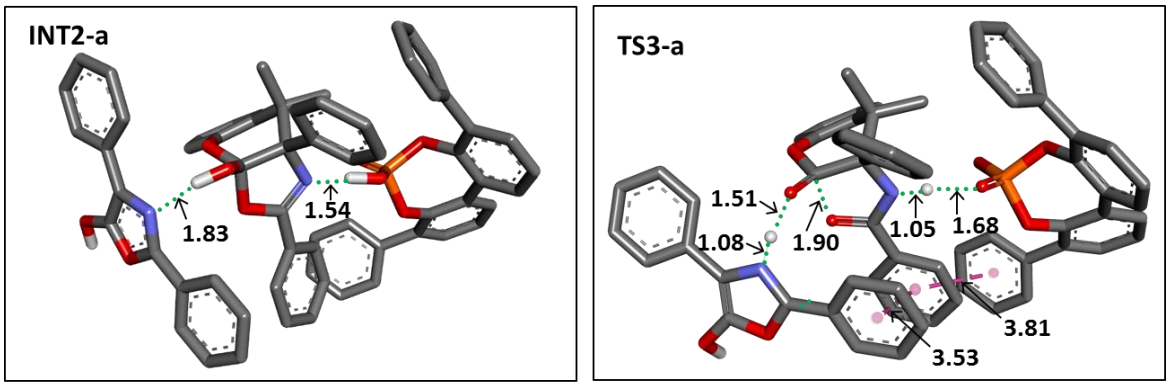

Figure 4.6 QM optimized structures associated with (*S*)-product via path a in mono-catalysis obtained at the M06-2X/6-31G*//3-21G level. Polar hydrogens are shown only for clarity. Distances are reported in Angstroms Å.

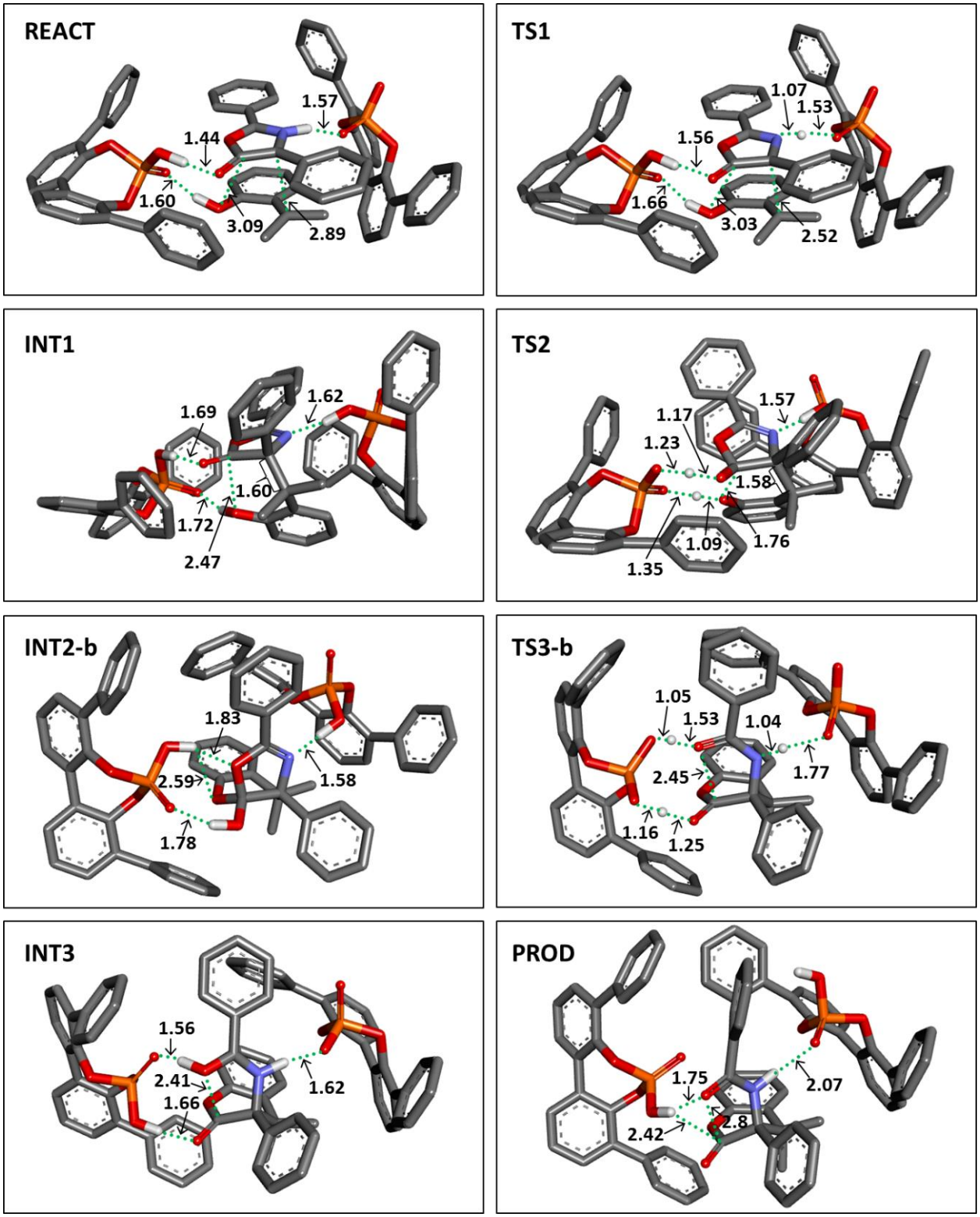

Figure 4.7 QM optimized structures associated with (*R*)-product in mono-catalysis obtained at the M06-2X/6-31G*//3-21G level. Polar hydrogens are shown only for clarity. Distances are reported in Angstroms Å.

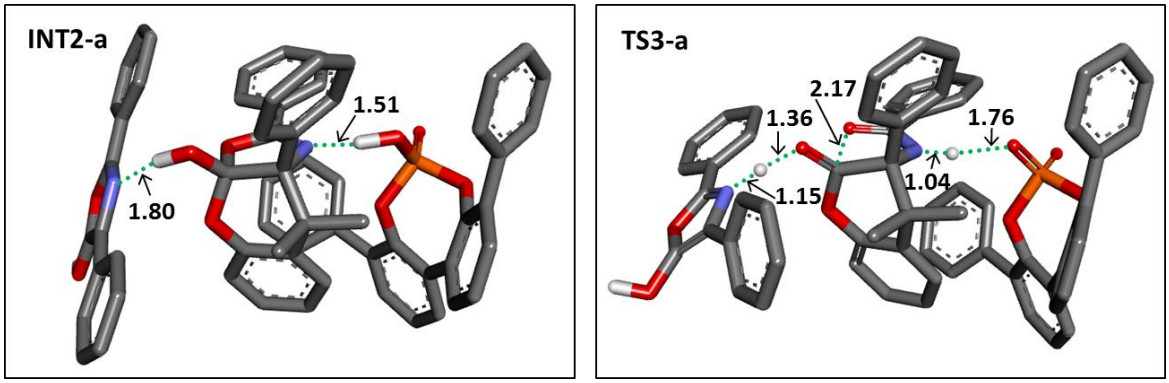

Figure 4.8 QM optimized structures associated with (*R*)-product via path a in mono-catalysis obtained at the M06-2X/6-31G*//3-21G level. Polar hydrogens are shown only for clarity. Distances are reported in Angstroms Å.

Consider the differences in barrier heights for **TS2** and **TS3** are originated from the differences in the energies of **INT1** and **INT2**, rather than differences in the energies of the transition states themselves. Key noncovalent interactions are illustrated in Figure 4.22 and their distances are provided in Table 4.2. **INT1-S** is found to be 2.9 kcal/mol lower in energy than the (*R*)-isomer. While the same number of H-bonding interactions are observed in both the INT1 models, π-stacking interactions found between the substrate and CPA1 (d4 and d5) are slightly stronger in **INT1-S** and steric repulsion is also lower than the (*R*)-isomer (d6 in *S* compared to d6-d8 in *R*). As a result, the more stability of INT1-S leads to the higher barrier of TS2 for the (*S*)-isomer. For **INT2**, by contrast, the (*S*)-isomer is found to be 2.5 kcal/mol higher in energy compared to the (*R*)-isomer. This is a result of the existence of parallel-displaced π-π stacking (d6 and d7), which is more stable energetically than T-shaped orientation, but steric repulsion is more pronounced in the (*R*)-isomer [79, 80]. This indicated that favorable π-stacking is a dominant factor rather than steric effects. Thus, TS3 can be predicted to be higher for the (*S*)-isomer.

Overall, **TS2** becomes the RDS for the (*S*)-product with the barrier of 12.0 kcal/mol while **TS3** is the RDS for the (*R*)-product with the barrier of 11.1 kcal/mol. As a consequence, the RDS to the formation of the (*R*)-product is lower in energy than the (*S*)-product by only 0.9 kcal/mol.

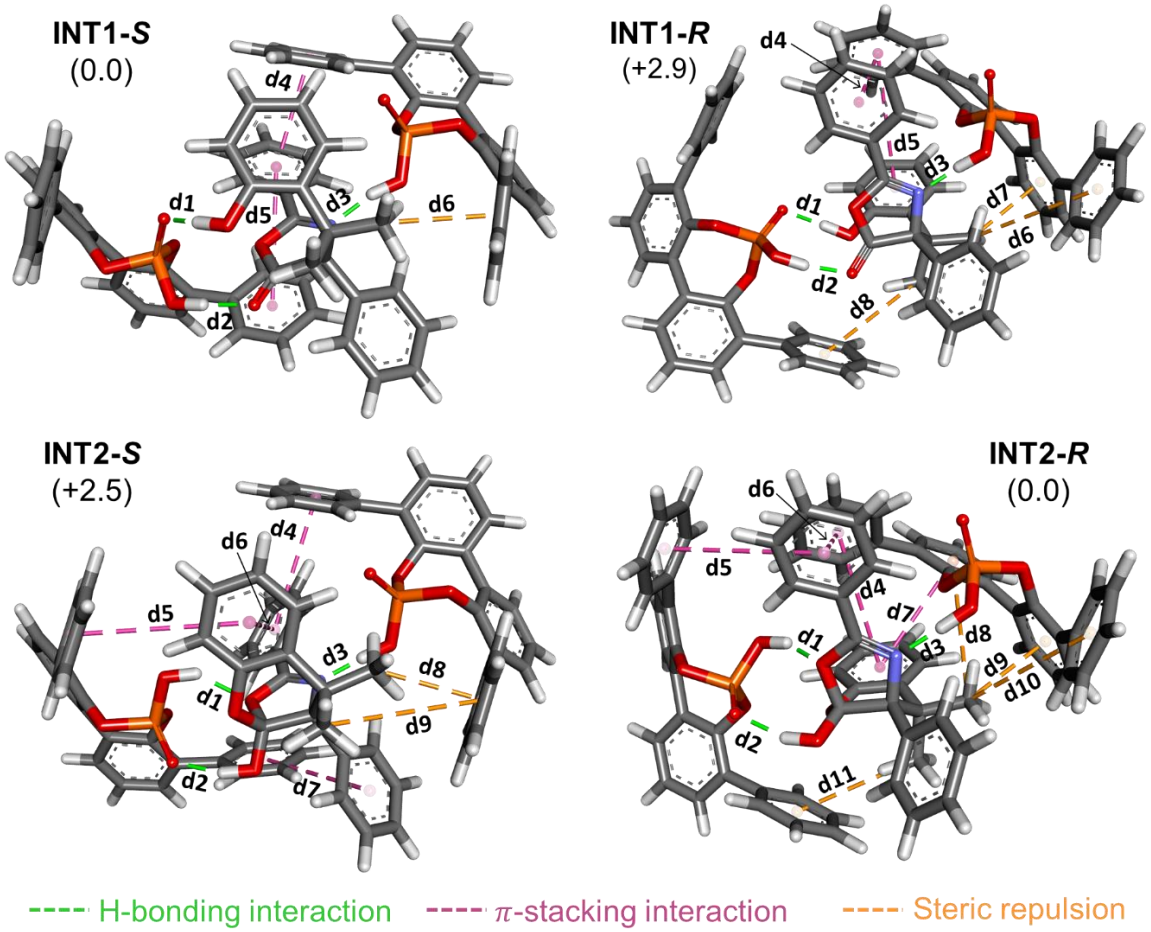

Figure 4.9 3D structures of INT1 and INT2 in mono-catalysis of (S)- and (R)- isomers. The values in parentheses are relative Gibbs free energies (in kcal/mol).

Table 4.2 The key interaction distances in the mono-catalytic reaction obtained at the QM (M062X/6-31G(d)//3-21G) level of theory (in Angstrom).

Structure	d1	d2	d3	d4	d5	d6	d7	d8	d9	d10	d11
INT1-S	1.75	1.68	1.63	3.85	4.57	3.60					
INT1-R	1.70	1.72	1.62	3.91	5.10	5.24	3.37	4.37			
INT2-S	1.92	1.72	1.55	4.54	5.23	5.82	5.29	3.33	4.99		
INT2-R	1.84	1.78	1.56	4.70	5.34	3.90	4.25	5.35	3.26	4.93	4.20

4.1.1 The effect of CPA substituents

In this subsection, the substituent effect on DA reactions has been elucidated by varying the 3,3' groups on the binaphthol ring, including (a) 2-naphthyl and (b) 9-anthracenyl, for only the reaction step with the largest barrier (**TS3-b**) for the (*S*)-isomer (Figure 4.10).

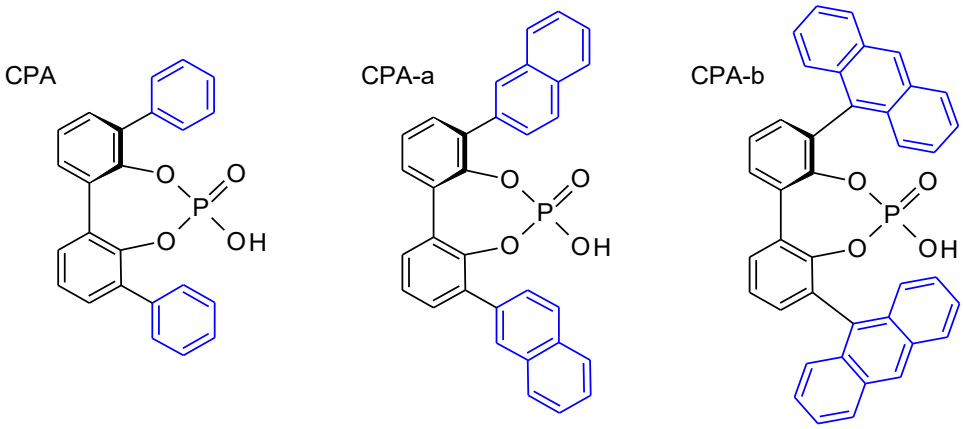

Figure 4.10 Models of CPA derivatives used for computational calculations

The energy profile of CPA-a and CPA-b compared to CPA as the reference condition for the mono-catalytic reaction, and their optimized structures are shown in Figure 4.11 and 4.12, respectively. The barrier to reaction for **TS3** by CPA-b is found to be 4.3 and 2.1 kcal/mol lower in energy than that by CPA or CPA-a, respectively. However, on the formation of **PROD**, which is the lowest energy structure, the reverse formation of **INT2** requires activation energy greater than 30 kcal/mol in the case of CPA. The results indicated that strong electron-donating substituents such as 2-naphthyl and 9-anthracenyl on CPA can lower the activation barriers to reaction, resulting in higher yields in agreement with the experimental observation.

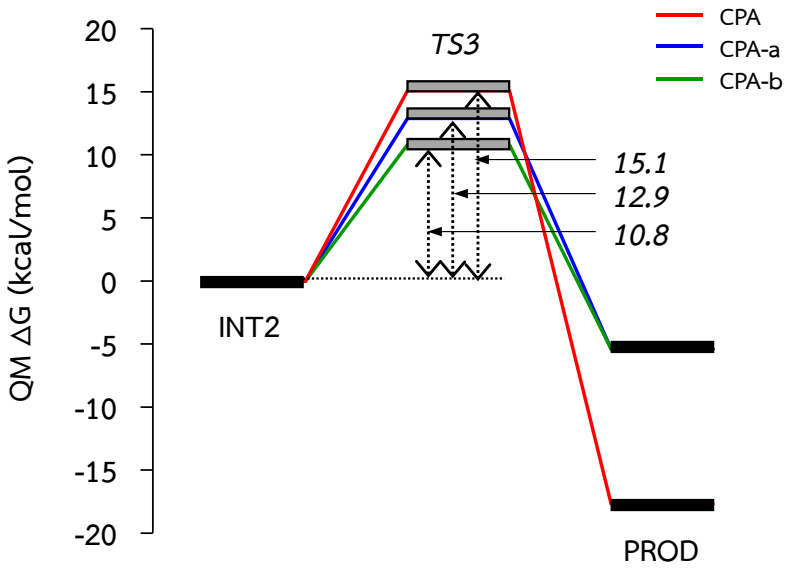

Figure 4.11 The QM ΔG energy profile of CPA, CPA-a, and CPA-b for mono-catalysis.

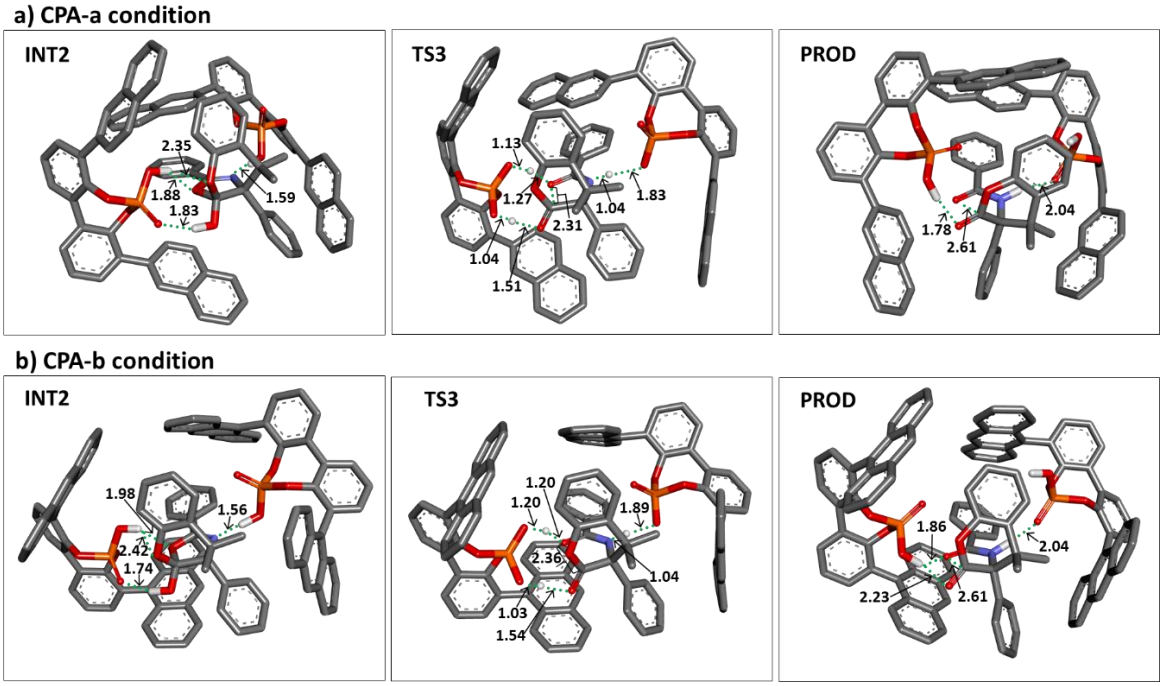

Figure 4.12 QM optimized structures associated with (*S*)-product in mono-catalysis involving (a) CPA-a and (b) CPA-b obtained at the M06-2X/6-31G*//3-21G level. Polar hydrogens are shown only for clarity. Distances are reported in Angstroms Å.

Table 4.3 The QM relative enthalpies ΔH and free energies ΔG of the stationary points obtained in this study for mono-catalytic system using CPA-a and CPA-b (in kcal/mol).

Structure	ΔH		ΔG	
	b	c	b	c
INT2	0.0	0.0	0.0	0.0
TS3	14.0	12.9	12.9	10.8
PROD	-2.6	-3.2	-5.4	-5.4

4.2 Co-catalytic DA reaction

From the calculations, we found that the reaction mechanism under co-catalytic condition also proceeds via the stepwise [4+2] cycloaddition followed by ring-opening reaction. The free energy reaction profile for the co-catalytic system is shown in Figure 4.13.

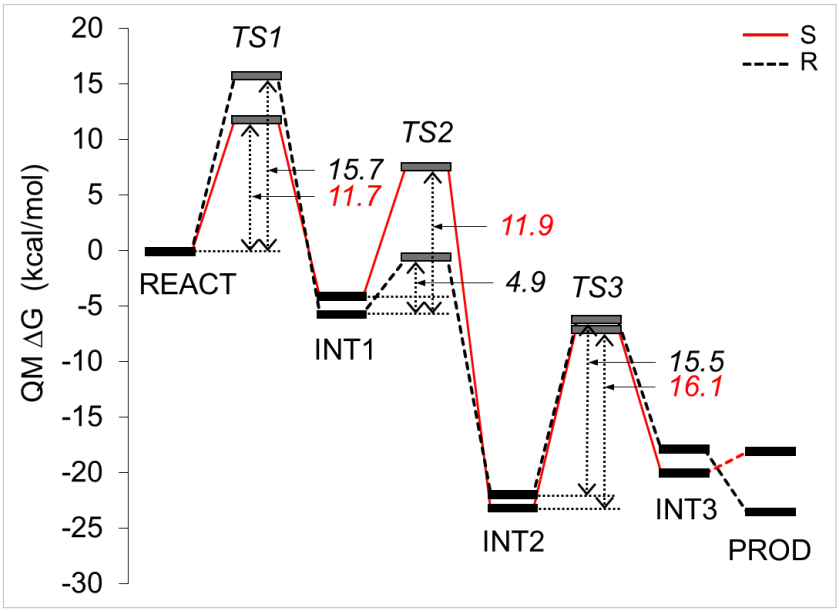

Figure 4.13 QM ΔG reaction profile of both (*S*)- and (*R*)- products for the co-catalytic reaction.

The mechanism of DA reaction catalyzed by CPA and *t*Bu-TBO is proposed according to Figure 4.14. The stationary points corresponding to the (*S*)- and (*R*)-products in the co-catalytic system are illustrated in Figure 4.15 and 4.16, respectively. The strong acidity of CPA and the strong basicity of TBO result in rapid proton transfers from CPA to TBO. Thus, the starting optimized geometry consists of the *o*-hydroxystyrene as *o*-QM, the azlactone in enol form, the deprotonated CPA, and the protonated TBO in **REACT**. The resulting complex model are tightly bound together due to the strong electrostatic attraction between CPA anion and TBO cation and H-bonding interactions with the o-QM and the azlactone. This provides a suitable chiral environment for subsequent enantioselective transformations, leading to highly enantioselective process in comparison to the mono-catalytic system.

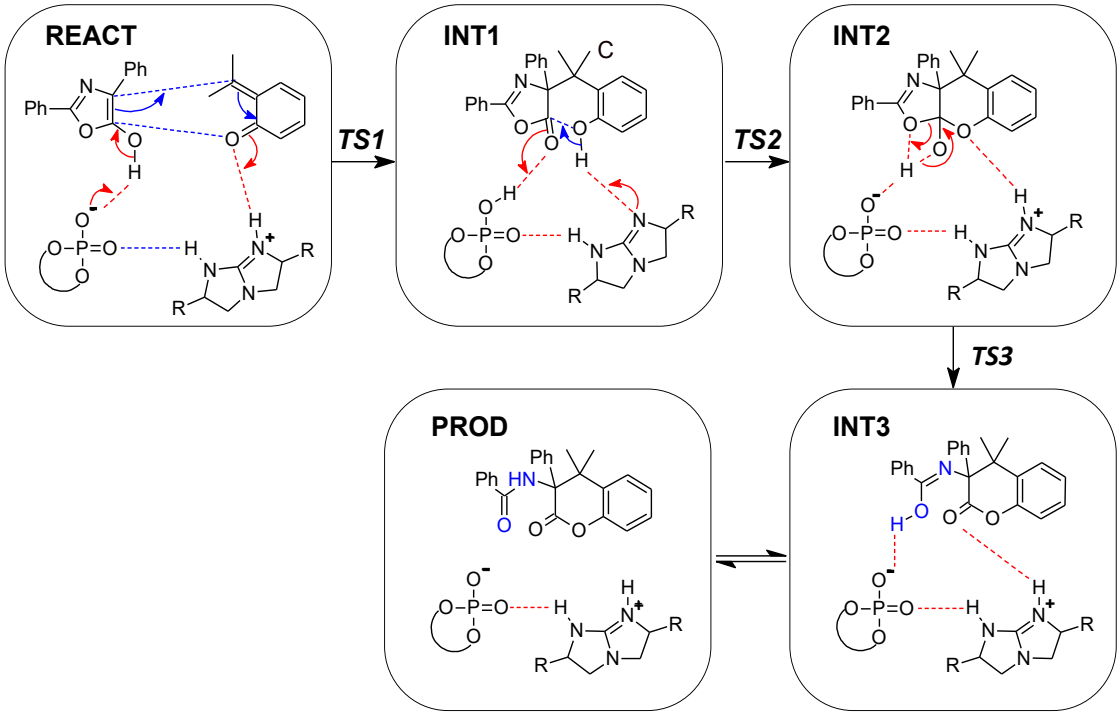

Figure 4.14 Schematic 2D illustration of the catalytic DA mechanism observed for chiral phosphoric acid merging with chiral bicyclic guanidine catalyst.

In step 1, CPA anion, which can act as a conjugated base, accepts a proton from the azlactone enol to form the azlactone enolate with the negative charge on the oxygen atom, facilitating the nucleophilic addition with the *o*-QM styrene to give a

dearomatized complex in **INT1** via C-C bond formation, and the TBO is regenerated. The bond formation occurs in in an asynchronous manner at TS1 in which the difference between the C---C and C---O bond distances in **TS1-S** is found to be 1.12 Å compared to 0.93 Å in **TS1-R**. The barrier to reaction for **TS1-S** is 11.7 kcal/mol lower in energy than the (*R*)-isomer. The activation barriers for TS1 are higher than those observed in the mono-catalytic process. This is a reflection of the instability of starting substrates in the co-catalytic system.

In step 2, The TBO base abstracts a proton from the hydroxyl group of the dearomatized complex, promoting ring closure to generate the DA adduct in INT2 via C-O fond formation (**TS2**), and followed by the subsequent protonation of CPA. The barriers to reaction for **TS2-R** is found to be 4.9 kcal/mol, which 7.0 kcal/mol lower in energy than the (*S*)-isomer, with the same C---O bond distances of 2.13 Å. The C-O bond length of the **INT2** cycloadducts are approximately 1.42 Å.

Finally, in step 3, CPA again functions as the base to remove a proton from the hydroxyl group of the cycloadduct, leading to ring-opening reaction and resulting in INT3. The activation energies required for C–O bond cleavage via **TS3-S** and **TS3-R** are 16.1 and 15.5 kcal/mol, respectively. The final product containing the amide group in **PROD** is obtained by subsequent proton rearrangement of the INT3 in enol form. **TS3-S** is found to be the highest barrier for the (*S*)-product (16.1 kcal/mol), while **TS1** and **TS3** are of comparable barrier heights for the (*R*)-product. However, the only 0.6 kcal/mol difference in the barriers for step 3 can be considered that might not be enantiocontrolling step for the reaction. If we consider the formation of the lowest energy structure of **INT2**, the reverse formation of **INT1** requires activation energy more than 30 kcal/mol for the (*S*)-isomer and 21 kcal/mol for the (*R*)-isomer. **TS1** and **TS2** are of comparable energy at approximately 12 kcal/mol for the (*S*)-product.

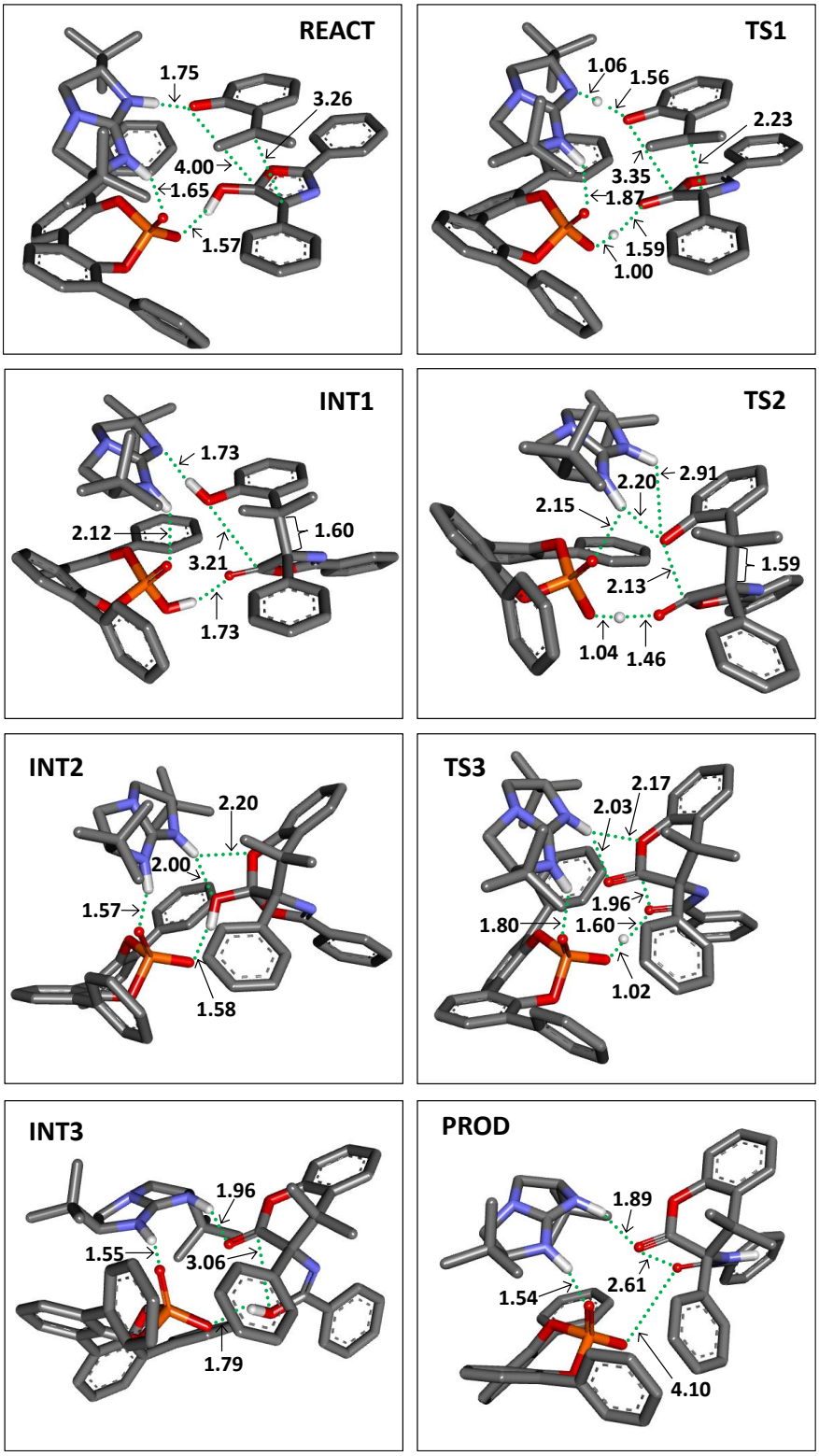

Figure 4.15 QM optimized structures associated with (*S*)-product in co-catalysis obtained at the M06-2X/6-31G*//3-21G level. Polar hydrogens are shown only for clarity. Distances are reported in Angstroms Å.

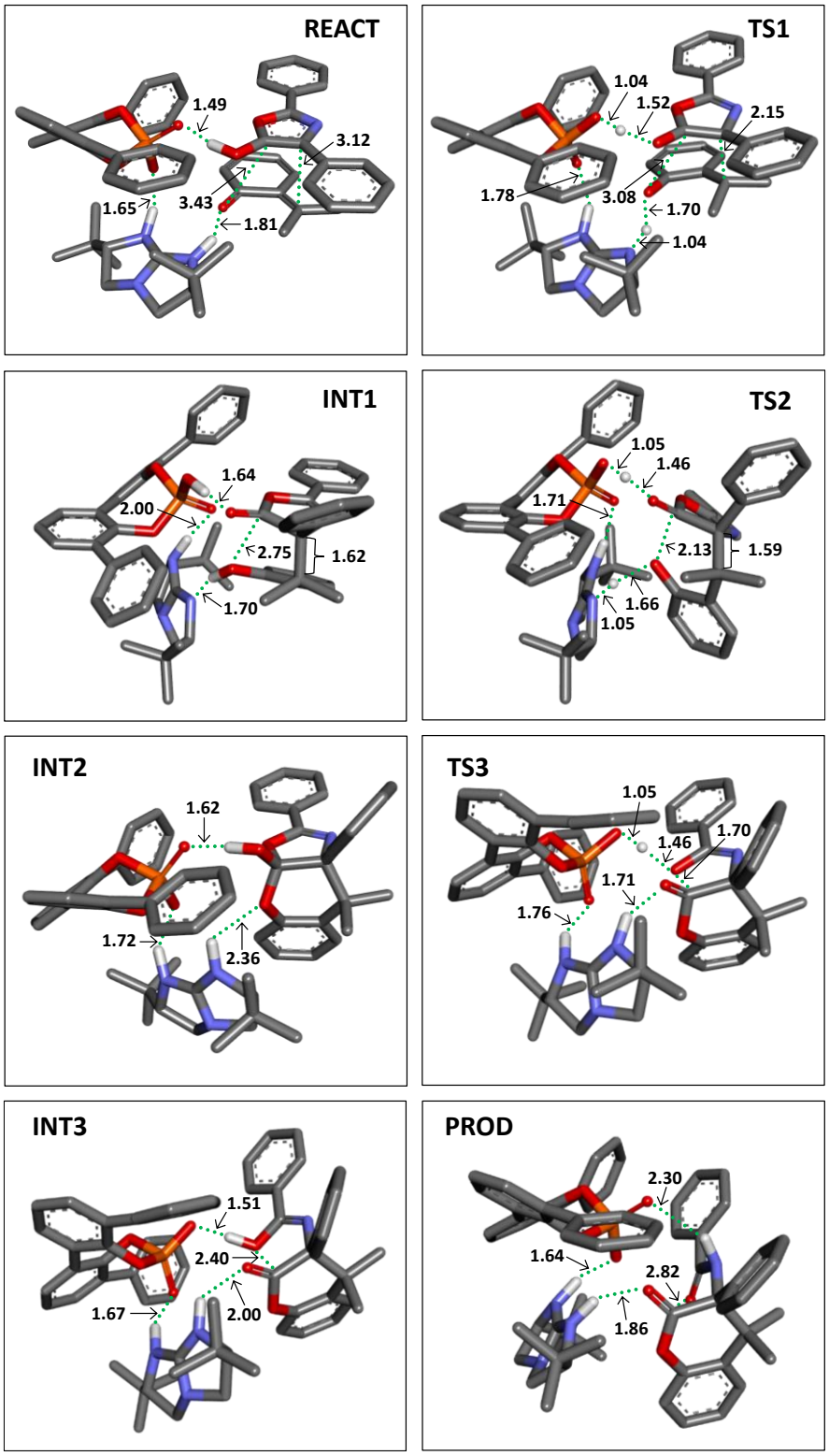

Figure 4.16 QM optimized structures associated with (*R*)-product in co-catalysis obtained at the M06-2X/6-31G*//3-21G level. Polar hydrogens are shown only for clarity. Distances are reported in Angstroms Å.

In contrast to the mono-catalytic system, the origin of the differences in the barrier heights for **TS1** and **TS2** are found to be a direct result of the stability of the transition state structures. Key noncovalent interactions are illustrated in Figure 4.17 and their distances are provided in Table 4.4. **TS1-S** is found to be 4.0 kcal/mol lower than the (*R*)-isomer. While H-bonding interaction is more pronounced in the (*R*)-isomer, the existence of π-stacking interaction (d5) is observed in the (*S*)-isomer and steric repulsion seen between the CPA phenyl rings and the *tert*-butyl groups of TBO (d10, d11, and d13), and between two methyl groups of the styrene and TBO (d8) are also significantly weaker than those seen in **TS1-R**. Moreover, the C-C bond is somewhat elongated in the former (d4, 2.23 Å in TS1-S vs 2.15 Å in TS1-R) that participate in reduction of steric clash between the *tert*-butyl groups of TBO with both the azlactone and CPA. The shorter C-C bond in **TS1-R** also manifest itself bond being formed that is unstable, resulting in the higher TS1 for the (*R*)-isomer. For **TS2**, by contrast, the (*R*)-isomer is found to be 7.0 kcal/mol lower in energy compared to the (*S*)-isomer. Again, this is a result of more effective H-bonding interactions between the N-H groups of TBO with both the dearomatized complex (d1) and CPA (d3), and reduced steric repulsion between the different compounds.

In summary, **TS1** and **TS2** are of comparable energy for the (*S*)-isomer with the barrier of 11.7 and 11.9 kcal/mol, respectively, while **TS1** is found to be the RDS for the (*R*)-product with the barrier of 15.7 kcal/mol. Consequently, the RDS to the formation of the (*S*)-product is lower in energy than that of the (*R*)-product by ~4 kcal/mol.

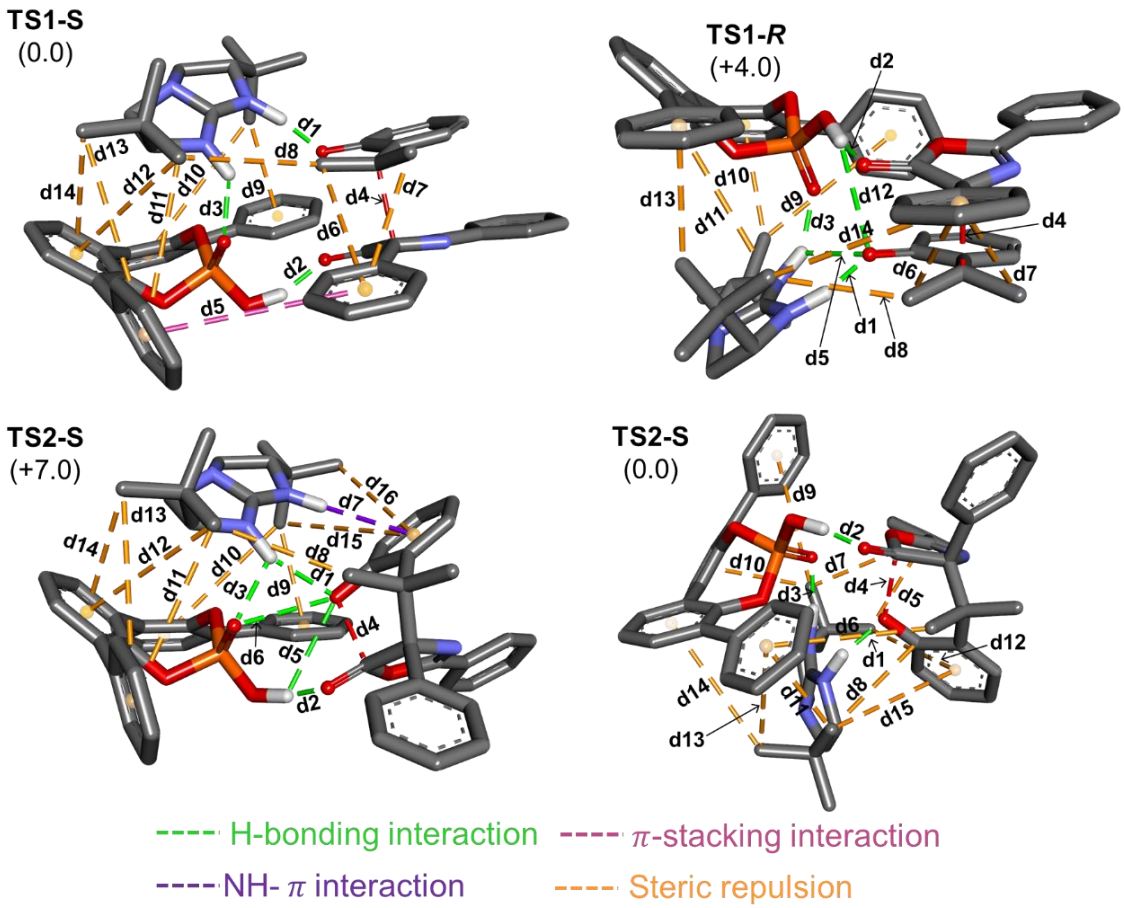

Figure 4.17 3D structures of TS1 and TS2 in co-catalysis of (S)- and (R)- isomers. The values in parentheses are relative Gibbs free energies (in kcal/mol).

Table 4.4 The key interaction distances in the co-catalytic reaction obtained at the QM (M062X/6-31G(d)//3-21G) level of theory (in Angstrom).

Structure	d1	d2	d3	d4	d5	d6	d7	d8	d9	d10	d11	d12	d13	d14	d15	d16
TS1-S	1.56	1.6	1.87	2.23	5.49	4.95	3.83	4.24	3.22	5.28	4.42	4.75	5.32	4.01		
TS1-R	1.70	1.52	1.77	2.15	2.39	3.92	3.93	3.46	4.78	3.37	3.97	3.02	3.32	4.83		
TS2-S	2.20	1.46	2.15	2.13	3.00	3.15	2.85	3.59	3.27	5.00	4.64	4.94	5.28	3.94	5.47	4.17
TS2-R	1.66	1.46	1.71	2.13	3.63	4.57	4.32	3.97	4.62	3.75	3.24	4.88	4.11	4.52	4.93	

4.3 Discussion of enantioselective catalytic reaction

The RDS in the mono-catalytic process is C-O bond-forming step or step 2 for the (*S*)-isomer (12.0 kcal/mol) and ring-opening step or step 3 for the (*R*)-isomer (11.1 kcal/mol). In contrast, the co-catalytic system displays more sizeable differences in the RDS barrier. While the RDS in the co-catalytic reaction is C-C bond-forming step or step 1 for the (*R*)-isomer (~16 kcal/mol) while C-C and C-O bond-forming steps (step 1 and step 2, respectively) are found to be comparable for the (*S*)-isomer (~12 kcal/mol)

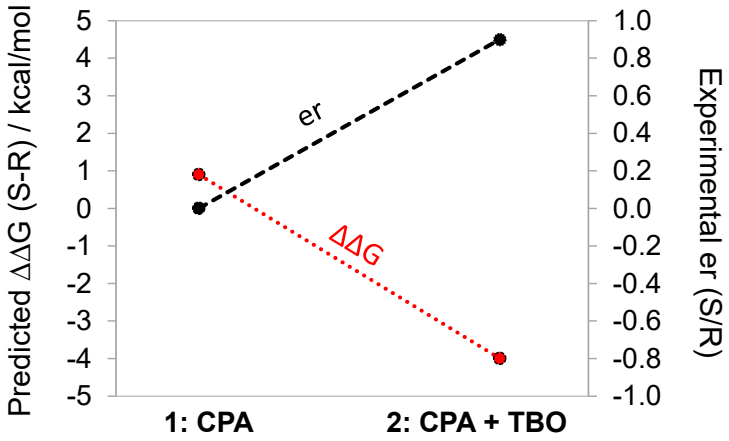

Figure 4.18 The relationship between the RDS energy difference and enantiomeric ratio for mono- and co- catalytic systems.

The difference in the RDS barriers ($\Delta\Delta G^{\ddagger}$) for the mono-catalytic reaction is only 0.9 kcal/mol while the experiment has been shown production of the (*S*)- and (*R*)-products in an almost equal ratios under mono-catalytic condition. It can be expected that the difference in the RDS barriers to reaction should be close to zero. Therefore, the calculated $\Delta\Delta G^{\ddagger}$ in mono-catalysis for the (*S*)-product is approximately the same as that for the (*R*)-product. In contrast, when adding TBO as co-catalyst, an increase in enantioselectivity is observed in which the (*S*)-isomer is found to be a major product with the enantiomeric ratio greater than 80%. It is found to be consistent with the difference in the RDS barriers of approximately 4.0 kcal/mol in favor of the (*S*)-product by the calculations. As a result, the (*S*)-product is heavily favored over the (*R*)-product in good agreement with the experiment.

CHAPTER 5
CONCLUSION

In this research, the enantioselective DA reaction between *o*-hydroxystyrene and azlactone catalyzed by (a) CPA only and by (b) merging CPA and TBO have been studied using DFT calculations in order to obtain the mechanism and explain the enetioselectivity. First of all, the results suggest preference for endo mode of the cycloaddition between *o*-hydroxystyrene and azlactone due to secondary orbital interactions. A stepwise and an asynchronous concerted DA mechanisms are located for the co-catalytic system, but the latter is not observed for the mono-catalytic system. However, it was found that the stepwise DA reaction proceeds via lower activation barrier in comparison to the concerted reaction; thus, energetically favorable for the former pathway has been investigated only. Based on QM calculations, the mono- and co-catalytic processes involving three main steps in which the two first steps are stepwise [4+2] cycloaddition, then followed by ring opening as the final step. Moreover, the results suggest that azlactone is sufficiently basic to act as a base in the catalytic reaction.

The first step is the initial C-C bond formation between the *o*-hydroxystyrene and the azlactone, leading to a dearomatized intermediate. The second step involves ring closure via the second formation of a C-O bond to generate a new six-membered ring or a cycloadduct. The final step is the azlactone ring opening followed by subsequent proton rearrangement, resulting in the formation of the final oxygenous cyclic product. Both CPA and TBO bifunctional catalysts play an important role in instantaneously activating both the *o*-hydroxystyrene and azlactone by hydrogen-bond formations. The noncovalent interactions show a significant contribution to the stability of the structures.

Both the (*S*)- and (*R*)- products in mono-catalytic DA reaction have comparable rate determining steps, corresponding to the asynchronous C-C bond between the dienophile and diene formationin the former, and ring opening in the latter due to the unique three-dimensional CPA arrangement. In the co-catalytic system, the formation

of the (S)-product is more energetically favorable in agreement with experimental observations. This confirms the predictive nature of the models generated here. This research shown that computational simulations offer a means in the future to develop innovative synthetic processes based on chiral catalysts such as CPA and TBO. In addition, the use of 6-31G(d) mixed with 3-21G basis set is sufficient for accurate calculations for this cycloaddition, instead of higher-level QM calculations to further computational expense.

REFERENCES

[1] O. Diels and K. Alder, "Synthesen in der hydroaromatischen Reihe", *Justus Liebigs Annalen der Chemie,* vol. 460 (1928), pp. 98-122.

[2] K. C. Nicolaou, S. A. Snyder, T. Montagnon, and G. Vassilikogiannakis, "The Diels–Alder Reaction in Total Synthesis", *Angewandte Chemie International Edition,* vol. 41 (2002), pp. 1668-1698.

[3] V. Eschenbrenner-Lux, K. Kumar, and H. Waldmann, "The Asymmetric Hetero-Diels–Alder Reaction in the Syntheses of Biologically Relevant Compounds", *Angewandte Chemie International Edition,* vol. 53 (2014), pp. 11146-11157,.

[4] J.-A. Funel and S. Abele, "Industrial Applications of the Diels–Alder Reaction", *Angewandte Chemie International Edition,* vol. 52 (2013), pp. 3822-3863.

[5] M. Gregoritza and F. P. Brandl, "The Diels–Alder reaction: A powerful tool for the design of drug delivery systems and biomaterials", *European Journal of Pharmaceutics and Biopharmaceutics,* vol. 97 (2015), pp. 438-453.

[6] K. Fukui, "Recognition of stereochemical paths by orbital interaction", *Accounts of Chemical Research,* vol. 4 (1971), pp. 57-64.

[7] L. M. Joshel and L. W. Butz, "The Synthesis of Condensed Ring Compounds. VII. The Successful Use of Ethylene in the Diels—Alder Reaction", *Journal of the American Chemical Society,* vol. 63 (1941), pp. 3350-3351.

[8] L. R. Domingo, M. J. Aurell, P. Pérez, and R. Contreras, "Quantitative characterization of the global electrophilicity power of common diene/dienophile pairs in Diels–Alder reactions", *Tetrahedron,* vol. 58 (2002), pp. 4417-4423,.

[9] A. I. Konovalov and V. D. Kiselev, "Diels—Alder reaction. Effect of internal and external factors on the reactivity of diene—dienophile systems", *Russian Chemical Bulletin,* vol. 52 (2003), pp. 293-311.

[10] K. N. Houk, J. Gonzalez, and Y. Li, "Pericyclic Reaction Transition States: Passions and Punctilios, 1935-1995", *Accounts of Chemical Research,* vol. 28 (1995), pp. 81-90.

[11] E. Goldstein, B. Beno, and K. N. Houk, "Density Functional Theory Prediction of the Relative Energies and Isotope Effects for the Concerted and Stepwise Mechanisms

of the Diels–Alder Reaction of Butadiene and Ethylene", *Journal of the American Chemical Society,* vol. 118 (1996), pp. 6036-6043.

[12] K. Itoh, K. Kitoh, and S. Kishimoto, "Concerted and stepwise mechanisms in the Diels–Alder and Michael reactions of furans with methyl 3-nitroacrylate — Experimental and theoretical studies", *Canadian Journal of Chemistry,* vol. 84 (2006), pp. 392-406.

[13] U. Rivero, M. Meuwly, and S. Willitsch, "A computational study of the Diels-Alder reactions between 2,3-dibromo-1,3-butadiene and maleic anhydride", *Chemical Physics Letters,* vol. 683 (2017), pp. 598-605.

[14] K. N. Houk, R. J. Loncharich, J. F. Blake, and W. L. Jorgensen, "Substituent effects and transition structures for Diels-Alder reactions of butadiene and cyclopentadiene with cyanoalkenes", *Journal of the American Chemical Society,* vol. 111 (1989), pp. 9172-9176.

[15] F. Shi, G.-J. Xing, Z.-L. Tao, S.-W. Luo, S.-J. Tu, and L.-Z. Gong, "An Asymmetric Organocatalytic Povarov Reaction with 2-Hydroxystyrenes", *The Journal of Organic Chemistry,* vol. 77 (2012), pp. 6970-6979.

[16] R.-Y. Zhu, C.-S. Wang, J. Zheng, F. Shi, and S.-J. Tu, "Organocatalytic Asymmetric Inverse-Electron-Demand 1,3-Dipolar Cycloaddition of N,N′-Cyclic Azomethine Imines", *The Journal of Organic Chemistry,* vol. 79 (2014), pp. 9305-9312.

[17] H.-H. Zhang, Y.-M. Wang, Y.-W. Xie, Z.-Q. Zhu, F. Shi, and S.-J. Tu, "Organocatalytic Chemo-, (E/Z)- and Enantioselective Formal Alkenylation of Indole-Derived Hydroxylactams Using o-Hydroxystyrenes as a Source of Alkenyl Group", *The Journal of Organic Chemistry,* vol. 79 (2014), pp. 7141-7151.

[18] Y.-C. Zhang, F. Jiang, S.-L. Wang, F. Shi, and S.-J. Tu, "Organocatalytic Chemo- and Regioselective Oxyarylation of Styrenes via a Cascade Reaction: Remote Activation of Hydroxyl Groups", *The Journal of Organic Chemistry,* vol. 79 (2014), pp. 6143-6152.

[19] Y. Liu, H.-H. Zhang, Y.-C. Zhang, Y. Jiang, F. Shi, and S.-J. Tu, "Organocatalytic enantioselective and (Z)-selective allylation of 3-indolylmethanol via hydrogen-bond activation", *Chemical Communications,* vol. 50 (2014), pp. 12054-12057.

[20] Z. Wang, F. Ai, Z. Wang, W. Zhao, G. Zhu, Z. Lin*, et al.*, "Organocatalytic Asymmetric Synthesis of 1,1-Diarylethanes by Transfer Hydrogenation", *Journal of the American Chemical Society,* vol. 137 (2015), pp. 383-389.

[21] W. Dai, H. Lu, X.-L. Jiang, T.-T. Gao, and F. Shi, "Organocatalytic asymmetric hydroarylation of o-hydroxyl styrenes via remote activation of phenylhydrazones", *Tetrahedron: Asymmetry,* vol. 26 (2015), pp. 109-117.

[22] M.-L. Li, D.-F. Chen, S.-W. Luo, and X. Wu, "Chiral Brønsted acid catalyzed intermolecular Friedel–Crafts alkylation of styrenes with indoles: construction of all-carbon quaternary stereocenters", *Tetrahedron: Asymmetry,* vol. 26 (2015), pp. 219-224.

[23] C.-C. Hsiao, S. Raja, H.-H. Liao, I. Atodiresei, and M. Rueping, "Ortho-Quinone Methides as Reactive Intermediates in Asymmetric Brønsted Acid Catalyzed Cycloadditions with Unactivated Alkenes by Exclusive Activation of the Electrophile", *Angewandte Chemie International Edition,* vol. 54 (2015), pp. 5762-5765.

[24] Y.-C. Zhang, Q.-N. Zhu, X. Yang, L.-J. Zhou, and F. Shi, "Merging Chiral Brønsted Acid/Base Catalysis: An Enantioselective [4 + 2] Cycloaddition of o-Hydroxystyrenes with Azlactones", *The Journal of Organic Chemistry,* vol. 81 (2016), pp. 1681-1688.

[25] R. W. Van De Water and T. R. R. Pettus, "*o*-Quinone methides: intermediates underdeveloped and underutilized in organic synthesis", *Tetrahedron,* vol. 58, pp. 5367-5405, 2002.

[26] N. J. Willis and C. D. Bray, "ortho-Quinone Methides in Natural Product Synthesis", *Chemistry – A European Journal,* vol. 18 (2012), pp. 9160-9173.

[27] H. Lv, L. You, and S. Ye, "Enantioselective Synthesis of Dihydrocoumarins via N-Heterocyclic Carbene-Catalyzed Cycloaddition of Ketenes and o-Quinone Methides", *Advanced Synthesis & Catalysis,* vol. 351 (2009), pp. 2822-2826.

[28] J.-J. Zhao, S.-B. Sun, S.-H. He, Q. Wu, and F. Shi, "Catalytic Asymmetric Inverse-Electron-Demand Oxa-Diels–Alder Reaction of In Situ Generated ortho-Quinone Methides with 3-Methyl-2-Vinylindoles", *Angewandte Chemie International Edition,* vol. 54 (2015), pp. 5460-5464.

[29] V. O. Dmitry, A. O. Vitaly, and N. K. Yuri, "ortho-Quinone methides as key intermediates in cascade heterocyclizations", *Russian Chemical Reviews,* vol. 86 (2017), p. 625.

[30] A. A. Jaworski and K. A. Scheidt, "Emerging Roles of in Situ Generated Quinone Methides in Metal-Free Catalysis", *The Journal of Organic Chemistry,* vol. 81 (2016), pp. 10145-10153.

[31] M. Tang, J.-J. Zhao, Q. Wu, M.-S. Tu, and F. Shi, "Organocatalytic Generation of o-Quinone Methides from Commonly Used o-Hydroxystyrenes at High Temperature for Enantioselective Cyclization", *Synthesis,* vol. 49 (2017), pp. 2035-2044.

[32] T.-P. Gao, J.-B. Lin, X.-Q. Hu, and P.-F. Xu, "A catalytic asymmetric hetero-Diels–Alder reaction of olefinic azlactones and isatins: facile access to chiral spirooxindole dihydropyranones", *Chemical Communications,* vol. 50 (2014), pp. 8934-8936.

[33] T.-P. Gao, D. Liu, J.-B. Lin, X.-Q. Hu, Z.-Y. Wang, and P.-F. Xu, "Direct construction of chiral quaternary dihydropyranones through highly enantioselective organocatalytic hetero-Diels–Alder reactions of olefinic azlactones", *Organic Chemistry Frontiers,* vol. 3 (2016), pp. 598-602.

[34] Y. Ying, Z. Chai, H.-F. Wang, P. Li, C.-W. Zheng, G. Zhao*, et al.*, "Bifunctional cinchona alkaloids-catalyzed asymmetric [4+2] cycloaddition reaction of β,γ-unsaturated α-keto esters with oxazolones", *Tetrahedron,* vol. 67 (2011), pp. 3337-3342.

[35] S. Dong, X. Liu, X. Chen, F. Mei, Y. Zhang, B. Gao*, et al.*, "Chiral Bisguanidine-Catalyzed Inverse-Electron-Demand Hetero-Diels–Alder Reaction of Chalcones with Azlactones", *Journal of the American Chemical Society,* vol. 132 (2010), pp. 10650-10651.

[36] P. P. de Castro, G. M. F. Batista, H. F. dos Santos, and G. W. Amarante, "Theoretical Study on the Epimerization of Azlactone Rings: Keto–Enol Tautomerism or Base-Mediated Racemization?", *ACS Omega,* vol. 3 (2018), pp. 3507-3512.

[37] M. Terada and H. Nii, "Highly Stereoselective [4+2] Cycloaddition of Azlactones to β,γ-Unsaturated α-Ketoesters Catalyzed by an Axially Chiral Guanidine Base", *Chemistry – A European Journal,* vol. 17 (2011), pp. 1760-1763.

[38] H. Hu, Y. Liu, J. Guo, L. Lin, Y. Xu, X. Liu*, et al.*, "Enantioselective synthesis of dihydrocoumarin derivatives by chiral scandium(iii)-complex catalyzed inverse-electron-demand hetero-Diels–Alder reaction", *Chemical Communications,* vol. 51 (2015), pp. 3835-3837.

[39] R. A. Mosey, J. S. Fisk, and J. J. Tepe, "Stereoselective syntheses of quaternary substituted **α**-amino acids using oxazol-5-(4H)-ones", *Tetrahedron: Asymmetry,* vol. 19 (2008), pp. 2755-2762.

[40] X.-Y. Yu, J.-R. Chen, Q. Wei, H.-G. Cheng, Z.-C. Liu, and W.-J. Xiao, "Catalytic Asymmetric Cycloaddition of In Situ-Generated ortho-Quinone Methides and Azlactones by a Triple Brønsted Acid Activation Strategy", *Chemistry – A European Journal,* vol. 22 (2016), pp. 6774-6778.

[41] J. Zhou, M.-L. Wang, X. Gao, G.-F. Jiang, and Y.-G. Zhou, "Bifunctional squaramide-catalyzed synthesis of chiral dihydrocoumarins via ortho-quinone methides generated from 2-(1-tosylalkyl)phenols", *Chemical Communications,* vol. 53 (2017), pp. 3531-3534.

[42] L. Zhang, Y. Liu, K. Liu, Z. Liu, N. He, and W. Li, "Asymmetric synthesis of dihydrocoumarins via the organocatalytic hetero-Diels–Alder reaction of ortho-quinone methides", *Organic & Biomolecular Chemistry,* vol. 15 (2017), pp. 8743-8747.

[43] T. Sperger, I. A. Sanhueza, and F. Schoenebeck, "Computation and Experiment: A Powerful Combination to Understand and Predict Reactivities", *Accounts of Chemical Research,* vol. 49 (2016), pp. 1311-1319.

[44] E. J. Corey, "Catalytic Enantioselective Diels–Alder Reactions: Methods, Mechanistic Fundamentals, Pathways, and Applications", *Angewandte Chemie International Edition,* vol. 41 (2002), pp. 1650-1667.

[45] A. Rulcova, I. Prokopova, L. Krausova, M. Bitman, R. Vrzal, Z. Dvorak*, et al.*, "Stereoselective interactions of warfarin enantiomers with the pregnane X nuclear receptor in gene regulation of major drug-metabolizing cytochrome P450 enzymes", *Journal of Thrombosis and Haemostasis,* vol. 8 (2010), pp. 2708-2717.

[46] J. Alemán and S. Cabrera, "Applications of asymmetric organocatalysis in medicinal chemistry", *Chemical Society Reviews,* vol. 42 (2013), pp. 774-793.

[47] I. R. Shaikh, "Organocatalysis: Key Trends in Green Synthetic Chemistry, Challenges, Scope towards Heterogenization, and Importance from Research and Industrial Point of View", *Journal of Catalysts,* pp. 35 (2014).

[48] I. M. J. W. S. PG Andersson, 2008. 231, 2008., "Modern Reduction Methods."

[49] T. Akiyama, J. Itoh, K. Yokota, and K. Fuchibe, "Enantioselective Mannich-Type Reaction Catalyzed by a Chiral Brønsted Acid", *Angewandte Chemie International Edition,* vol. 43 (2004), pp. 1566-1568.

[50] D. Uraguchi and M. Terada, "Chiral Brønsted Acid-Catalyzed Direct Mannich Reactions via Electrophilic Activation", *Journal of the American Chemical Society,* vol. 126 (2004), pp. 5356-5357.

[51] D. Parmar, E. Sugiono, S. Raja, and M. Rueping, "Complete Field Guide to Asymmetric BINOL-Phosphate Derived Brønsted Acid and Metal Catalysis: History and Classification by Mode of Activation; Brønsted Acidity, Hydrogen Bonding, Ion Pairing, and Metal Phosphates", *Chemical Reviews,* vol. 114 (2014), pp. 9047-9153.

[52] K. Kanomata, Y. Toda, Y. Shibata, M. Yamanaka, S. Tsuzuki, I. D. Gridnev*, et al.*, "Secondary stereocontrolling interactions in chiral Brønsted acid catalysis: study of a Petasis–Ferrier-type rearrangement catalyzed by chiral phosphoric acids", *Chemical Science,* vol. 5 (2014), pp. 3515-3523.

[53] J. P. Reid and J. M. Goodman, "Goldilocks Catalysts: Computational Insights into the Role of the 3,3′ Substituents on the Selectivity of BINOL-Derived Phosphoric Acid Catalysts", *Journal of the American Chemical Society,* vol. 138 (2016), pp. 7910-7917.

[54] R. B. Sunoj, "Transition State Models for Understanding the Origin of Chiral Induction in Asymmetric Catalysis", *Accounts of Chemical Research,* vol. 49 (2016), pp. 1019-1028.

[55] R. Maji, S. C. Mallojjala, and S. E. Wheeler, "Chiral phosphoric acid catalysis: from numbers to insights," *Chemical Society Reviews,* vol. 47, pp. 1142-1158, 2018.

[56] I. D. Gridnev, M. Kouchi, K. Sorimachi, and M. Terada, "On the mechanism of stereoselection in direct Mannich reaction catalyzed by BINOL-derived phosphoric acids", *Tetrahedron Letters,* vol. 48 (2007), pp. 497-500.

[57] T. Marcelli, P. Hammar, and F. Himo, "Phosphoric Acid Catalyzed Enantioselective Transfer Hydrogenation of Imines: A Density Functional Theory Study of Reaction

Mechanism and the Origins of Enantioselectivity", *Chemistry – A European Journal,* vol. 14 (2008), pp. 8562-8571.

[58] L. Simón and J. M. Goodman, "A Model for the Enantioselectivity of Imine Reactions Catalyzed by BINOL–Phosphoric Acid Catalysts", *The Journal of Organic Chemistry,* vol. 76 (2011), pp. 1775-1788.

[59] C. Palomo, M. Oiarbide, and R. López, "Asymmetric organocatalysis by chiral Brønsted bases: implications and applications", *Chemical Society Reviews,* vol. 38 (2009), pp. 632-653.

[60] D. Leow and C.-H. Tan, "Chiral Guanidine Catalyzed Enantioselective Reactions", *Chemistry – An Asian Journal,* vol. 4 (2009), pp. 488-507.

[61] D. Leow and C.-H. Tan, "Catalytic Reactions of Chiral Guanidines and Guanidinium Salts," *Synlett*, pp. 1589-1605 (2010).

[62] Z. Jiang, Y. Pan, Y. Zhao, T. Ma, R. Lee, Y. Yang*, et al.*, "Synthesis of a Chiral Quaternary Carbon Center Bearing a Fluorine Atom: Enantio- and Diastereoselective Guanidine-Catalyzed Addition of Fluorocarbon Nucleophiles", *Angewandte Chemie International Edition,* vol. 48 (2009), pp. 3627-3631.

[63] M. W. Wong and A. M. E. Ng, "Asymmetric Michael Addition Using Bifunctional Bicyclic Guanidine Organocatalyst: A Theoretical Perspective", *Australian Journal of Chemistry,* vol. 67 (2014), pp. 1100-1109.

[64] B. Cho, C.-H. Tan, and M. W. Wong, "Origin of Asymmetric Induction in Bicyclic Guanidine-Catalyzed Thio-Michael Reaction: A Bifunctional Mode of Lewis Acid-Brønsted Acid Activation", *The Journal of Organic Chemistry,* vol. 77 (2012), pp. 6553-6562.

[65] Y. Shibata and M. Yamanaka, "DFT Study of the Mechanism and Origin of Enantioselectivity in Chiral BINOL-Phosphoric Acid Catalyzed Transfer Hydrogenation of Ketimine and α-Imino Ester Using Benzothiazoline", *The Journal of Organic Chemistry,* vol. 78 (2013), pp. 3731-3736.

[66] T. A. K. R. D. Dennington, and J. M. Millam, GaussView 5.0.8, Gaussian, 2008.

[67] M. Yamanaka, J. Itoh, K. Fuchibe, and T. Akiyama, "Chiral Brønsted Acid Catalyzed Enantioselective Mannich-Type Reaction", *Journal of the American Chemical Society,* vol. 129 (2007), pp. 6756-6764.

[68] X. Tian, N. Hofmann, and P. Melchiorre, "Asymmetric Vinylogous Diels–Alder Reactions Catalyzed by a Chiral Phosphoric Acid", *Angewandte Chemie International Edition,* vol. 53 (2014), pp. 2997-3000.

[69] M. Terada, "Axially Chiral Guanidines as Efficient Brønsted Base Catalysts for Enantioselective Transformations", *Journal of Synthetic Organic Chemistry, Japan,* vol. 68 (2010), pp. 1159-1168.

[70] M. J. Frisch, G. W. Trucks, H. B. Schlegel, G. E. Scuseria, M. A. Robb, J. R. Cheeseman*, et al.*, *Gaussian 09 Revision A.02*: Gaussian Inc. Wallingford CT 2009 (2009).

[71] Y. Zhao and D. G. Truhlar, "The M06 suite of density functionals for main group thermochemistry, thermochemical kinetics, noncovalent interactions, excited states, and transition elements: two new functionals and systematic testing of four M06-class functionals and 12 other functionals", *Theoretical Chemistry Accounts,* vol. 120 (2008), pp. 215-241.

[72] Y. Zhao and D. G. Truhlar, "Density Functionals with Broad Applicability in Chemistry", *Accounts of Chemical Research,* vol. 41 (2008), pp. 157-167.

[73] M. Linder and T. Brinck, "Stepwise Diels–Alder: More than Just an Oddity? A Computational Mechanistic Study", *The Journal of Organic Chemistry,* vol. 77 (2012), pp. 6563-6573.

[74] M. Linder and T. Brinck, "On the method-dependence of transition state asynchronicity in Diels–Alder reactions", *Physical Chemistry Chemical Physics,* vol. 15 (2013), pp. 5108-5114.

[75] G. Gaddamanugu, *Performance of ab initio and DFT methods in modeling Diels-Alder reactions* vol. 50 (2011).

[76] G. Ujaque, P. S. Lee, K. N. Houk, M. F. Hentemann, and S. J. Danishefsky, "The Origin of endo Stereoselectivity in the Hetero-Diels–Alder Reactions of Aldehydes with ortho-Xylylenes: CH–**π**, **π**–**π**, and Steric Effects on Stereoselectivity", *Chemistry – A European Journal,* vol. 8 (2002), pp. 3423-3430.

[77] J. I. García, J. A. Mayoral, and L. Salvatella, "Do Secondary Orbital Interactions Really Exist?", *Accounts of Chemical Research,* vol. 33, pp. 658-664, 2000.

[78] C. S. Wannere, A. Paul, R. Herges, K. N. Houk, H. F. Schaefer Iii, and P. Von Ragué Schleyer, "The existence of secondary orbital interactions", *Journal of Computational Chemistry,* vol. 28 (2007), pp. 344-361.

[79] M. O. Sinnokrot and C. D. Sherrill, "Highly Accurate Coupled Cluster Potential Energy Curves for the Benzene Dimer: Sandwich, T-Shaped, and Parallel-Displaced Configurations", *The Journal of Physical Chemistry A,* vol. 108 (2004), pp. 10200-10207.

[80] G. B. McGaughey, M. Gagné, and A. K. Rappé, "**π**-Stacking Interactions: ALIVE AND WELL IN PROTEINS", *Journal of Biological Chemistry,* vol. 273 (1998), pp. 15458-15463.

APPENDIX

APPENDIX A: Supporting Information

Table S1. The key distances obtained from DFT calculation at the M06-2X/6-31G*//3-21G level (in Angstroms Å).

(a) Mono-catalytic condition

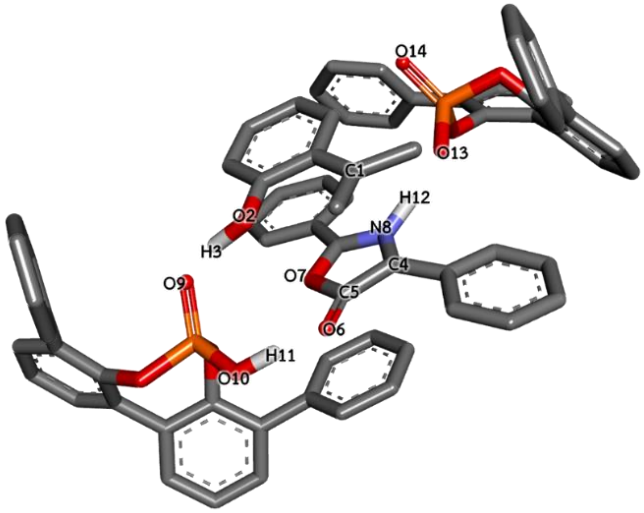

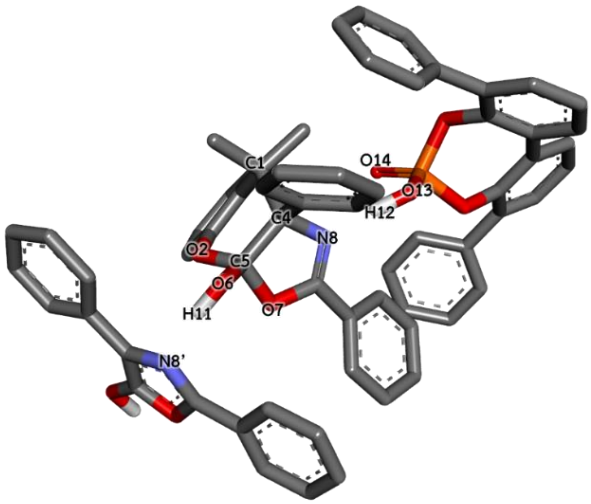

(*S*)-product	REACT	TS1	INT1	TS2	INT2-b (INT2-a)	TS3-b (TS3-a)	PROD
C1-C4	2.853	2.559	1.612	1.587	1.573 (1.576)	1.586 (1.577)	1.581
O2-C5	3.092	3.009	2.656	1.769	1.397 (1.396)	1.330 (1.364)	1.355
O2-H3	1.002	0.994	0.982	1.091	1.920	2.676	5.198
H3-O9	1.613	1.665	1.754	1.36	0.981	1.140	5.399
O6-H11	1.444	1.538	1.684	1.145	0.990 (0.991)	1.462 (1.514)	1.914

O10-H11 (N8'-H11)	1.050	1.023	0.998	1.261	1.724 (1.833)	1.044 (1.080)	0.983
N8-H12	1.070	1.081	1.630	1.578	1.555 (1.536)	1.054 (1.047)	1.019
H8-O13	1.536	1.492	1.027	1.037	1.043 (1.051)	1.680 (1.681)	1.808
C5-O7	1.393	1.393	1.360	1.386	1.470 (1.453)	2.334 (1.901)	2.559
H3-O7	2.982	2.962	2.989	2.411	1.920	1.256	5.895

(*R*)-product	REACT	TS1	INT1	TS2	INT2-b (INT2-a)	TS3-b (TS3-a)	PROD
C1-C4	2.890	2.523	1.598	1.577	1.570 (1.574)	1.584 (1.590)	1.575
O2-C5	3.094	3.031	2.472	1.757	1.402 (1.398)	1.322 (1.338)	1.360
O2-H3	1.004	0.993	0.985	1.090	2.590	2.654	7.142
H3-O9	1.602	1.661	1.723	1.353	0.983	1.046	5.732
O6-H11	1.443	1.568	1.696	1.174	0.987 (0.993)	1.252 (1.364)	2.420
O10-H11 (N8'-H11)	1.052	1.019	0.998	1.232	1.780 (1.799)	1.161 (1.147)	0.992
N8-H12	1.064	1.074	1.619	1.572	1.584 (1.507)	1.043 (1.038)	1.017
H12-O13	1.574	1.553	1.027	1.037	1.038 (1.062)	1.766 (1.765)	2.069
C5-O7	1.392	1.393	1.363	1.390	1.463 (1.447)	2.451 (2.167)	2.800
H3-O7	2.890	2.908	2.842	2.459	1.836	1.534	5.881

(b) Co-catalytic condition

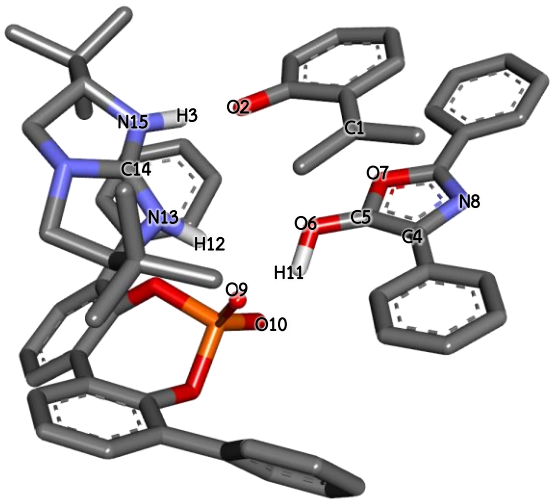

(*S*)-product	REACT	TS1	INT1	TS2	INT2	TS3	INT3	PROD
C1-C4	3.264	2.23	1.607	1.595	1.571	1.574	1.573	1.587
O2-C5	4.004	3.351	3.21	2.129	1.414	1.397	1.356	1.363
O2-H3	1.753	1.561	1.004	2.908	2.203	2.173	2.368	2.643
H3-N15	1.027	1.065	1.732	1.023	1.022	1.022	1.021	1.021
O2-H12	3.858	3.534	2.432	2.2	4.423	4.03	4.497	4.852
H12-N13	1.039	1.020	1.014	1.029	1.055	1.029	1.062	1.069
O9-H12	1.657	1.869	2.123	2.153	1.573	1.798	1.554	1.541
O10-H11	1.570	1.004	0.984	1.040	1.587	1.018	1.789	5.835
H11-O6	1.012	1.597	1.732	1.460	1.016	2.393	2.468	4.339
C5-O7	1.357	1.366	1.360	1.383	1.432	1.962	3.097	2.613
H3-O6	4.425	4.264	3.807	5.514	1.998	2.029	1.963	1.891
H12-O6	4.286	3.832	3.825	3.791	2.867	2.043	2.765	2.883
H11-O7	3.089	3.697	3.694	2.912	2.488	1.603	0.996	3.147
N8-H11	4.092	4.887	5.14	4.701	3.785	3.370	2.663	1.010

(*R*)-product	REACT	TS1	INT1	TS2	INT2	TS3	INT3	PROD
C1-C4	3.123	2.148	1.622	1.59	1.585	1.584	1.578	1.593
O2-C5	3.431	3.075	2.748	2.125	1.421	1.418	1.358	1.344
O2-H3	1.805	1.698	1.012	1.656	2.355	2.574	2.904	2.856
H3-N15	1.022	1.038	1.7	1.054	1.015	1.045	1.02	1.024
O2-H12	2.671	2.386	3.78	3.105	4.175	4.023	4.332	4.223
H12-N13	1.047	1.032	1.018	1.032	1.038	1.028	1.043	1.049
O9-H12	1.646	1.775	2.002	1.714	1.715	1.764	1.671	1.640
O10-H11	1.488	1.035	1.001	1.049	1.621	1.046	1.514	2.297
H11-O6	1.032	1.597	1.643	1.461	1.002	2.489	2.939	2.713
C5-O7	1.351	1.357	1.347	1.383	1.431	1.699	2.403	2.823
H3-O6	3.456	4.264	3.678	3.586	3.497	1.712	2.002	1.862
H12-O6	4.540	4.477	5.655	4.522	5.431	4.138	4.427	3.737
H11-O7	2.335	2.454	2.386	2.482	2.349	1.462	1.022	3.034
N8-H11	4.101	4.411	4.425	4.445	3.992	3.340	3.002	1.024

Table S2. Mulliken charges distribution of each molecule in the system calculated by M06-2X/6-31G*//3-21G basis set.

CPA leading to the (*S*)-product

Molecules	REACT	TS1	INT1	TS2	INT2	TS3	INT3	PROD
o-Hydroxystyrene	0.646	0.533	0.064	0.678	0.068	0.097	0.722	-0.019
Azlactone	0.136	0.228			(0.035)	(-0.028)		
CPA1	-0.729	-0.723	-0.041	-0.060	-0.083 (-0.086)	-0.755 (-0.757)	-0.736	0.042
CPA2 (Azlactone)	-0.053	-0.038	-0.023	-0.618	0.016 (0.051)	0.657 (0.785)	0.014	-0.023
Total Charge	0.000	0.000	0.000	0.000	0.000	0.000	0.000	0.000

CPA leading to the (*R*)-product

Molecules	REACT	TS1	INT1	TS2	INT2	TS3	INT3	PROD
o-Hydroxystyrene	0.641	0.493	0.062	0.667	0.045	0.080	0.695	-0.011
Azlactone	0.126	0.255			(0.025)	(-0.014)		
CPA1	-0.747	-0.742	-0.068	-0.077	-0.078 (-0.094)	-0.759 (-0.773)	-0.725	0.023
CPA2 (Azlactone)	-0.019	-0.006	0.006	-0.590	0.033 (0.069)	0.678 (0.786)	0.030	-0.013
Total Charge	0.000	0.000	0.000	0.000	0.000	0.000	0.000	0.000

CPA + *t*Bu-TBO leading to the (*S*)-product

Molecules	REACT	TS1	INT1	TS2	INT2	TS3	INT3	PROD
o-Hydroxystyrene	0.013	-0.366	-0.067	-0.723	-0.075	-0.790	0.015	0.068
Azlactone	-0.069	-0.378						
CPA	-0.711	-0.001	0.019	-0.067	-0.725	-0.042	-0.768	-0.809
Guanidine	0.767	0.745	0.049	0.790	0.800	0.832	0.753	0.741
Total Charge	0.000	0.000	0.000	0.000	0.000	0.000	0.000	0.000

CPA + *t*Bu-TBO leading to the (*R*)-product

Molecules	REACT	TS1	INT1	TS2	INT2	TS3	INT3	PROD
o-Hydroxystyrene	-0.050	-0.399	-0.053	-0.722	-0.075	-0.734	-0.053	0.017
Azlactone	-0.037	-0.361						
CPA	-0.702	-0.023	-0.002	-0.019	-0.738	-0.044	-0.742	-0.773
Guanidine	0.788	0.783	0.055	0.740	0.813	0.777	0.794	0.755
Total Charge	0.000	0.000	0.000	0.000	0.000	0.000	0.000	0.000

Table S3 Computational details in this study.

System	Details	3-21G/6-31G*	6-31+G**	6-311+G**	6-311++G**
Mono-catalysis	Atoms	80+61	141	141	141
	Basis function	1082	1917	2238	2293
	Primitive Gaussian	2020	3185	3564	3619
	α e^-	306	306	306	306
	β e^-	306	306	306	306
Co-catalysis	Atoms	66+70	136	136	136
	Basis function	992	1076	1992	2955
	Primitive Gaussian	1870	2809	3146	3209
	α e^-	264	264	264	264
	β e^-	264	264	264	264

APPENDIX B: Publication

The Journal of Organic Chemistry, vol. 84 (2019), pp 4025–4032

JOC The Journal of Organic Chemistry Article
Cite This: J. Org. Chem. 2019, 84, 4025−4032 pubs.acs.org/joc

Theoretical Investigation of the Enantioselective [4 + 2] Cycloaddition Reaction of *o*-Hydroxystyrene and Azlactone

Napassorn Jensupakarn,[†] M. Paul Gleeson,*[,‡] Duangkamol Gleeson,[§] and Kanokthip Boonyarattanakalin*[,†]

[†]College of Nanotechnology, King Mongkut's Institute of Technology Ladkrabang, Bangkok 10520, Thailand
[‡]Department of Biomedical Engineering, King Mongkut's Institute of Technology Ladkrabang, Bangkok 10520, Thailand
[§]Faculty of Science, King Mongkut's Institute of Technology Ladkrabang, Bangkok 10520, Thailand

Supporting Information

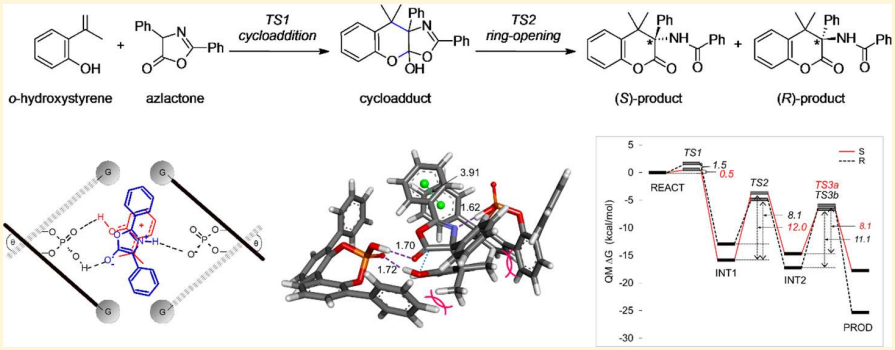

ABSTRACT: Theoretical studies have been undertaken to rationalize the origin of the enantioselective Diels−Alder reaction (DA) of *o*-hydroxystyrene and azlactone catalyzed by (a) chiral BINOL-phosphoric acid (CPA) and (b) CPA and chiral guanidine (TBO). The sequence of events leading to increased enantioselectivity under the latter conditions have been studied using density functional theory (DFT) methods. The computational results indicate that both the mono- and co-catalytic processes proceed via stepwise [4 + 2] cycloaddition reactions involving three steps, which are (1) C−C bond formation, (2) C−O bond formation, and (3) the opening of the azlactone ring. This results in the formation of an oxygenous cycle with one chiral center. The origin of greater enantioselectivity under the latter catalytic conditions are discussed in terms of the structural characteristics and energetics of the intermediates and transition states formed on the potential energy surface of the competing reactions.

1. INTRODUCTION

The Diels−Alder (DA) reaction is one of the most important reactions used for synthesis of carbo- and heterocyclic compounds in organic chemistry.[1] It is formally a [4 + 2] cycloaddition reaction of a conjugated diene and a dienophile, which react to produce a molecule with an unsaturated six-membered ring by the formation of two new chemical bonds in either a one-step or a two-step mechanism. The stepwise pathway involves two transition states (TSs) separated by an intermediate that is either diradical or zwitterionic in nature, which is then followed by ring closure. A difference in the lengths of the two bonds being formed indicate an asynchronous process, which is expected to result in enhanced charge transfer and lower activation barriers.[2] DA reactions can be activated by the substitution of electron donating or withdrawing groups on the diene or the dienophile, or external factors such as catalysts can be used to influence the reaction mechanism and the product compositions.[3] DA cycloaddition reactions are heavily utilized in pharmaceutical and agrochemical applications[4] and have been extensively studied from an experimental and theoretical point of view.[5]

Enantioselective DA reactions make use of chiral catalysts[6] which can not only accelerate the rate of reactions but also enhance product selectivity in comparison with uncatalyzed processes. Catalytic asymmetric DA reactions have been widely used for the synthesis of cyclohexene frameworks with up to four contiguous stereocenters.[7]

The Shi group[8] recently demonstrated the enantioselective [4 + 2] cycloaddition of *o*-hydroxystyrene and azlactone to produce a dihydrocoumarin scaffold, an important structural unit in numerous natural product and pharmaceutical molecules.[9] The [4 + 2] cycloaddition could be catalyzed by chiral BINOL-phosphoric acid (CPA) and chiral five-membered bicyclic guanidine (TBO) as chiral Brønsted acid and chiral Brønsted base catalysts, respectively (Scheme 1). The distribution of *S* and *R* enantiomers was found to depend

Received: January 4, 2019
Published: March 6, 2019

DOI: 10.1021/acs.joc.9b00032
J. Org. Chem. 2019, 84, 4025−4032

The Journal of Organic Chemistry Article

Scheme 1. Overall Reaction Consisting of [4 + 2] Cycloaddition and Ring Opening

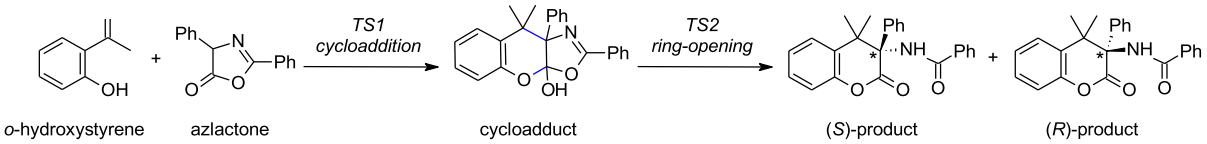

heavily on the nature of the diene, the dienophile, and the catalyst combination used. The *S*-configured product is found to predominate under conditions involving a chiral Brønsted acid and a base such as CPA and TBO, whereas in the presence of a chiral Brønsted acid alone, products are found to display much lower enantioselectivity. Indeed, CPAs are proven organocatalysts for numerous enantioselective DA cycloadditions acting in a bifunctional way to activate the electrophile, the nucleophile, or both.[10] The proposed mechanism reaction was suggested to proceed via a [4 + 2] cycloaddition process followed by ring opening to afford the final product.

In the presence of CPA, *o*-hydroxystyrene can be converted into either a highly reactive carbocation or its resonance structure, *o*-quinone methide (*o*-QM) intermediate, by protonation.[11] Azlactone can be utilized as a suitable reaction partner in a number of catalytic cycloaddition reactions due to its multiple reactive sites.[12] The latter can be activated by the Brønsted basic site of CPA to form an enolate intermediate by deprotonation followed by nucleophilic attack and ring opening.[13] Studies have shown that reactions with CPA can proceed via a bifunctional activation mode to provide an oxo-heterocycle with high enantioselectivity.[14] However, the enantioselective role of TBO-catalyzed DA cycloadditions reactions remain less explored.[15] It can be envisaged that multiple noncovalent interactions among CPA, TBO, the diene, and the dienophile are critical for controlling the enantioselectivity.[16]

In this work we have employed computational chemistry methods to explore the enantioselective catalytic mechanisms of *o*-hydroxystyrene and azlactone using the catalysts CPA and TBO. Electronic structure calculations have been undertaken to model the minimum and transition state structures of the DA reaction in the presence of (a) CPA and (b) CPA and TBO. We have employed density functional theory (DFT) gas-phase cluster models to construct potential energy surfaces for both isomers under the two mono- and co-catalytic conditions. From a consideration of the structures and energies obtained, we discuss the origin of the stereoselectivity observed, which by extension could be exploited in the design of future enantioselective DA reactions.

2. COMPUTATIONAL METHODS

Simulations of the DA reactions have been evaluated in the gas phase using *o*-hydroxystyrene as the diene and azlactone as the dienophile, as shown in Figure 1. These structures were simulated in their higher energy tautomeric form (Figure 2). (*R*)-BINOL-derived chiral phosphoric acid (CPA) substituted with phenyl groups at the 3- and 3′-positions and chiral bicyclic guanidine (1,4,6-triazabicyclo[3.3.0]oct-4-ene; TBO) bearing two *tert*-butyl groups were used for Brønsted acid and base catalysts, respectively (Figure 1).

Two separate catalytic systems were evaluated: namely, the mono-catalytic and co-catalytic systems. DA reactions using each model were undertaken to evaluate the endo *Si* face and *Re* face attacks in order to explain the origin of the enantioselectivity. Two molecules of

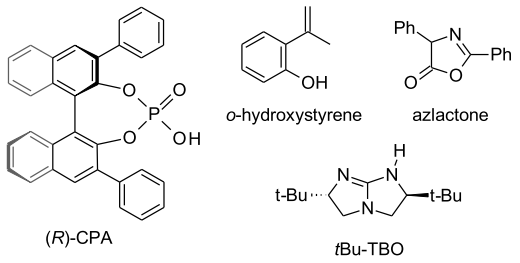

Figure 1. Molecular models used for computational calculations.

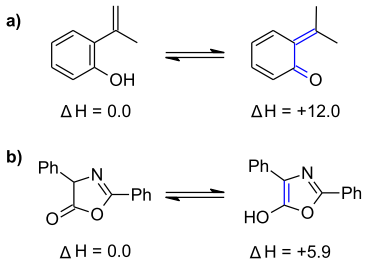

Figure 2. *o*-Hydroxystyrene (diene) and azactone (dienophile) tautomers and their relative energies (kcal/mol) at the M06-2X/6-31+G(d,p) level of theory.

CPA were used in monocatalysis to facilitate the required acid/base transfer processes in line with others.[17] The naphthalene ring of (*R*)-BINOL (gray color in Figure 1) was removed for computational efficiency similar to the case in other studies.[13]

The QM calculations were performed in the Gaussian 09[18] package. Density functional theory (DFT) calculations used the M06-2X functional[18] as recommended by Linder and Brinck.[5b,19] The 6-31G(d) basis set[20] was used for all atoms involved in bond breaking, formation, and H-bonding. The 3-21G basis set was used for the phenyl substituents of CPA and t*Bu* of TBO, as these play a primarily a steric role. All structures were fully optimized at the M06-2X/6-31G(d):3-21G level of theory in the gas phase. Single-point energies at the M06-2X/6-31+G(d,p) were subsequently obtained. Vibrational analysis was undertaken to confirm the identity of all stationary points obtained and to allow for the determination of the Gibbs free energy corrections to the reaction profile.

3. RESULTS

The structures and energetics of the mono- and co-catalytic models were assessed in terms of both the *si* and *re* based mechanisms. In principle the DA mechanism can be either concerted or stepwise; hence, both possible mechanisms were taken into consideration. Both concerted and stepwise DA reactions were investigated; however, only the latter was observed. Consequently, we report the stepwise reaction pathway for the systems according to Scheme 2. The energies of the stationary points obtained for the endo *si*- and *re*-DA mechanisms are given in Table 1. The stationary points for the *R* product from the mono-catalytic process and the *S* product for the co-catalytic process are illustrated in Figures 3 and 5, respectively. Illustrations of the stationary points of the

DOI: 10.1021/acs.joc.9b00032
J. Org. Chem. 2019, 84, 4025−4032

Scheme 2. 2D Illustration of (a) the DA Mechanism Catalyzed by Chiral Phosphoric Acid and (b) Catalytic DA Mechanism Observed for Chiral Phosphoric Acid Combined with Chiral Guanidine Catalyst

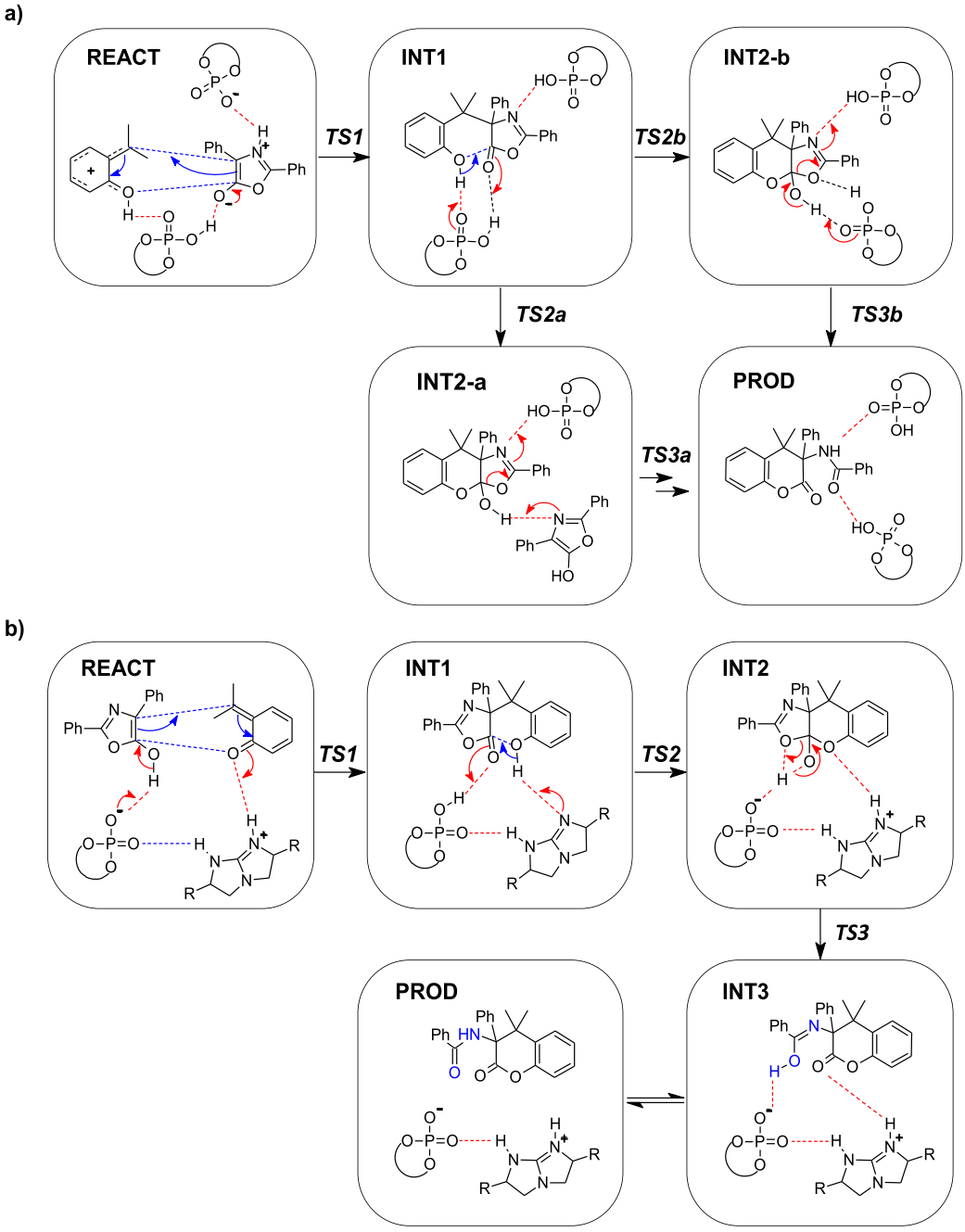

remaining two mechanisms evaluated can be found in Figures S3 and S4 in the Supporting Information. The sum of the Mulliken charge on each structure has been compiled and can be found in Table S1.

Both reactions occur via high-energy tautomers of each reagent (Figure 2). The *o*-hydroxystyrene diene tautomer is 12.0 kcal/mol higher in energy than the corresponding enol on the basis of isolated gas-phase calculations at the M06-2X/6-31+G(d,p) level. In comparison, the azlactone requires 5.9 kcal/mol to adopt the requisite enol conformation needed to undergo reaction.[8] Interestingly, modeling the reagents in these tautomers alongside CPA and/or TBO led to additional proton rearrangement (Scheme 2). In the *R* mono-catalytic system proton transfer from one acidic CPA molecule to the oxazole nitrogen results in the transfer of the azlactone enol proton to the *o*-hydroxystyrene ketone. In the co-catalytic system, by contrast, proton transfer from CPA to TBO is observed in the initial cluster model.

3.1. Mono-catalytic System. The optimized mono-catalytic model consists of the azlactone, *o*-hydroxystyrene, and two CPA molecules to facilitate the DA reaction. The *si* and *re* models are similar in terms of the interaction made but differ subtly in terms of their 3D orientation due to the steric effect of the CPA phenyl rings (Figure 3). The nitrogen atom

DOI: 10.1021/acs.joc.9b00032
J. Org. Chem. 2019, 84, 4025−4032

Table 1. Computed Relative Gibbs Free Energies of Stationary Points Obtained in This Study (in kcal/mol)

state	*S* product	*R* product
	Monocatalysis	
REACT	0	0
TS1	0.5	1.5
INT1	−15.8	−12.9
TS2	−3.8	−4.9
INT2	−14.7	−17.2
TS3a/b	−6.6/0.6	−4.0/−6.1
	Co-catalysis	
REACT	0	0
TS1	11.7	15.7
INT1	−4.3	−5.7
TS2	7.5	−0.8
INT2	−23.2	−22
TS3	−7.1	−6.5
INT3	−20.1	−17.9
PROD	−18.2	−23.5

of the azlactone is initially protonated by the phosphoric acid **CPA1** forming an azlactone enolate with a large partial negative charge on the oxygen atom. The styrene tautomer is subsequently protonated to form the tertiary carbocation intermediate.

The reaction proceeds via the formation of a bond between the C4 atom of the azlactone and the styrene tertiary carbon (**TS1**), leading to the dearomatized intermediate **INT1**. The transition states are asynchronous in nature with much shorter C−C distances in comparison to C−O distances. The difference in the C−C and C−O distances in **TS1-S** was found to be 0.45 Å in comparison to to 0.51 Å in **TS1-R**. The barrier to reaction for **TS1-R** was 1.5 kcal/mol, which was 1.0 kcal/mol higher than that for **TS1-S** (Figure 3 and Figure S3). Little difference between the *si*- and *re*-based transition states is observed for **TS1**, both displaying comparable nonbonded interactions.

In step 2, **CPA2** activates the styrene-azlactone complex via a proton-shuttling process that promotes ring closure to generate the DA adduct via C−O bond formation (**TS2**). The

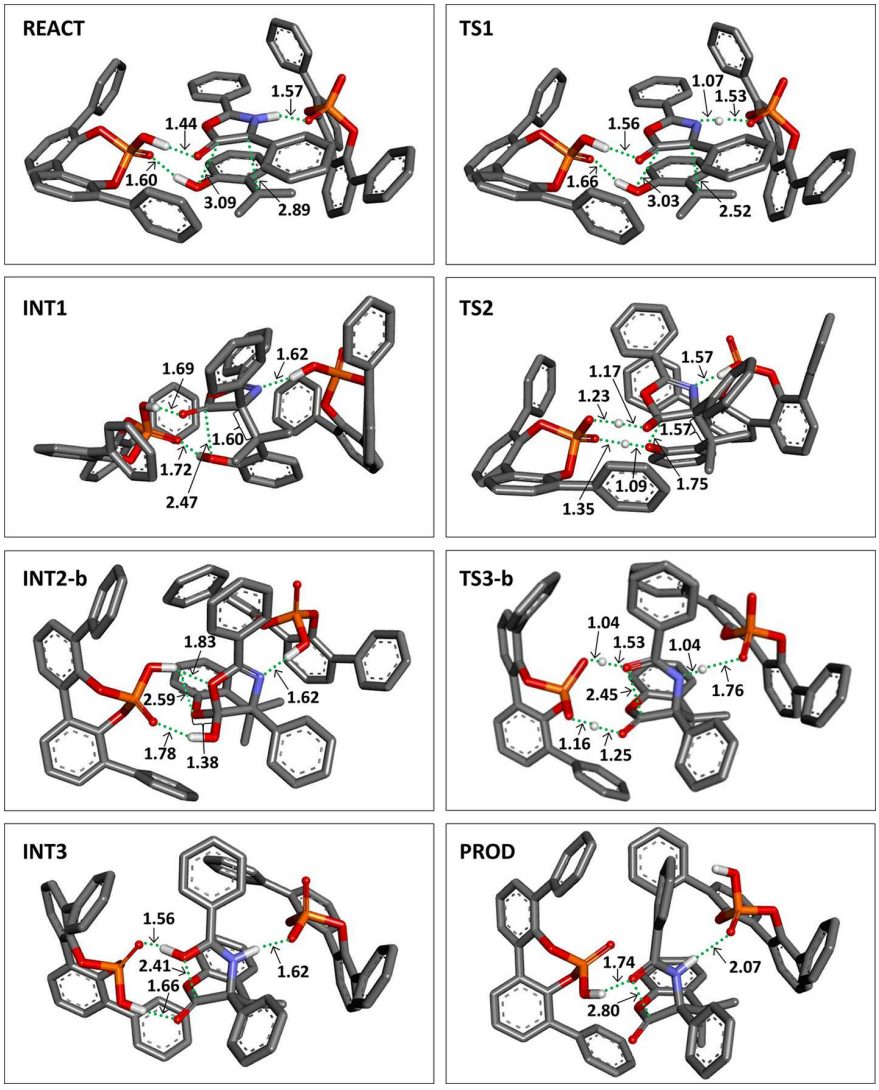

Figure 3. QM optimized structures associated with the *R* product obtained in the monocatalysis model. Polar hydrogens are displayed only for clarity. Distances are shown in Å.

DOI: 10.1021/acs.joc.9b00032
J. Org. Chem. 2019, 84, 4025−4032

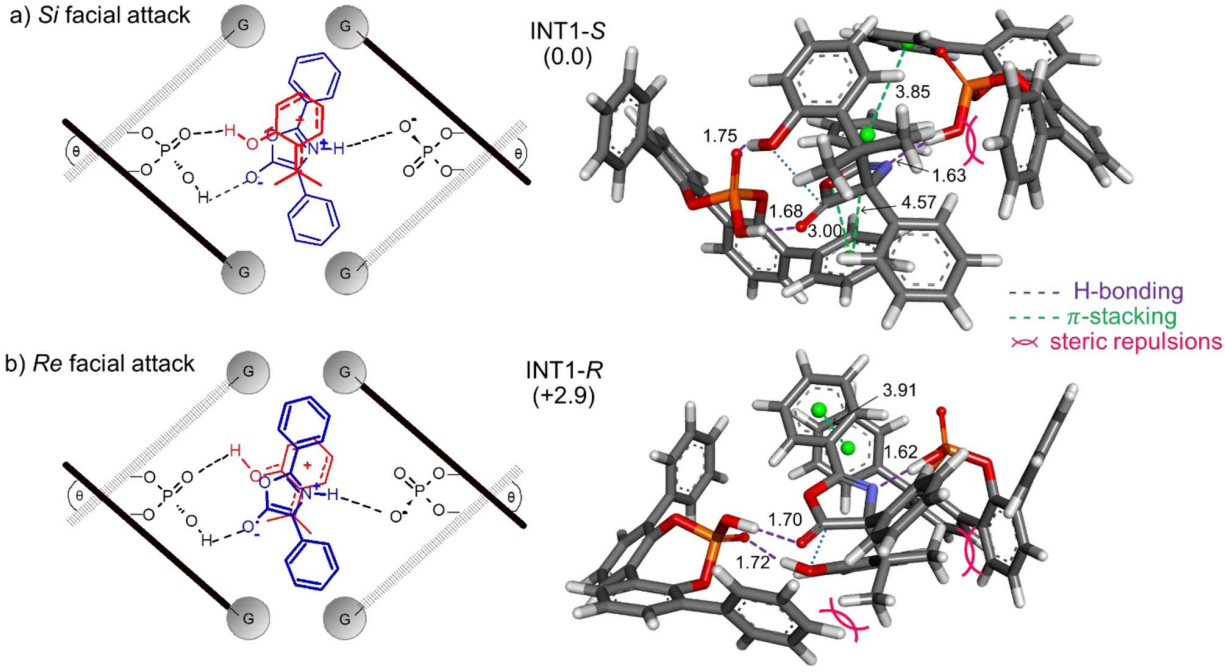

Figure 4. Schematic representation models and 3D structures of (a) **TS2-S** and (b) **TS2-R** for C−C bond formation in monocatalysis of *S* and *R* product. The numbers in parentheses are relative Gibbs free energies (in kcal/mol) (G is an aryl group substituted at the 3,3′-positions of CPA in the ball model and substrates in the tube model).

barriers for the *R*- and the *S*-mediated processes are 8.1 and 12.0 kcal/mol, respectively, with C−O distances of 1.77 and 1.76 Å, respectively. The C−O bond length of the **INT2** products are found to be 1.42 Å. The final step involves protonation of the oxazole nitrogen by **CPA1** leads to the azlactone ring opening in **TS3**. This requires concomitant proton transfer of the alcohol proton to a base which could be CPA (step b) or potentially an additional, and more basic, azlactone molecule (step a). In the case of **TS3-b**, the enolate complex is generated by the proton transfer to **CPA2**, resulting in a ring-opening activation energy of 15.2 kcal/mol (see Figure S5 in the Supporting Information). Alternatively, a second azlactone molecule can act as the base, giving rise to **TS3-a**. The increased basicity of the azlactone results in a barrier 7.1 kcal/mol lower in energy for the *S* product, but only a minor change for the *R* product. The final step requires proton rearrangement to form the corresponding amide group (**PROD**).

The origin of the differences in barrier heights for **TS2** and **TS3** is primarily down to differences in the energies of **INT1** and **INT2**, rather than differences in the energies of the transition states themselves. **INT1-R** is found to be 2.9 kcal/mol higher in energy than the *S* isomer in spite of the similar interaction present (Figure 4). While there is the same number of H-bond interactions, π-stacking is more pronounced in the *S* isomer and steric repulsion is lower, resulting in a higher **TS2** for the former. For **INT2** in contrast, the *S* isomer is found to be 2.5 kcal/mol higher in energy in comparison to the *R* isomer (Figure S6) and an analysis of the structures shows that this is again due to improved π-stacking between the substrates and CPA. This means **TS3** is predicted to be higher for the *S* isomer.

In summary, it is found that the rate determining step (RDS) to formation of the *R* product is marginally lower in energy than that for the *S* product (by 0.9 kcal/mol). **TS2** is found to be rate determining for the *S* product (12.0 kcal/mol), while **TS3** is found to be rate determining for the *R* product (11.1 kcal/mol).

3.2. Co-catalytic System. The proposed DA reaction mechanism catalyzed by CPA/*t*Bu-TBO was investigated according to Scheme 2b. We found that the DA reaction under co-catalytic conditions also proceeds via the stepwise mechanism (Figure 5). The starting geometry (**REACT**) consists of the azlactone in the enol form and the styrene as *o*-quinone methide (*o*-QM), **CPA** in its deprotonated form, and **TBO** in its protonated form. The resulting complex is tightly bound together due to the strong electrostatic attraction between guanidinium cation and phosphate anion and H-bond interactions with the azlactone and *o*-QM.

C−C bond formation occurs in an asynchronous manner at **TS1** with activation energies of 11.7 and 15.7 kcal/mol for *Si* and *Re* faces, respectively. The barriers to reaction for **TS1** are higher than those observed for the mono-catalytic process and are a reflection of the greater instability of starting complexes in the latter. The lower activation barrier for **TS1-S** is due to the greater asynchronicity between the C−C and C−O bonds in comparison to the case for **TS1-R** (1.12 and 0.93 Å, respectively) (Figure 5 and Figure S4). The dearomatized intermediates display C−C bond lengths of 1.607 and 1.622 Å for the *S* and *R* **INTs**, respectively, and the **TBO** catalyst is regenerated. In step 2, **TBO** abstracts a proton from the alcohol of **INT1** leading to ring closure. The activation barrier for **TS2-S** is 4.9 kcal/mol, 7.0 kcal/mol higher than **TS2-R**. **CPA** subsequently removes a proton from the OH group of **INT2**, thereby activating the ring-opening reaction and resulting in **INT3**. The activation energies required for C−O bond cleavage via **TS3-S** and **TS3-R** are 16.1 and 15.5 kcal/mol, respectively. The final oxygenous cyclic product is

DOI: 10.1021/acs.joc.9b00032
J. Org. Chem. 2019, 84, 4025−4032

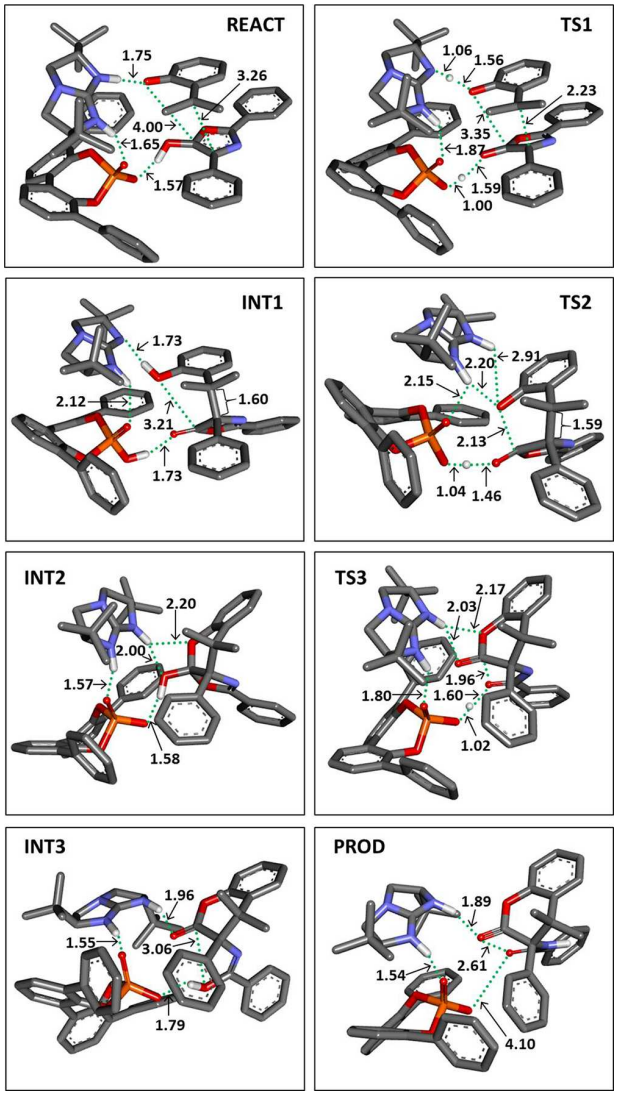

Figure 5. QM optimized structures associated with *S* product obtained in co-catalysis. Polar hydrogens are displayed only for clarity. Distances are shown in Å.

obtained by proton rearrangement, and it is found that the *R* product is marginally more stable than the *S* product due to more effective interaction with the chiral catalysts. **TS3-R** is found to be the highest barrier for the *S* product (16.1 kcal/mol), while **TS1** and **TS3** are of comparable barrier height for the *R* product (15.7 and 15.5 kcal/mol, respectively). However, on formation of **INT2**, the lowest energy structure, reverse formation of **INT1**, requires barriers of greater than 30 kcal/mol for the *S* isomer and 21 kcal/mol for the *R* isomer. For the *S* isomer, **TS1** and **TS2** are of comparable magnitude at approximately 12 kcal/mol.

In contrast to the mono-catalytic process, the differences in the barriers for steps 1 and 2 are found to be a direct result of the stabilization of the transition state structures by CPA and TBO. **TS1** for the *S* isomer is found to be 4.0 kcal/mol lower than for the *R* isomer. The C−C bond is somewhat elongated in the former (2.23 vs 2.15 Å), and reduced steric clash between the *tert*-butyl groups of TBO and both the azlactone and CPA is observed (Figure 6). This also manifests itself in the form of reduced charge transfer onto the azlactone (Table S1). **TS2** of the *R* isomer is found to be 7.0 kcal/mol lower than that of the *S* isomer (Figure S7). Again, this is a result of demonstrably more effective H-bonding interactions between CPA and TBO in particular at the transition state as well as reduced steric repulsion between the different components (Figure S7).

In summary, the RDS to formation of the *S* product is dramatically lower in energy than that of the *R* product (by ∼4 kcal/mol) for the co-catalytic process. **TS1** is found to be the rate determining step for the *R* product (15.7 kcal/mol), while **TS1** and **TS2** are found to be of comparable energy for the *S* product (11.7 and 11.9 kcal/mol, respectively).

4. DISCUSSION

The free energy profiles for the mono- and co-catalytic DA reactions are shown in Figure 7. The RDS in mono-catalytic reaction is the C−O bond formation, or step 2, for the *S*) isomer (12.0 kcal/mol) and ring opening, or step 3, for the *R* isomer (11.1 kcal/mol). The DA process for the co-catalytic system displays more sizable differences in the rate-determining barrier. The RDS in the co-catalytic reaction was found to be C−C bond formation, or step 1 for the *R* - isomer (∼16 kcal/mol), while the C−C and C−O bond formation steps were found to be comparable for the *S* isomer (∼12 kcal/mol).

It has been shown experimentally that under the mono-catalytic conditions (CPA alone) both enantiomeric products are produced with lower enantioselectivity (%er ≈ 60 on average). In contrast, when TBO is added as cocatalyst, a marked increase in selectivity is observed, favoring the *S* enantiomer (%er > 80). It would therefore be expected that the difference in the rate-determining barrier to reaction should be close to zero for the mono-catalytic reaction and favor the *S* isomer for the the co-catalytic system. We found that the calculated $\Delta\Delta G^{\ddagger}$ in monocatalysis for the *S* product is approximately the same as that for the *R* product. In the case of the co-catalytic process, the $G^{\ddagger}$ value is 4.0 kcal/mol in favor of the *S* product. As a result, the *S* product is heavily favored over the *R* product in line with experiment (Figure 8).

5. CONCLUSION

DFT studies of the enantioselective DA reaction between *o*-hydroxystyrene and azlactone catalyzed by CPA only and CPA in combination with *t*Bu-TBO catalyst were carried out to reveal the reaction mechanism and rationalize the origin of the enantioselectivity. The reaction mechanisms in mono- and co-catalytic systems proceed through stepwise DA cycloaddition followed by ring opening. The bifunctionality of CPA and *t*Bu-TBO plays an important role in simultaneously activating both *o*-hydroxystyrene and azlactone via hydrogen-bonding interactions. In the mono-catalytic DA reaction, both the *R* and *S* products have predicted rate determining steps of comparable magnitude. This corresponds to the asynchronous formation of a C−C bond between the diene and dienophile in the former and ring opening in the latter due to the unique 3D arrangement of the CPA catalysts. In the co-catalytic system involving CPA and TBO, formation of the *S* product is more facile, in line with experimental observations confirming the predictive nature of the models generated here. This and other research studies[21] appear to show that simulations offer a

DOI: 10.1021/acs.joc.9b00032
J. Org. Chem. 2019, 84, 4025−4032

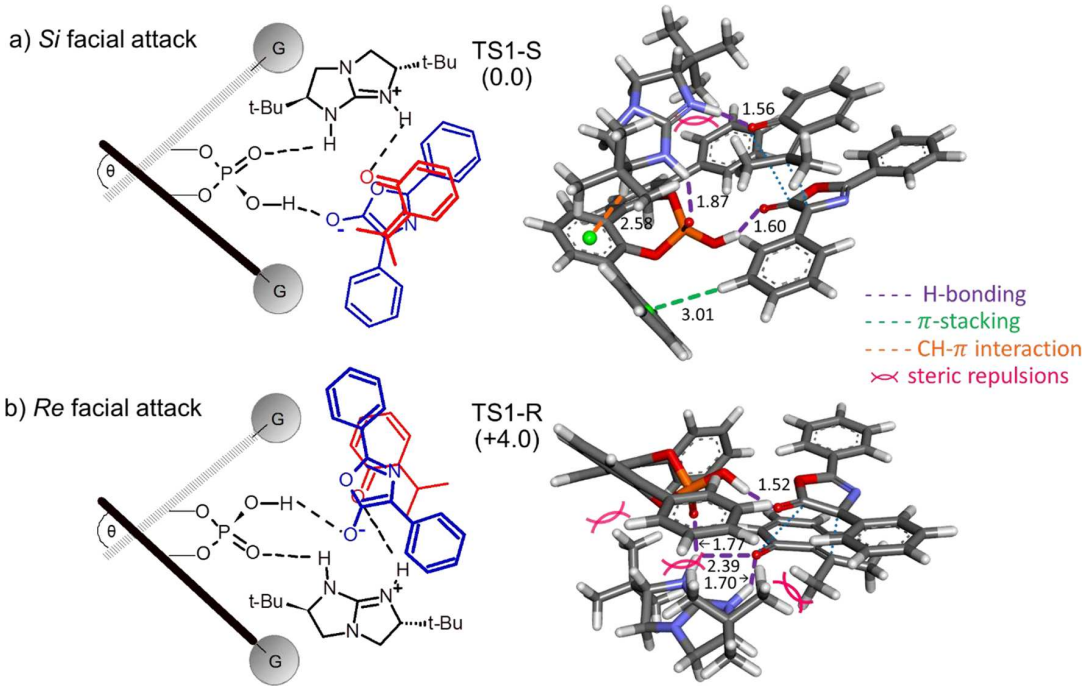

Figure 6. Schematic representation models and 3D structures of (a) **TS1-S** and (b) **TS1-R** for C−C bond formation in co-catalysis of *S* and *R* products. The numbers in parentheses are relative Gibbs free energies (in kcal/mol) (G is aryl group substituted at the 3,3′-positions of CPA in the ball model and substrates in the tube model).

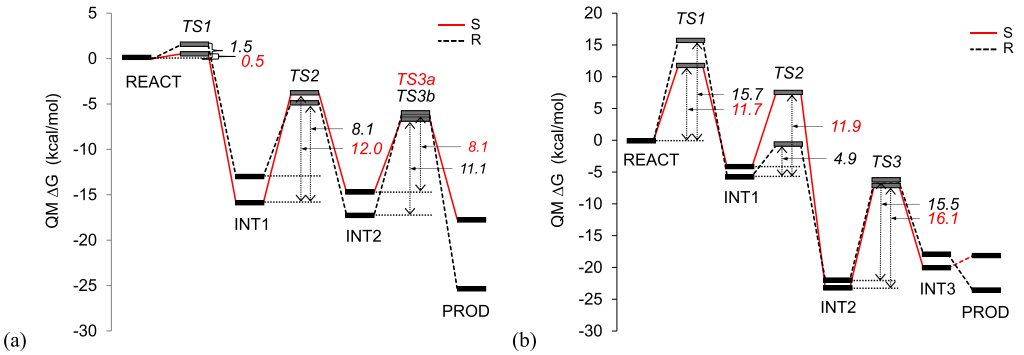

Figure 7. QM Δ*G* reaction profile of both *S* and *R* products for (a) mono-catalytic and (b) co-catalytic Diels−Alder reactions. **TS3b** is shown for *R* due to the lower activation energy in comparison with **TS3a**.

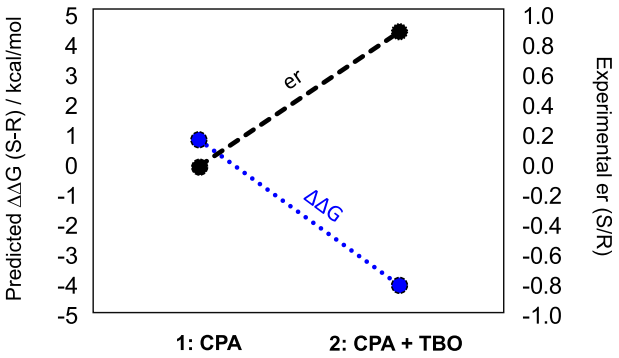

Figure 8. Relationship between the RDS energy difference and enantiomeric ratio for mono-catalytic (1) and co-catalytic (2) systems.

means to develop novel synthetic processes based on chiral catalysts such as CPA and TBO in the future.

■ ASSOCIATED CONTENT

Supporting Information

The Supporting Information is available free of charge on the ACS Publications website at DOI: 10.1021/acs.joc.9b00032.

Energies, Mulliken charges, transition state vibrational frequencies, and 3D images (PDF)

Coordinates of optimized stationary points (ZIP)

■ AUTHOR INFORMATION

Corresponding Authors

*E-mail for M.P.G.: paul.gl@kmitl.ac.th.

*E-mail for K.B.: kanokthip.bo@kmitl.ac.th.

DOI: 10.1021/acs.joc.9b00032
J. Org. Chem. 2019, 84, 4025−4032

ORCID

M. Paul Gleeson: 0000-0001-6998-7446

Notes

The authors declare no competing financial interest.

■ ACKNOWLEDGMENTS

M.P.G. wishes to acknowledge funding provided by King Mongkut's Institute of Technology Ladkrabang.

■ REFERENCES

(1) Nicolaou, K. C.; Snyder, S. A.; Montagnon, T.; Vassilikogiannakis, G. *Angew. Chem., Int. Ed.* **2002**, *41*, 1668−1698.
(2) Domingo, L. R.; Sáez, J. A. *Org. Biomol. Chem.* **2009**, *7*, 3576−3583.
(3) Konovalov, A. I.; Kiselev, V. D. *Russ. Chem. Bull.* **2003**, *52*, 293−311.
(4) (a) Funel, J.-A.; Abele, S. *Angew. Chem., Int. Ed.* **2013**, *52*, 3822−3863. (b) Gregoritza, M.; Brandl, F. P. *Eur. J. Pharm. Biopharm.* **2015**, *97*, 438−453.
(5) (a) Goldstein, E.; Beno, B.; Houk, K. N. *J. Am. Chem. Soc.* **1996**, *118*, 6036−6043. (b) Linder, M.; Brinck, T. *J. Org. Chem.* **2012**, *77*, 6563−6573.
(6) Corey, E. J. *Angew. Chem., Int. Ed.* **2002**, *41*, 1650−1667.
(7) (a) Jørgensen, K. A. *Angew. Chem., Int. Ed.* **2000**, *39*, 3558−3588. (b) Enders, D.; Hüttl, M. R. M.; Grondal, C.; Raabe, G. *Nature* **2006**, *441*, 861.
(8) Zhang, Y.-C.; Zhu, Q.-N.; Yang, X.; Zhou, L.-J.; Shi, F. *J. Org. Chem.* **2016**, *81*, 1681−1688.
(9) Kontogiorgis, C. A.; Hadjipavlou-Litina, D. J. *J. Med. Chem.* **2005**, *48*, 6400−6408.
(10) Parmar, D.; Sugiono, E.; Raja, S.; Rueping, M. *Chem. Rev.* **2014**, *114*, 9047−9153.
(11) (a) Shi, F.; Xing, G.-J.; Tao, Z.-L.; Luo, S.-W.; Tu, S.-J.; Gong, L.-Z. *J. Org. Chem.* **2012**, *77*, 6970−6979. (b) Zhang, Y.-C.; Jiang, F.; Wang, S.-L.; Shi, F.; Tu, S.-J. *J. Org. Chem.* **2014**, *79*, 6143−6152. (c) Wang, Z.; Ai, F.; Wang, Z.; Zhao, W.; Zhu, G.; Lin, Z.; Sun, J. *J. Am. Chem. Soc.* **2015**, *137*, 383−389. (d) Dai, W.; Lu, H.; Jiang, X.-L.; Gao, T.-T.; Shi, F. *Tetrahedron: Asymmetry* **2015**, *26*, 109−117. (e) Zhang, H.-H.; Wang, Y.-M.; Xie, Y.-W.; Zhu, Z.-Q.; Shi, F.; Tu, S.-J. *J. Org. Chem.* **2014**, *79*, 7141−7151. (f) Liu, Y.; Zhang, H.-H.; Zhang, Y.-C.; Jiang, Y.; Shi, F.; Tu, S.-J. *Chem. Commun.* **2014**, *50*, 12054−12057. (g) Li, M.-L.; Chen, D.-F.; Luo, S.-W.; Wu, X. *Tetrahedron: Asymmetry* **2015**, *26*, 219−224. (h) Tang, M.; Zhao, J.-J.; Wu, Q.; Tu, M.-S.; Shi, F. *Synthesis* **2017**, *49* (09), 2035−2044.
(12) (a) de Castro, P. P.; Carpanez, A. G.; Amarante, G. W. *Chem. - Eur. J.* **2016**, *22*, 10294−10318. (b) Hewlett, N. M.; Hupp, C. D.; Tepe, J. J. *Synthesis* **2009**, *2009*, 2825−2839. (c) Hu, H.; Liu, Y.; Guo, J.; Lin, L.; Xu, Y.; Liu, X.; Feng, X. *Chem. Commun.* **2015**, *51*, 3835−3837. (d) Liu, X.; Wang, Y.; Yang, D.; Zhang, J.; Liu, D.; Su, W. *Angew. Chem., Int. Ed.* **2016**, *55*, 8100−8103. (e) Zhou, J.; Wang, M.-L.; Gao, X.; Jiang, G.-F.; Zhou, Y.-G. *Chem. Commun.* **2017**, *53*, 3531−3534. (f) Ma, C.; Zhou, J.-Y.; Zhang, Y.-Z.; Mei, G.-J.; Shi, F. *Angew. Chem., Int. Ed.* **2018**, *57*, 5398−5402.
(13) Jiang, J.; Qing, J.; Gong, L.-Z. *Chem. - Eur. J.* **2009**, *15*, 7031−7034.
(14) (a) Zhang, L.; Liu, Y.; Liu, K.; Liu, Z.; He, N.; Li, W. *Org. Biomol. Chem.* **2017**, *15*, 8743−8747. (b) Yu, X.-Y.; Chen, J.-R.; Wei, Q.; Cheng, H.-G.; Liu, Z.-C.; Xiao, W.-J. *Chem. - Eur. J.* **2016**, *22*, 6774−6778.
(15) Leow, D.; Tan, C.-H. *Synlett* **2010**, *2010*, 1589−1605.
(16) (a) Wheeler, S. E.; Seguin, T. J.; Guan, Y.; Doney, A. C. *Acc. Chem. Res.* **2016**, *49*, 1061−1069. (b) Seguin, T. J.; Wheeler, S. E. *ACS Catal.* **2016**, *6*, 7222−7228.
(17) Tian, X.; Hofmann, N.; Melchiorre, P. *Angew. Chem., Int. Ed.* **2014**, *53*, 2997−3000.
(18) (a) Zhao, Y.; Truhlar, D. G. *Theor. Chem. Acc.* **2008**, *120*, 215−241. (b) Zhao, Y.; Truhlar, D. G. *Acc. Chem. Res.* **2008**, *41*, 157−167.
(19) Linder, M.; Brinck, T. *Phys. Chem. Chem. Phys.* **2013**, *15*, 5108−5114.
(20) Gaddamanugu, G. *Indian J. Chem. Sect. A* **2011**, *50*, 1579−1586.
(21) (a) Shibata, Y.; Yamanaka, M. *J. Org. Chem.* **2013**, *78*, 3731−3736. (b) Simón, L.; Goodman, J. M. *J. Org. Chem.* **2010**, *75*, 589−597. (c) Jiang, Z.; Pan, Y.; Zhao, Y.; Ma, T.; Lee, R.; Yang, Y.; Huang, K.-W.; Wong, M. W.; Tan, C.-H. *Angew. Chem., Int. Ed.* **2009**, *48*, 3627−3631. (d) Cho, B.; Tan, C.-H.; Wong, M. W. *Org. Biomol. Chem.* **2011**, *9*, 4550−4557. (e) Cho, B.; Tan, C.-H.; Wong, M. W. *J. Org. Chem.* **2012**, *77*, 6553−6562.

DOI: 10.1021/acs.joc.9b00032
J. Org. Chem. 2019, 84, 4025−4032

AUTHOR BIOGRAPHY

Name	Miss Napassorn Jensupakarn
Date of Birth	21 February 1994
Address	No. 24 Soi.Chokchai4(56) Jucntion13, Chokchai4 Road, Ladprao Subdistrict, Ladprao District, Bangkok 10230
Education	Bachelor's Degree of Engineer from College of Nanotechnology, King Mongkut's Institute of Technology Ladkrabang (KMITL)

Conferences :

1. Poster presentation at The 5th Thailand International Nanotechnology Conference (NanoThailand 2016) during November 27-29, 2016.
2. Oral presentation at Pure and Applied Chemistry International Conference 2019 (PACCON 2019) during February 7-8, 2019.

Academic Publication:

1. Napassorn Jensupakarn, M. Paul Gleeson, Duangkamol Gleeson, and Kanokthip Boonyarattanakalin, "Theoretical Investigation of the Enantioselective [4 + 2] Cycloaddition Reaction of *o*-Hydroxystyrene and Azlactone", *The Journal of Organic Chemistry*, vol. 84 (2019), pp 4025–4032.